A FRAMEWORK FOR DEVELOPING OPTIMAL TENSILE STRENGTH RELATIONSHIPS BASED ON CHARACTERIZATION TOOLS WITH FOCUS ON: PARTICLE SIZE, LUBRICANT SENSITIVITY, AND TABLET SHAPE

BY

SONIA MODARRES RAZAVI

A dissertation submitted to the

Graduate School—New Brunswick

Rutgers, The State University of New Jersey

in partial fulfillment of the requirements

for the degree of

Doctor of Philosophy

Graduate Program in Mechanical And Aerospace Engineering

Written under the direction of

Alberto M. Cuitiño

and approved by

_____

_____

_____

_____

New Brunswick, New Jersey

OCTOBER, 2017

ABSTRACT OF THE DISSERTATION

A Framework for Developing Optimal Tensile Strength Relationships Based on Characterization Tools with Focus on: Particle Size, Lubricant Sensitivity, and Tablet Shape

by

SONIA MODARRES RAZAVI

Dissertation Director: Alberto M. Cuitiño

This work is a collection of problems all focused on mechanical strength of pharmaceutical tablets. The first problem focuses on relating material strength to the breaking force of non-flat faced tablets. We propose a general framework for determining optimal relationships for tensile strength of doubly convex tablets under diametrical compression. This approach is based on the observation that tensile strength is directly proportional to the breaking force and inversely proportional to a non-linear function of geometric parameters and materials properties. This generalization reduces to the analytical expression commonly used for flat faced tablets, i.e., Hertz solution, and to the empirical relationship currently used in the pharmaceutical industry for convex-faced tablets, i.e., Pitt's equation. Under proper parameterization, optimal tensile strength relationship can be determined from experimental results by minimizing a figure of merit of choice. This optimization is performed under the first-order approximation that a flat faced tablet and a doubly curved tablet have the same tensile strength if they have the same relative density and are made of the same powder, under equivalent manufacturing conditions. Furthermore, we provide a set of recommendations and best practices for

assessing the performance of optimal tensile strength relationships in general. Based on these guidelines, we identify two new models, namely the general and mechanistic models, which are effective and predictive alternatives to the tensile strength relationship currently used in the pharmaceutical industry.

The second problem targets the utilization of a non-destructive technique to assess tablet strength. An ultrasound measurement system was employed as a non-destructive method to evaluate its reliability in predicting the tensile strength of tablets and investigate the benefits of incorporating it in a continuous line, manufacturing solid dosage forms. Tablets containing lactose, acetaminophen, and magnesium stearate were manufactured continuously and in batches. The effect of two processing parameters, compaction force and level of shear strain were examined. Elastic modulus and tensile strength of tablets were obtained by ultrasound and diametrical mechanical testing, respectively. It was found that as the blend was exposed to increasing levels of shear strain, the speed of sound in the tablets decreased and the tablets became both softer and mechanically weaker. Moreover, the results indicate that two separate tablet material properties (e.g., relative density and elastic modulus) are necessary in order to predict tensile strength. A strategy for tensile strength prediction is proposed that uses the existing models for elastic modulus and tensile strength of porous materials. Ultrasound testing was found to be very sensitive in differentiating tablets with similar formulation but produced under different processing conditions (e.g., different level of shear strain), thus, providing a fast and non-destructive method for hardness prediction that could be incorporated to a continuous manufacturing process.

The third problem aims to adopt a Quality by Design paradigm to better control the mechanical strength of tablets as a critical quality attribute by understanding the effects of critical process parameters and critical material attributes. To this end, the effect of particle size distribution, lubricant concentration, and mixing time on the tensile strength and stiffness of tablets were studied. Two grades of lactose, lactose α-monohydrate and spray-dried lactose, were selected. Tablets were compressed to different relative densities ranging from 0.8 to 0.94 using an instrumented compactor

simulator, and compaction curves showing the force-displacement profiles during compaction were obtained. The total work input during the compaction process is found to be higher for spray-dried lactose compared to lactose monohydrate. We propose a general model, which predicts the elastic modulus and tensile strength envelope that a specific powder can obtain based on its lubrication sensitivity for different particle size distributions. This was possible by introducing a new parameter in the existing tensile strength and elastic modulus models. A wide range of lubrication conditions was explored and the model exhibited a good predictability. The mechanical properties of lactose monohydrate tablets were noticeably dependent on particle size, unlike spray-dried lactose where little to almost no sensitivity to initial particle size was observed. The model is designed in a general fashion that can capture all the possible mechanical integrity behaviors in response to different lubrication conditions and initial particle size. Our model can be extended to all the powders that undergo different deformation mechanisms and is applicable for more complex pharmaceutical formulations.

Acknowledgements

This dissertation is a result of the contribution of many individuals, which I have had the pleasure to work with. I have to first start by thanking my supportive and kind advisor, Prof. Alberto Cuitiño. I am forever indebted to him for making me a more confident person by giving me a lot of opportunities, yet letting me find my way freely. I would like to thank Prof. Marcial Gonzalez, who has helped me tremendously without any hesitation. I have learnt a lot from him both scientifically and personally and for that I am truly grateful. I would also like to express my gratitude toward my other committee members, Prof. Mina Pelegri, who is an inspirational role model for all the women engineers and Prof. German Drazer, whom I had the pleasure to work with. I have always admired his attention to details.

I want to thank the Engineering Research Center for Structured Organic Particulate Systems (C-SOPS) for the financial support and providing an excellent environment to understand and address industry needs and interact with both academic and industrial collaborators. To the C-SOPS members, I was privileged to be surrounded by so many dedicated and talented colleagues. I will always cherish the friendships and memories I have made with each and every one of you. I would like to specifically thank Golshid Keyvan, Bereket Yohannes, Gerardo Callegari, Savitha Panikar, Pallavi Pawar, Yifan Wang, Zhanjie Liu, and Sarang Oka.

I want to express my appreciation to my amazing officemates and my dear friends, especially Mahsa and Shirin, for all the discussions and laughs over the coffee breaks. You made my PhD life much more fun and meaningful.

Words cannot describe my endless love and gratitude I have for my family. My parents have been my rock in life. My mom, Farzaneh, who has always been by my side despite the long distance through good and rough days. My dad, Reza, whom our phone

conversations may have not lasted more than 5 minutes but the positive energy would have kept me going through the day. I am so fortunate to have my biggest role models as my parents and always strive to make them feel proud and happy. My big sister, Sara, whom I always look up to. I am the proudest sister to have her in my life. My niece, Nila, who brings joy to my life and holds a special place in my heart. I dream of a day when we all live at least in the same time zone!!

Last but not least, my lifelong partner, Navid, I cannot imagine passing one moment of my life without you. I know these couple of sentences cannot deliver my feelings toward you. Throughout all these years you have stood beside me and have always encouraged me to move forward and never give up. What I am and where I am today was definitely not possible without you in my life. I love you honey.

Dedication

To my spectacular parents, Farzaneh & Reza

my lovely sister, Sara

&

my better half, Navid

Table of Contents

List of Figures

List of Tables

Chapter 1

Introduction

1.1 Background

Solid dosage forms account for almost 80% of all marketed pharmaceutical products in the United States [6]. Tablets are the most common dosage form, due to their relatively low manufacturing cost, high production rates, acceptable shelf life, dosage accuracy, and contolled drug release [7, 8]. Tablets are mainly fabricated by pressing powders into various shapes and geometries. The compacted powder is always a mixture of two or more powder ingredients. The ingredients are classified into two groups: active pharmaceutical ingredients (APIs) and excipients. API, which delivers the therapeutic effect, is formulated with excipients to ensure desirable tablet behavior from its production to release in human body.

1.2 Powder Compaction

Direct compression, compared to dry granulation and wet granulation, is the simplest and preferred route to produce oral solid dosage forms, which refers to the compaction of the dry mixed of the individual ingredients [9]. Tableting (i.e., powder compaction) is the last stage in a tablet production, if coating is not required.

The compaction mechanism starts with particle re-arrangement, which refers to particles moving into closer packing and volume reduction. With an increase in the compaction pressure particles deform either plastically, elastically, or fracture into smaller particles (i.e., fragmentation) [10]. In most cases, more than one of the aforementioned mechanisms occur [11]. The applied energy is completely recovered in elastic deformation, unlike plastic deformation and fragmentation where the the particles undergo

irreversible deformation. Interparticulate attraction occurs between the particles as their surfaces are brought closer together resulting in bond formation. Finally, elastic recovery occurs during the decompression stage [12]. There are three dominating bonding mechansims that act between particulate solids: solid bridges, intermolecular forces, and mechanical interlocking [13]. The sum of number of bonds remained after the decompression stage and the strength of each bond are reflected in the tablet strength.

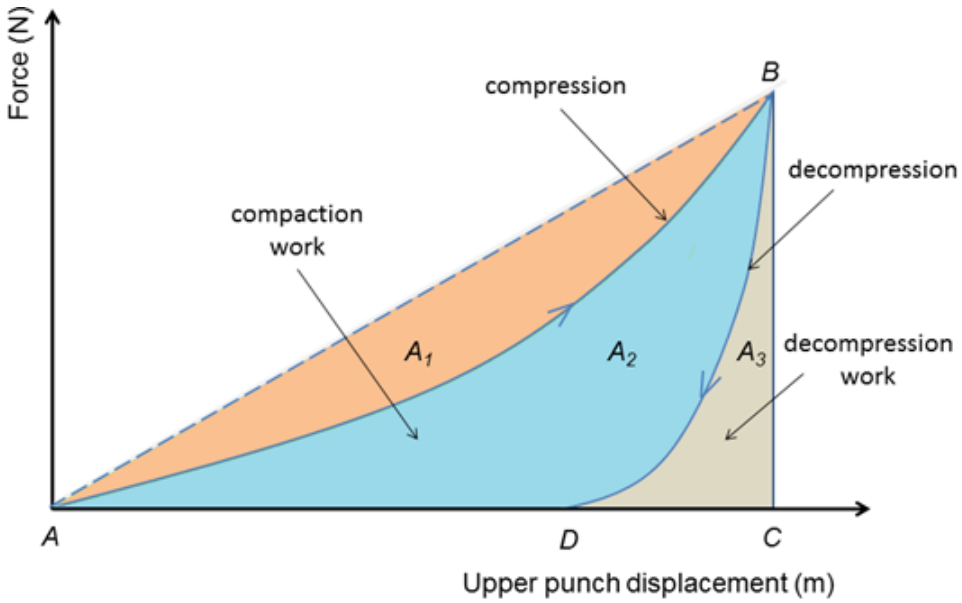

Figure 1.1: Schematic of a compaction curve; upper punch force vs. upper punch displacement [1].

Single station compaction simulators are the ideal devices to study powder deformation behavior by accurate recording of upper punch force and displacement, if the die wall friction is negligible [14]. This profile depends on the material and equipment. Fig. 1.1 schematically shows how the forces evolve during powder compression. Ideally, the force-displacement cruve follows the triangle ABC. However, in reality compression takes place along curve AB followed by decompression along curve BD. Area A_1 represents the work of friction and area A_3 is the work recovered during decompression stage. The area under the curve AB, $(A_2 + A_3)$ represents the net work of compaction. The bigger the area A_2 is, the better the compressibility. Materials that undergo a large irreversible deformation are expected to yield a large net work [14].

Both powder properties (e.g., particle size [15] and crystal structure of the material [16]) and processing parameters (e.g., compression force, compression speed [17, 18]) affect the compaction behavior and tablet properties [19].

1.3 Compaction Cycle

Tablet compaction is divided into four distinct stages. These stages include die filling, metering, compressing, and ejection. In the filling stage, the powder is introduced into the die followed by metering stage, where the the weight is adjusted and the excessive powder is pushed out of the die. Powder compression usually consists of two steps: pre-compression and main compression. In the pre-compression step, a low compression force is applied to the powder to release air trapped between the powder particles. During the main compression loading the punches get closer and the thickness of the powder bed decreases until it reaches its minimum, where the maximum compaction pressure is applied (Point B in Fig. 1.1). When the force is released, the unloading stage starts and some of the energy is recovered and tablet expands axially. The last stage of the tablet compaction is the ejection, where the tablet is ejected from the die. Fig. 1.2 schematically shows a high speed rotary press in motion.

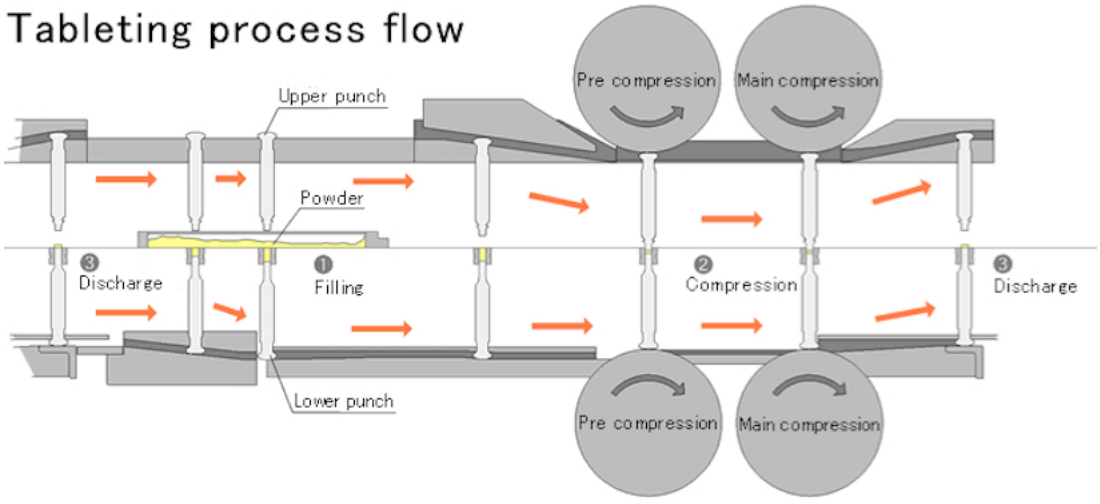

Figure 1.2: Tablet compression cycle stages. Courtesy of Kikusui Seisakusho Ltd., Kyoto, Japan.

The main types of tablet presses are mechanical and hydraulic. In mechanical presses

the distance between the punches can be controlled and powders are compressed to constant thickness. In hydraulic presses the force exerted on powders is the processing variable and powders are compressed to constant force.

In order to adequately characterize the mechanical properties of powders, properties during and after compaction of tablets are extracted and analyzed. Although powder mixing is not the focus of this disseration, but since different mixing techniques were employed that affect the powder properties and their compaction behavior, a section is dedicated to briefly introduce mixing mechanisms and techniques.

1.4 Mixing Mechanisms

Mixing mechanism can be categorized in two ways: the scale at which mixing occurs and the driving force. The former can be classified as macro-mixing and micro-mixing and the latter is classified into convective, dispersive, and shear mixing [20, 21, 22]. Macro-mixing refers to the transportation and mixing of group of particles, while micro-mixing focuses on the mixing at individual particle level. The two classifications are obviously correlated; convective mixing is a macro-mixing and dispersive and shear mixing are micro-mixing. Shearing occurs in all the mixers. Shear mixing is caused by slipping planes within the powder bed. There exists velocity gradients between individual particles or particle planes [23]. Three types of mixers that were used in this work are: V-blender, Resonant Acoustic Mixing (RAM), and Glatt GCG-70 continuous blender. A brief description of each blender is provided as follows:

V-blender

V-blender, a popular tumble mixer, uses tumbling motion of a vessel containing powder ingredients. A combination of all the aforementioned mixing mechanisms exists. However, faster convective mixing occurs compared to dispersive mixing. The charging method of the material into the V-blender, the volume of the loaded material, mixer speed, and the number of revolutions may all affect the mixing efficiency.

For understanding the performance and mechanism of this type of mixer the reader is

referred to [24, 25, 26].

Resonant Acoustic Mixer (RAM)

RAM, which is rather a new and not thoroughly studied mixer, transfers low frequency, high-intensity acoustic energy to the material to be mixed. There are no impellers used in RAM technology, so a wide range of mixing conditions can be achieved with a simple vessel design [27]. All three mixing mechanisms (convection, dispersion, and shear) are expected to be present. Micro-mixing zones as well as the bulk movement of the materials take place throughout the entire vessel.

The total mixing power, P_{mix}, which is independent of the material properties, can be calculated by the following empirical equiation:

$$P_{mix} = 0.707\ F_{rms} \left(\frac{\Delta P}{100}\right) \left(\frac{a_{peak}\ g}{2\pi f}\right) = E_{mix} \times \frac{m}{t_{mix}} \tag{1.1}$$

where ΔP is the difference in power intensity of the loaded from the unloaded masses, F_{rms} is the machine force constant ($\simeq$ 70 N), g is the gravitational constant, a_{peak} is the peak acceleration experienced at the specific power intensity and f is the frequency of (61 Hz) at which the resonant acoustic mixer operates. The value of 0.707 is the correction factor. Measuring the total mixing time, t_{mix}, and the total powder mass, m, the total energy per unit mass, E_{mix} can be determined. Fill level, blending time, and acceleration are the key parameters that affect the RAM performance [28].

For more information regarding the performance and technology of RAM, please refer to [27, 28, 29].

Glatt Continuous Blender

Continuous powder mixing has received more attention by the increasing interest toward continuous pharmaceutical oral solid dose manufacturing. Continuous blenders use rotating blades that force the ingredients to transport and mix along the way. Like RAM, continuous blenders are independent of material properties. Blade configuration (i.e., orientation and number of blades) and impeller speed, which determines the mass

flow rate, affect the mixing performance [30, 31, 32, 33].

1.5 Tablet Tensile Strength

It is important to assure that tablets have sufficient strength to endure post-compaction loading such as coating, packaging, handling, and storage. The dissolution profile of a drug tablet is also influenced by its mechanical properties [34]. Hardness is thus an important quality factor that is tested during tablet production [35]. The mechanical strength of tablets is typically measured by traditional destructive tests, such as three-point bending, four-point bending, diametrical compression, and axial tensile strength tests [36, 37, 38, 39].

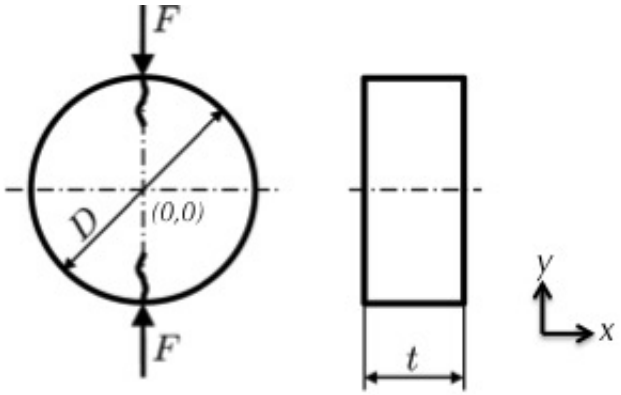

Figure 1.3: Geometry and failure behavior in a flat faced cylindrical tablet.

Among these experimental techniques, the diametrical compression test, also referred to as Brazilian test [40], is the most conventional method used in the pharmaceutical industry to measure the breaking force of a tablet. The test consists in placing and compressing a tablet along its diameter between two rigid platens as shown in Fig. 1.3. Hertz [41] developed a mathematical description for the stress states of an elastic disk under point loading diametrical compression, where here the equations are presented considering a tablet as the sample:

$$\sigma_x = \frac{-2F}{\pi t}\left[\frac{x^2(D-y)}{((D-y)^2+x^2)^2} + \frac{x^2(D+y)}{((D+y)^2+x^2)^2} - \frac{1}{2D}\right] \tag{1.2}$$

$$\sigma_y = \frac{-2F}{\pi t}\left[\frac{(D-y)^3}{((D-y)^2+x^2)^2} + \frac{(D+y)^3}{((D+y)^2+x^2)^2} - \frac{1}{2D}\right] \tag{1.3}$$

$$\sigma_{xy} = \frac{2F}{\pi t}\left[\frac{x(D-y)^2}{((D-y)^2+x^2)^2} + \frac{x(D+y)^2}{((D+y)^2+x^2)^2}\right] \tag{1.4}$$

where F is the breaking force, D is the diameter of the tablet, and t is its thickness. Maximum principal tensile stress occuring in the center of the disc and along the x-direction is predicted to be the cause of failure assuming the maximum stress criterion ($\sigma_y = \sigma_{xy} = 0$). Thus, by replacing x and y with zero, corresponding to the center of the tablet, in Eq. (1.2), Hertz solution is obtained:

$$\sigma_t = \frac{2F}{\pi D t} \tag{1.5}$$

where σ_t is the tensile strength. The above expression is only valid for flat cylindrical tablets that fail in tension across the symmetry plane of the loaded diameter.

Hardness (i.e., breaking force) has been traditionally reported and still used as a critical quality attribute (CQA). However, tensile strength is a better representative of the tablet strength, which actually is a measure of tablet strength and is independent of the tablet dimensions [42, 43].

1.6 Compressibility, Compactibility, and Tabletability

Tye et al. [44] introduced three important terms that give a lot of information about tablet compaction: Tabletability (tensile strength vs. compaction pressure), compressibility (relative density vs. compaction pressure), and compactability (tensile strength vs. relative density). There is a big difference between compressibility and compactability of powders. Compressibility refers to the ability of the powder to undergo volume reduction under pressure, whereas compactibility is the ability of a powder to form a coherent compact.

Relative density is used to characterize powders at different stages of densification. By applying more force to the powder bed the relative density of the tablet increases.

There are two main factors that affect the tablet properties (e.g., hardness, disintegration, and dissolution profiles): (i) material properties (e.g., constituents of the powder mixture, particle size and shape) and (ii) processing parameters (e.g., mixing conditions, compaction force, compaction speed, etc.). By understanding the behavior of processing parameters on the performance of the tablet, the tablet properties can actually be engineered.

1.7 Organization of the Dissertation

Given the brief introduction of powder compaction and some relevant terminologies in Chapter 1, the three specific objectives of this dissertation are summarized as follows:

1. Finding an optimal relationship for tensile strength of doubly convex tablets under diametrical compression.

2. Predicting tensile strength of pharmaceutical tablets by ultrasound measurement in continuous manufacturing.

3. Quantifying the lubrication and particle size distribution effects on tensile strength and stiffness of tablets.

A chapter has been dedicated for each specific objective. Each chapter starts with the background of the problem and relevant published literature. Materials and methods used in the work are provided followed by the results and key findings. Each chapter ends with a summary and concluding remarks. Chapter 5 provides an overall conclusion and a set of recommendations for future studies.

Chapter 2

General and Mechanistic Optimal Relationships for Tensile Strength of Doubly Convex Tablets Under Diametrical Compression

2.1 Introduction

Diametrical compression test was first implemented by Carneiro and Barcellos [40] to measure the tensile failure of flat cylindrical concrete samples using the equation Eq. (1.5) developed by Timoshenko and Goodier [45] and Frocht [46]. In 1968, the test was employed on lactose tablets to determine their tensile strength [47] and has been used ever since. There has been controversy about the applicability of the Hertz solution. For example, Procopio et al. [48] discussed that the strain at which failure occurs under diametrical load is an important crtierion for the validity of Hertz solution. It bears emphasis that all compacted powders are brittle [37] and, in sharp contrast to ductile materials, they do not exhibit significant permanent deformations before failure. Nowadays, tablets are no longer produced only in a flat cylindrical shape and are manufactured in different shapes and dimensions to aid identification, subsequent processing or to just simply enhance marketability. In this chapter, the tensile strength determination of a doubly convex cylindrical tablet is presented.

The diametrical compression test can still be used for non-flat faced tablets. However, the conversion of a breaking force to tensile strength is not that simple. In sharp contrast to flat faced tablets, there is no closed-form analytical solution that relates tensile strength and breaking force for curved faced tablets.

Tensile strength and breaking force increase exponentially with increasing relative density for typical pharmaceutical powders, tableting speeds, and tablet shapes (see, e.g.,

[44, 49, 50, 51]). In addition, the breaking force exhibits a strong dependence on the shape of the tablet and only a mild dependence on the diametrical compression speed. In order to find an optimal tensile strength relationship for curved faced tablets, Pitt et al. [52] used a photoelastic method to measure the stress distribution of doubly convex tablets subject to diametrical load. For doubly convex cylindrical gypsum discs, they established the following empirical relationship [53] between geometric parameters, breaking force and tensile strength:

$$\sigma_t = \frac{10F}{\pi D^2 \left[2.84 \left(\frac{t}{D}\right) - 0.126 \left(\frac{t}{W}\right) + 3.15 \left(\frac{W}{D}\right) + 0.01\right]} \tag{2.1}$$

where W is the length of the cylindrical portion of the tablet (see Fig. 2.1). This equation is valid for any brittle doubly convex disc with $0.1 \leq W/D \leq 0.3$, and also for discs with $W/D = 0.06$ and $D/R < 1.0$. However, it is worth noting that Pitt's equation (2.1) does not reduce to the Hertz solution (1.5) when the geometric parameters correspond to those of a flat faced tablet. Pitt and Heasley [54] subsequently modified Eqs. (1.5) and (2.1) to be applicable for elongated tablets by multiplying both equations by a factor of 2/3—this factor is exact only for the limiting case of large length to width ratios.

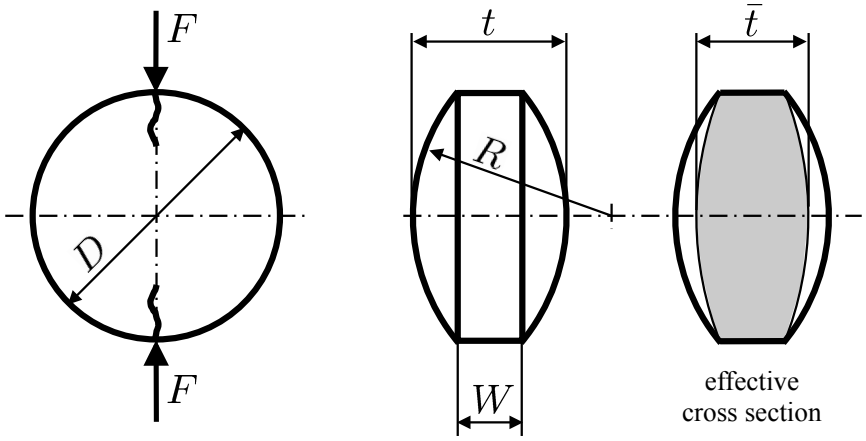

Figure 2.1: Geometry and failure behavior in a doubly convex tablet under diametrical compression.

Shang et al. [2] adopted the form of Pitt's original equation and calibrated its empirical coefficients to an extensive experimental campaign of doubly convex microcrystalline

cellulose (MCC) tablets with various curvatures and of various relative densities. Specifically, they fit experimental measurements to

$$\sigma_t = \frac{F}{\pi D^2 \left[a\left(\frac{t}{D}\right) + b\left(\frac{t}{W}\right) + c\left(\frac{W}{D}\right) + d\right]} \tag{2.2}$$

where a, b, c, and d are empirical coefficients (see Table 2.1 for numerical values). This equation, which from now on is referred to as the *4-parameter model*, has the same application space as Pitt's equation but shows a better fit to experimental data. They also simplified Eq. (2.2) by observing that there are only two independent geometric parameters (e.g., t/D and W/D) and that the correct limiting behavior for flat geometries can be enforced analytically. Thus, they proposed

$$\sigma_t = \frac{F}{\pi D^2 \left[a\left(\frac{t}{D}\right) + c\left(\frac{W}{D}\right)\right]} \tag{2.3}$$

which we refer to as the *1-parameter model*, where $a = 0.14$ and $c = 0.5 - a = 0.36$ are empirical parameters. It is interesting to note that Shang et al. [55] reported that the optimal values for a and c do not necessarily sum up to one-half (i.e., they do not enforce the correct limiting behavior in Eq. (2.3)) when calibrated to detailed finite element numerical results (e.g., $a = 0.187$ and $c = 0.284$ are proposed). Furthermore, and in contrast to Shang's results, Podczeck et al. [56] calibrated finite element simulations to $a = 0$ and $c = 0.5$, for doubly convex geometries with $0.06 \leq W/D \leq 0.5$ and $D/R \leq 1.85$, which fail in accord with Fig. 2.1. These results suggest that the elucidations of optimal tensile strength relationships and of optimal procedures to calibrate their parameters are important areas worthy of further research.

Table 2.1: A comparison of existing models according to their optimal coefficients, 90% confidence intervals and residual errors obtained from each figure of merit, for all flat and doubly convex tablets. ($\underline{\circ}$ indicates that $\circ$ is an assumption.)

Models	a	b	c	d	e f g	σ-norm	Q-norm	$Q\sigma$-norm
Pitt's [53]	0.284	0.0126	0.315	0.001	$\underline{1}$ $\underline{1}$ $\underline{1}$	14.96	0.469	2.26
1-parameter [2]	0.14	$\underline{0}$	$\frac{1}{2}-a$	b	$\underline{1}$ - $\underline{1}$	–	0.260	–
1-parameter	0.1717 ±4.9%	$\underline{0}$	$\frac{1}{2}-a$	b	$\underline{1}$ - $\underline{1}$	–	0.236	–
1-parameter	0.1612 ±4.2%	$\underline{0}$	$\frac{1}{2}-a$	b	$\underline{1}$ - $\underline{1}$	8.11	–	–
1-parameter	0.1530 ±4.8%	$\underline{0}$	$\frac{1}{2}-a$	b	$\underline{1}$ - $\underline{1}$	–	–	1.07
4-parameter [2]	0.227	−0.00432	0.117	0.0192	$\underline{1}$ $\underline{1}$ $\underline{1}$	–	0.191	–
4-parameter	0.2256 ±10%	−0.0033 ±60.4%	0.142 ±23.7%	0.0192 ±36.5%	$\underline{1}$ $\underline{1}$ $\underline{1}$	–	0.164	–
4-parameter	0.1224 ±22.9%	0.0079 ±46.2%	0.3267 ±15.1%	−0.0055 ±170.2%	$\underline{1}$ $\underline{1}$ $\underline{1}$	6.22	–	–
4-parameter	0.1625 ±14.7%	0.0027 ±94.6%	0.2595 ±15%	0.0029 ±294.2%	$\underline{1}$ $\underline{1}$ $\underline{1}$	–	–	0.772

There is some controversy over which MCC undergoes elasto-plastic deformation and thus it is invalid to use Eq. (1.5) for this material [48]. We argue that the brittle failure is the key parameter in using the Hertz solution and MCC, or in general compacted granular tablets, break in a brittle-like manner.

In the present work we propose a general framework for determining optimal relationships for tensile strength of doubly convex tablets under diametrical compression. This approach is based on the observation that tensile strength is directly proportional to the breaking force and inversely proportional to a non-linear function of geometric parameters and materials properties. Under proper parametrization, the tensile strength relationship can be determined from experimental results by solving an optimization problem that minimizes a figure of merit of choice. Based on this general framework,

we develop three new optimal tensile strength relationships and three different figures of merit to determine their optimal parameters. We also provide a set of guidelines for assessing the performance of optimal tensile strength relationships, with which we compare the new models with two models previously proposed in the literature (i.e., equations (2.2) and (2.3)). This analysis reveals that two of the new models, namely the general and mechanistic models, are effective and predictive alternatives to the tensile strength relationship currently used in the pharmaceutical industry.

2.2 Material and Methods

In the current study, microcrystalline cellulose MCC (Batch no. 1H59965, Avicel Ph102, FMC biopolymer, Newark, DE) was employed. The true density of the pure MCC was provided by the manufacturer and equal to 1540 kg/m^3 and the original powder has particle sizes between 0.23 μm and 700 μm.

Figure 2.2: Presster, a linear mechanical replicator of any rotary tablet press.

Tablets were manufactured using a 10 mm flat faced B tooling in a linear compaction emulator (The Metropolitan Computing Corporation of East Hanover, NJ) to simulate a Fette 2080 press (Fig. 2.2). A dwell time of 28.88 ms, corresponding to a production speed of 38, 700 tablets per hour, was used. Tablets were stored for two weeks at ambient

room temperature and inside a sealed, clear plastic bag prior to the determination of the breaking force.

The thickness and diameter of the tablets were carefully measured by a digital caliper ($\pm$0.01 mm, Absolute digimatic Caliper), and the mass was recorded by a precision balance ($\pm$0.001 g, Adventurer Ohaus). From these measurements, the volume and bulk density of tablets were caluclated. The relative density of the tablets was determined by the following equation

$$\bar{\rho} = \frac{\rho_b}{\rho_t} \tag{2.4}$$

where ρ_b is the bulk density of the tablet and ρ_t is the true density of the powder. As depicted in Fig. 2.3, the tablets were diametrically compressed using an Instron testing machine (Model 4411, Instron, MA, USA) at a loading rate of 10 mm/min (see Table 2.2 for numerical values). All tablets exhibited failure under pure tensile stress with no significant permanent deformations during diametrical loading—verifying the assumption of brittle fracture.

Figure 2.3: Instron 4411- 5kN tension compression test machine, used for diametrical compression tests. Compression platens are not installed in the figure.

Table 2.2: Characteristics of flat faced tablets and their calculated tensile strength values. Tensile strength values were calculated using Hertz solution Eq. (1.5).

	Actual mass (g)	Thickness (mm)	Actual diameter (mm)	Break force (N)	Tensile strength (MPa)
1	0.2969	2.79	10.04	339.4	7.71
2	0.272	2.55	10.03	323.1	8.04
3	0.2718	2.58	10.05	299.1	7.34
4	0.2706	2.84	10.06	193.1	4.30
5	0.268	3	10.06	136.7	2.88
6	0.2687	3.03	10.08	141.4	2.95
7	0.267	3.42	10.08	84.2	1.55
8	0.2428	3.66	10.1	38.7	0.67
9	0.2416	3.61	10.09	39.3	0.69
10	0.2828	3.03	10.07	189.6	3.96
11	0.2696	3.02	10.06	150.2	3.15
12	0.2701	2.96	10.06	159.6	3.41
13	0.3022	2.8	10.04	372.7	8.44
14	0.2995	2.8	10.04	299.9	6.79
15	0.2999	2.8	10.04	365.6	8.28
16	0.3105	2.82	10.02	472.0	10.63
17	0.3261	2.9	10.02	483.1	10.58
18	0.3249	2.86	10.01	553.4	12.30
19	0.3584	3.17	10.03	588.5	11.78
20	0.357	3.2	10.03	606.2	12.02
21	0.3592	3.15	10.01	610.3	12.32
22	0.3626	3.19	10.02	616.1	12.27
23	0.3661	3.24	10.02	621.0	12.18
24	0.3775	3.28	10.01	645.4	12.51
25	0.3726	3.28	10.02	620.5	12.02
26	0.2716	3.58	10.08	59.2	1.04
27	0.2693	3.56	10.07	78.8	1.40
28	0.2659	3.05	10.06	110.6	2.29

2.3 Results

2.3.1 Optimal Tensile Strength Relationships

The tensile strength σ_t is related to the breaking force F under diametrical compression by the following general equation

$$\sigma_t = \frac{F}{\pi D^2 Q} \tag{2.5}$$

where Q is a non-linear function of geometric parameters and material properties. For example, for flat faced elastic isotropic cylindrical tablets, $Q = t/2D$ when the tablet is under concentrated loads [45] and $Q = t/2D[1-(b/D)^2]^{3/2}$ when the tablet is under loads uniformly distributed on a stripe of width b [57]. Analytical expressions for Q can also be derived under the assumption of radial pressures acting on the tablet (see, e.g., [58] for uniform radial pressure and [59] for parabolic radial pressure) and for flattened cylinders subject to uniform diametrical compression [60]. The function Q may additionally account for the effect of anisotropy [61] and plastic behavior [48], among other material behavior. It may also account for the lack of plane stress conditions, and the size and shape of the tablet, among other geometric characteristics.

For given powder and manufacturing conditions, we firstly presume that the tensile strength σ_t depends on the relative density, $\bar{\rho}$, the size s and shape S of the tablet,

$$\sigma_t := \sigma_t(\bar{\rho}, s, S) \tag{2.6}$$

Basically, there is an inevitable variability in the strength of tablets with same size, shape and relative density distribution. In addition, the relative density distribution depends on the shape of the tablet. These factors will statisitcally condition the spatial distribution and severity of the microscopic and material defects within the region of the tablet subject to the higher stresses where fracture will initiate and propagate from [37].

Here as a first order approximation, we assume that σ_t is a material property that solely depends on the relative density $\bar{\rho}$ of the tablet, for given powder and manufacturing

conditions, as also shown in [44] and [62]. To this end, several assumptions are taken into consideration. First, the spatial distribution of density is assumed to have a second order effect. Second, the size-dependency of tablet strength is not taken into account for flat and doubly convex tablets with very similar diameters. This simplification is based on the observation that the region of the tablet subject to the higher stresses under diametrical compression is centered in the cross section. Third, the variability of tablet strength is assumed negligible, that is the Weibull modulus m of the material (i.e., a reciprocal measure of the strength variability of the brittle material) is assumed to have a very large value and thus the distribution of measured strength to be very narrow [63].

The function $\sigma_t(\bar{\rho})$ can then be readily obtained from an experimental campaign of flat faced cylindrical tablets. We also assume that Q is strictly a geometric function, for given powder properties or manufacturing variables. Based on such assumptions, the function Q can be determined from experimental results by solving the following optimization problem

$$\min_{Q:\mathcal{S}\to\mathbb{R}} \left[\sum_{\{S_i,\bar{\rho}_i\}\in\mathcal{S}\times\mathcal{D}} \left(\sigma_t(\bar{\rho}_i) - \frac{F_i}{\pi\ D_i^2\ Q(S_i)} \right)^2 \right]^{1/2} =: \min_{Q:\mathcal{S}\to\mathbb{R}} \sigma\text{−norm}$$

where $\mathcal{S}$ is the space of all possible tablet shapes that fail in tension under diametrical compression, $\mathcal{D}$ is an interval of tablet relative densities (e.g., from the smallest density at which a solid tablet free of macroscopic defects is formed, to full compaction or relative density of 1.00), and D_i is the diameter of shape S_i along which the breaking force F_i is applied. In the above expression, $\sigma_t(\bar{\rho}_i)$ is obtained from a flat faced cylindrical made with the same powder and under the same manufacturing conditions is employed for making the tablet with shape S_i and relative density $\bar{\rho}_i$. Alternatively, the function Q can be determined by solving any of the following equivalent problems

$$\min_{Q:\mathcal{S}\to\mathbb{R}} \left[\sum_{\{S_i,\bar{\rho}_i\}\in\mathcal{S}\times\mathcal{D}} \left(Q(S_i) - \frac{F_i}{\pi\ D_i^2\ \sigma_t(\bar{\rho}_i)} \right)^2 \right]^{1/2} =: \min_{Q:\mathcal{S}\to\mathbb{R}} Q\text{−norm}$$

$$\min_{Q:\mathcal{S}\to\mathbb{R}} \left[\sum_{\{S_i,\bar{\rho}_i\}\in\mathcal{S}\times\mathcal{D}} \left(Q(S_i)\ \sigma_t(\bar{\rho}_i) - \frac{F_i}{\pi\ D_i^2} \right)^2 \right]^{1/2} =: \min_{Q:\mathcal{S}\to\mathbb{R}} Q\sigma-\text{norm}$$

It bears emphasis that these equivalent optimization problems determine Q by enforcing Eq. (2.5), that is they determine an optimal tensile strength relationship. If there were no experimental uncertainty and second order effects mentioned above were negligible, these three optimization problems behave similarly and have the same solution. However, in reality, experimental uncertainty is unavoidable and the form of Q has to be approximated and parametrized. Thus, our goal is to find the optimal form for Q and the most stable optimization problem to determine its fitting parameters (i.e., for example, the minimization of the Q-norm, the σ-norm, or the $Q\sigma$-norm).

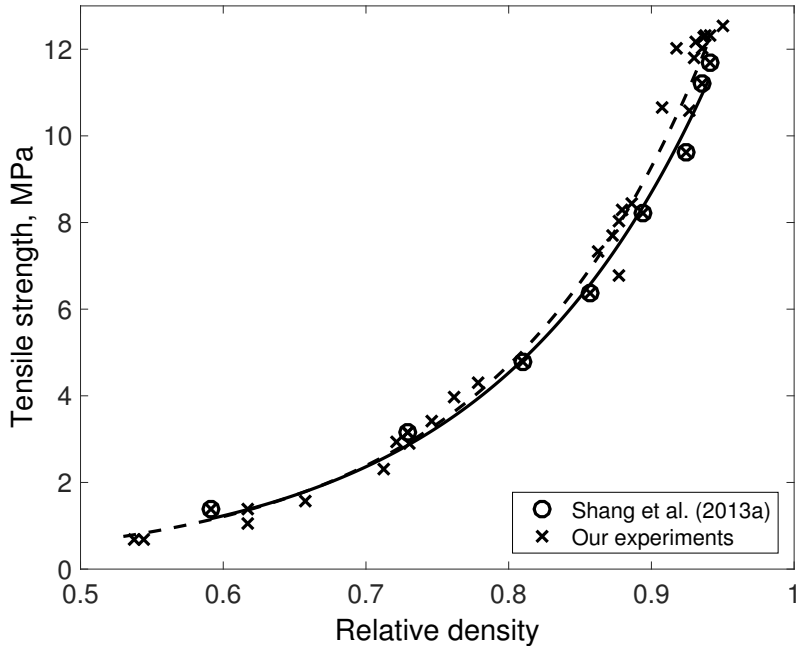

Figure 2.4: Relationship between tensile strength and relative density of flat faced tablets. According to Eq. (2.4), A and B are 24.68 kPa and 6.516 for the full curve and 20.65 kPa and 6.787 for the dashed curve, respectively.

In the interest of applicability, we restrict attention to doubly convex tablets whose shapes can be parametrized by t/D, t/W, W/D as depicted in Fig. 2.1. Specifically, we consider MCC tablets for which Shang et al. [2] have obtained the relationship between tensile strength and relative density using flat faced tablets (see Fig. 2.4 and Table 2.3

for the numerical values extracted from [2]). The experimental data is best fit to an exponential function, that is

$$\sigma_t = A\ \mathrm{e}^{B\bar{\rho}} \tag{2.7}$$

where $A = 24.68$ kPa and $B = 6.516$. Shang and co-workers have additionally reported results for an extensive experimental campaign of doubly convex tablets with various curvatures and of various relative densities. The relative density of each tablet is computed by dividing the tablet density over the material true density, i.e., 1590 kg/m^3 for MCC [55].

Table 2.3: Tensile strength and relative density of flat faced tablets extracted from [2].

Relative density	Tensile strength, MPa
0.5910	1.39
0.7290	3.14
0.8103	4.79
0.8568	6.38
0.8942	8.22
0.9239	9.63
0.9355	11.19
0.9406	11.70

For the sake of simplicity, we assume a form for Q that only captures the leading order term of each geometric parameter, that is

$$Q = a\left(\frac{t}{D}\right)^e + b\left(\frac{t}{W}\right)^f + c\left(\frac{W}{D}\right)^g + d$$

with the constraint that $Q \to t/2D$ as $W \to t$, in order to enforce the correct limit for flat tablets. Thus, the relationship between tensile strength, breaking force, and

geometric parameters, i.e., Eq. (2.5), simplifies to

$$\sigma_t = \frac{F}{\pi D^2 \left[a \left(\frac{t}{D}\right)^e + b \left(\frac{t}{W}\right)^f + c \left(\frac{W}{D}\right)^g + d \right]} \tag{2.8}$$

where the parameters $\{a, b, c, d, e, f, g\}$ are either assumed known or optimally estimated from a set of experimental observations (e.g., Shang's dataset [2]) using different figures of merit (e.g., σ-norm, Q-norm, and $Q\sigma$-norm). If $e = f = g = 1$, the 4-parameter model is recovered, i.e., Eq. (2.2). However, if Pitt's coefficients are used in the 4-parameter model then the correct limit for flat tablets is not attained, indicating that there is a different set of coefficients that further minimizes the problem presented above. Similarly, if $b = 0$, $c = 1/2 - a$ and $e = g = 1$, the 1-parameter model is recovered, i.e., Eq. (2.3). Table 2.1 summarizes the optimal values for the parameters of these two particular forms of Q when determined from the dataset reported in [2] using MATLAB multistart algorithm [64] and each of the three figures of merit. In addition, the 90% confidence bound of each optimal parameter and the residual error obtained from each optimization are reported in the table. It bears emphasis that the optimization is performed under the assumption that a flat faced tablet and doubly curved tablet have the same tensile strength if they have the same relative density.

The minimization of the Q-norm has been used by previous authors and therefore the corresponding fitted parameters are close to those reported in [2]. It is interesting to note that our optimal values for the parameters result in a smaller residual error than that obtained with previously reported values. This may be attributed to the good performance of the multistart algorithm employed or to rounding errors in the values of $\sigma_t(\bar{\rho})$ retrieved from [2]. In the case of the 4-parameter model, the improvement over Pitt's equation is evident. These results also reveal that the 1-parameter model leads to a well-defined stable optimization problem (i.e., error bounds are small and solutions are less sensitive to the figure of merit) and that the 4-parameter model leads to a better physical description of the tensile strength (i.e., the residual errors are systematically smaller than those obtained with the 1-parameter model).

It is important to note that the fidelity and robustness of these optimal tensile strength

relationships can be further improved by: (i) considering a more general, mechanistically informed expression for Q, (ii) extending the size and variety of the experimental dataset, (iii) restricting attention to those tablets which failed under pure tensile stress (see, e.g., [2, 55, 56] for other failure mechanisms). These three aspects are examined next in turn.

General Model

The correct limit of Q for flat tablets, i.e., $Q \to t/2D$ as $W \to t$, can be imposed analytically by writing Eq. (2.8) as follows

$$\sigma_t = \frac{F}{\pi D^2 \left[a \left(\frac{W}{D}\right)^e + b \left(\frac{t}{W}\right)^f + \frac{1}{2}\left(\frac{t}{D}\right) - a \left(\frac{t}{D}\right)^e - b \right]} \tag{2.9}$$

where $\{a, b, e, f\}$ are the fitting parameters. We note that Eq. (2.9), referred to as the *general model*, not only exhibits the correct limit for flat geometries and captures the leading order behavior of Q but it also reduces the dimension of the search space from 7 to 4. Coincidentally, the general model and the 4-parameter model (i.e., any re-calibration of Pitt's equation) have a search space of dimension 4. Therefore, the general model requires a computation effort for the optimization of its parameters similar to that of previous models but it allows for a better physical description of the tensile strength. Moreover, by imposing $e = f = 1$ on Eq. (2.9)—or the correct limit on Eq. (2.2)—a new *2-parameter model* is recovered

$$\sigma_t = \frac{F}{\pi D^2 \left[a \left(\frac{t}{D}\right) + b \left(\frac{t}{W}\right) + \left(\frac{1}{2} - a\right) \frac{W}{D} - b \right]} \tag{2.10}$$

where $\{a, b\}$ are the fitting parameters.

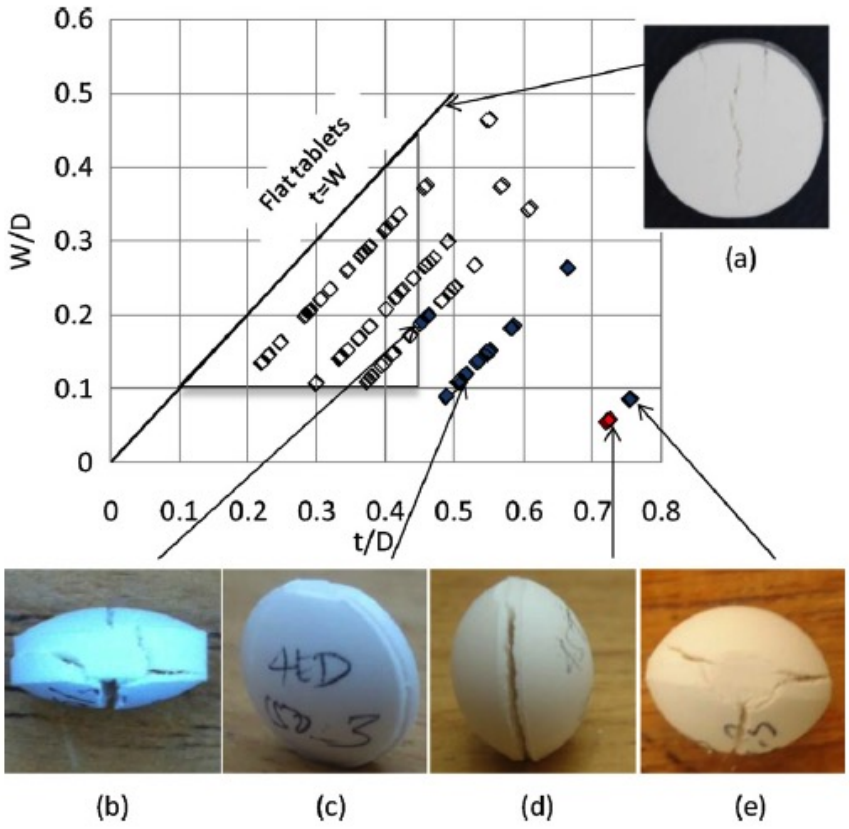

Figure 2.5: Failure modes of doubly convex MCC tablets [2].

In order to assess the behavior of the proposed models, we restrict attention to those tablets with diameter $D = 10.318$ mm reported in [2], which exhibited crack formation and propagation under pure tensile stress. Fig. 2.5 illustrates the change in the failure mode under diametrical load as the radius of curvature incerases in the doubly convex tablets. Specifically, we excluded ball ($D/R = 1.842$), extra deep ($D/R = 1.374$) and some deep tablets ($D/R = 0.988$) having $W/D \approx 0.2$ and $t/D \approx 0.45$.

The optimal values for the parameters of the 1-parameter (2.3), 2-parameter (4.5), 4-parameter (2.2), and general (2.9) models are reported in Table 2.4. Confidence bounds and residual errors are also reported in the table.

Table 2.4: A comparison between all models according to their optimal coefficients, 90% confidence intervals and residual errors obtained from each figure of merit, for only those flat and doubly convex tablets that failed under pure tensile stress. ($\underline{\circ}$ indicates that $\circ$ is an assumption.)

Models	a	b	c	d	e	f	g	σ-norm	Q-norm	Qσ-norm
Pitt's [53]	0.284	0.0126	0.315	0.001	$\underline{1}$	$\underline{1}$	$\underline{1}$	13.3	0.43	2.13
1-parameter	0.1316 ±10.1%	$\underline{0}$	$\frac{1}{2}-a$	b	$\underline{1}$	-	$\underline{1}$	–	0.196	–
1-parameter	0.1236 ±7.5%	$\underline{0}$	$\frac{1}{2}-a$	b	$\underline{1}$	-	$\underline{1}$	6.43	–	–
1-parameter	0.1016 ±9.5%	$\underline{0}$	$\frac{1}{2}-a$	b	$\underline{1}$	-	$\underline{1}$	–	–	0.739
2-parameter	−0.0202 ±164.7%	0.0285 ±20.7%	$\frac{1}{2}-a$	$-b$	$\underline{1}$	$\underline{1}$	$\underline{1}$	–	0.16	–
2-parameter	−0.0538 ±51.3%	0.0278 ±16%	$\frac{1}{2}-a$	$-b$	$\underline{1}$	$\underline{1}$	$\underline{1}$	4.71	–	–
2-parameter	−0.0550 ±50.1%	0.0278 ±16.9%	$\frac{1}{2}-a$	$-b$	$\underline{1}$	$\underline{1}$	$\underline{1}$	–	–	0.568
4-parameter	0.1406 ±35%	0.0077 ±107.7%	0.2626 ±28.8%	−0.0037 ±430.5%	$\underline{1}$	$\underline{1}$	$\underline{1}$	–	0.139	–
4-parameter	−0.0382 ±114.8%	0.0296 ±24.9%	0.5615 ±13.3%	−0.0390 ±37.2%	$\underline{1}$	$\underline{1}$	$\underline{1}$	4.5	–	–
4-parameter	−0.0132 ±328.5%	0.0262 ±29.5%	0.5193 ±14%	−0.0332 ±46.5%	$\underline{1}$	$\underline{1}$	$\underline{1}$	–	–	0.539
general	0.3231 ±10.9%	0.0240 ±36%	a	$\frac{1}{2}\frac{t}{D}-b$	1.6963 ±12%	−263.5 ±∞%	e	–	0.146	–
general	0.0484 ±267.6%	0.8688 ±83%	a	$\frac{1}{2}\frac{t}{D}-b$	−0.8553 ±82.7%	−0.3147 ±43.4%	e	3.85	–	–
general	0.7289 ±689.1%	2.3185 ±409%	a	$\frac{1}{2}\frac{t}{D}-b$	−0.3151 ±283.8%	−0.2156 ±209.9%	e	–	–	0.463

The residual errors for 1-parameter and 4-parameter models are noticeably reduced in comparison to Table 2.1, confirming that those tablets that did not fail under tensile stress should not be included and treated as the rest of the tablets. Furthermore, it is evident from the table that the 2-parameter outperforms the 1-parameter model,

suggesting that t/W is required in the expression for Q—though perhaps to a power f different from 1. Finally, the 4-parameter and the general models have very similar residual errors for all three figures of merit and, in particular, the 4-parameter model exhibits a better performance for the Q-norm.

This last observation provides additional insight into the role of flat faced tablets in the optimization process. The 4-parameter model does not have the correct limiting behavior for flat faced tablets. However, only 5.7% are flat faced tablets in the dataset and thus their contribution to the overall residual error is negligible. In other words, the optimization process reduces the error for doubly convex tablets in detriment to the predictability of the model for shallow/flat tablets. Specifically, the 4-parameter model exhibits, in average, a 65% larger error for flat faced tablets and a 5% smaller error for curved tablets than the general model. The inclusion of more flat tablets in the dataset may, however, have the opposite effect. We further study this issue in the next subsection.

Role of Flat Faced Tablets in the Optimization Process

We extended the experimental dataset in [2] with a new series of tests on flat faced tablets. Specifically, 28 flat tablets of pure MCC were manufactured according to the description explained in Section 2.2. The new fitting parameters to the exponential function (2.4) are $A = 20.65$ kPa and $B = 6.787$, as depicted in Fig. 2.4. We specifically tested few tablets with relatively low and high relative densities to capture a wider range. Even though, the manufacturing conditions were different, the two fitting exponential curves are very close to each other. Thus, combining the data points is acceptable for the purpose of this study.

Table 2.5 shows the optimal values for the parameters of the 1-parameter (2.3), 2-parameter (4.5), 4-parameter (2.2), and general (2.9) models when calibrated with the extended experimental campaign. Flat faced tablets now represent 21.3% of the total number of tablets (cf. 5.7% in the previous section). In contrast to results in Table 2.4, the general model exhibits smaller residual errors than those of the 4-parameter model for all the figures of merit. This result confirms that, by including more flat faced

tablets in the dataset, the limiting behavior of the 4-parameter model is improved only in detriment of its overall behavior. Specifically, the 4-parameter model now exhibits, in average, a 1% smaller error for flat faced tablets and a 17% larger error for curved tablets than the general model. The general model, however, automatically exhibits the correct limit, rendering the unnecessary need of a large number of experiments for flat geometries. The cost- and time-effectiveness of using the general model is evident. It bears emphasis that experimental errors and uncertainty in the functionality of the geometric function Q render the problem ill-posed (i.e., the solution is not unique, sensitive to errors, and dependent on the norm which is minimized). Experimental errors cannot be eliminated but one can minimize the figure of merit that provides more stability to the optimization process. According to our case study, this is the case of the $\sigma-$norm and thus the optimization problem reduces to

$$\min_{a,b,e,f} \left[\sum_{i \in \mathcal{P}} \left(\sigma_t(\bar{\rho}_i) - \frac{F_i}{\pi \ D_i^2 \ \left[a \left(\frac{W_i}{D_i} \right)^e + b \left(\frac{t_i/D_i}{W_i/D_i} \right)^f + \frac{1}{2} \left(\frac{t_i}{D_i} \right) - a \left(\frac{t_i}{D_i} \right)^e - b \right]} \right)^2 \right]^{1/2}$$

where $\mathcal{P}$ is a set of experimental points and $\sigma_t(\bar{\rho}_i)$ is obtained from a small number of flat faced tablets.

Mechanistic Interpretation

A major source of uncertainty is the fact that the functionality of Q is unknown in general. However, further insight can be gained by recasting the problem in terms of an effective cross-sectional surface area, $\bar{A}$, associated with strength, that is

$$\sigma_t = \frac{2F}{\pi \bar{A}} \tag{2.11}$$

where $\bar{A} = tD$ for flat-faced tablets (cf. Eq. (1.5)). For doubly convex tablets, we parametrize $\bar{A}$ by an effective thickness $\bar{t}$ (see Fig. 2.1) as follows

$$\bar{A} = D^2 \left[2 \left(\frac{\bar{t}}{D} - \frac{W}{D} \right) \left[\frac{1}{3} + \frac{1}{15} \left(\frac{\bar{t}}{D} - \frac{W}{D} \right)^2 \right] + \frac{W}{D} \right] + \mathcal{O}\left(\frac{(\bar{t} - W)^5}{D^3} \right) \tag{2.12}$$

Table 2.5: Recalibration of optimal coefficients, 90% confidence interval and residual errors for flat and doubly convex tablets that failed under pure tensile stress, using a larger group of flat faced tablets in the optimization process. ($\underline{\circ}$ indicates that $\circ$ is an assumption.)

Models	a	b	c	d	e	f	g	σ-norm	Q-norm	Qσ-norm
1-parameter	0.1145 ±12.4%	$\underline{0}$	$\frac{1}{2}-a$	b	$\underline{1}$	-	$\underline{1}$	–	0.229	–
1-parameter	0.0949 ±11%	$\underline{0}$	$\frac{1}{2}-a$	b	$\underline{1}$	-	$\underline{1}$	8.95	–	
1-parameter	0.0654 ±17.7%	$\underline{0}$	$\frac{1}{2}-a$	b	$\underline{1}$	-	$\underline{1}$	–	–	1.025
2-parameter	−0.0380 ±99%	0.0287 ±23.3%	$\frac{1}{2}-a$	$-b$	$\underline{1}$	$\underline{1}$	$\underline{1}$	–	0.200	–
2-parameter	−0.1117 ±29.4%	0.0321 ±16.6%	$\frac{1}{2}-a$	$-b$	$\underline{1}$	$\underline{1}$	$\underline{1}$	6.90	–	–
2-parameter	−0.1205 ±29.1%	0.0330 ±18.2%	$\frac{1}{2}-a$	$-b$	$\underline{1}$	$\underline{1}$	$\underline{1}$	–	–	0.838
4-parameter	0.0442 ±109%	0.0198 ±46.6%	0.4183 ±18.1%	−0.0185 ±99.5%	$\underline{1}$	$\underline{1}$	$\underline{1}$	–	0.187	–
4-parameter	−0.1187 ±31.2%	0.0415 ±15.7%	0.6975 ±7.9%	−0.0655 ±18.8%	$\underline{1}$	$\underline{1}$	$\underline{1}$	6.26	–	–
4-parameter	−0.1316 ±29.2%	0.0444 ±16.6%	0.7211 ±8%	−0.0720 ±20.8%	$\underline{1}$	$\underline{1}$	$\underline{1}$	–	–	0.776
general	3.0992 ±1313%	3.9923 ±972.5%	a	$\frac{1}{2}\frac{t}{D}-b$	−0.1640 ±593.1%	−0.2006 ±508.3	e	–	0.178	–
general	0.0342 ±278.9%	0.6553 ±76.4%	a	$\frac{1}{2}\frac{t}{D}-b$	−0.9648 ±82%	−0.436 ±41.1	e	5.54	–	–
general	0.1344 ±517.8%	0.8150 ±199.8%	a	$\frac{1}{2}\frac{t}{D}-b$	−0.6065 ±182.4%	−0.4411 ±186.3	e	–	–	0.687

This parametrization is made only in the interest of simplicity. However, a geometric interpretation of the above equation suggests that $\bar{t}/D$ may be a function of D/R, which we postulate to be

$$\frac{\bar{t}}{D} = \frac{W}{D} + \alpha \left(\frac{D}{R}\right)^{\beta} \left(\frac{t}{D} - \frac{W}{D}\right)$$

where $\alpha > 0$ and $\beta \geq 0$ are fitting parameters. As a result, a new relationship between geometric parameters, breaking force, and tensile strength is obtained, i.e.,

$$\sigma_t = \frac{2F}{\pi D^2 \left[2\alpha \left(\frac{D}{R}\right)^{\beta} \left(\frac{t}{D} - \frac{W}{D}\right) \left[\frac{1}{3} + \frac{\alpha^2}{15} \left(\frac{D}{R}\right)^{2\beta} \left(\frac{t}{D} - \frac{W}{D}\right)^2\right] + \frac{W}{D}\right]} \tag{2.13}$$

which is referred to as the *mechanistic model*. It is interesting to note that the mechanistic model has a substantially different functionality compared to the one of the general model (2.9). In the case of $\bar{t} = (t + W)/2$, however, the 1-parameter model is approximately recovered with $a = 1/6$, which is very close to the optimal value obtained in our case study (see Table 2.1). Thus, a more clear connection between the mechanistic model and the general model is desirable, which is beyond the scope of this work.

Table 2.6: Mechanistic model optimal coefficients, 90% confidence bound and residual errors from each figure of merit, for those tablets in the extended dataset that failed under pure tensile stress.

Model	α	β	σ-norm	Q-norm	Qσ-norm
mechanistic	0.5817	3.9736	–	0.172	–
	±8.6%	±25.5%			
mechanistic	0.5562	3.9877	5.97	–	–
	±9.4%	±15.4%			
mechanistic	0.5377	5.0030	–	–	0.699
	±9.4%	±18.3%			

The optimal values for α and β, determined from the extended dataset with four different shapes of tablets (Section 2.3.1) using each of the three figures of merit, are presented in Table 2.6. The residual errors are comparable to those of the general model and the stability is remarkable, as shown by the tight confidence bounds. The optimal values are clearly insensitive to the figure of merit. In addition, the search space of the mechanistic model is of dimension 2 whereas the one of the general model is of dimension 4. Fig. 2.6 compares the predictability between the four models discussed in this study. The error distributioin plot for each model is presented in Fig. 2.7. The

mechanistic model has the largest number of small errors compared to the other models. Thus, the mechanistic model is preferable both in terms of efficacy and efficiency.

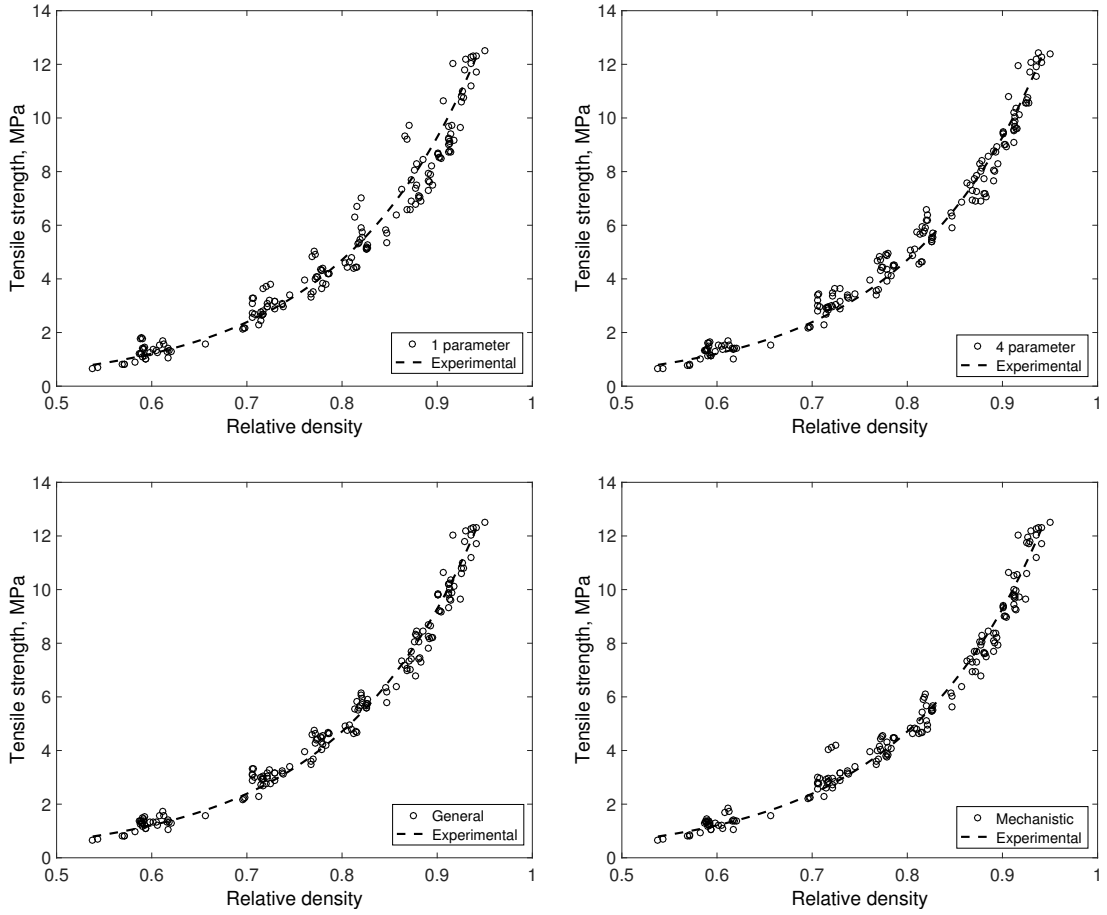

Figure 2.6: The relationship between tensile strength and relative density of the experimental data using $\sigma-$norm.

2.4 Summary and Conclusion

We have proposed a general framework for determining optimal relationships for tensile strength of doubly convex tablets under diametrical compression. The approach is based on the observation that tensile strength is directly proportional to the breaking force and inversely proportional to Q, a non-linear function of geometric parameters and materials properties. This generalization reduces to the analytical expression commonly used for flat faced tablets, i.e., Hertz solution, for $Q = t/2D$. Here, we have assumed that Q is solely a function of geometric parameters that, for doubly convex tablets, reduces to

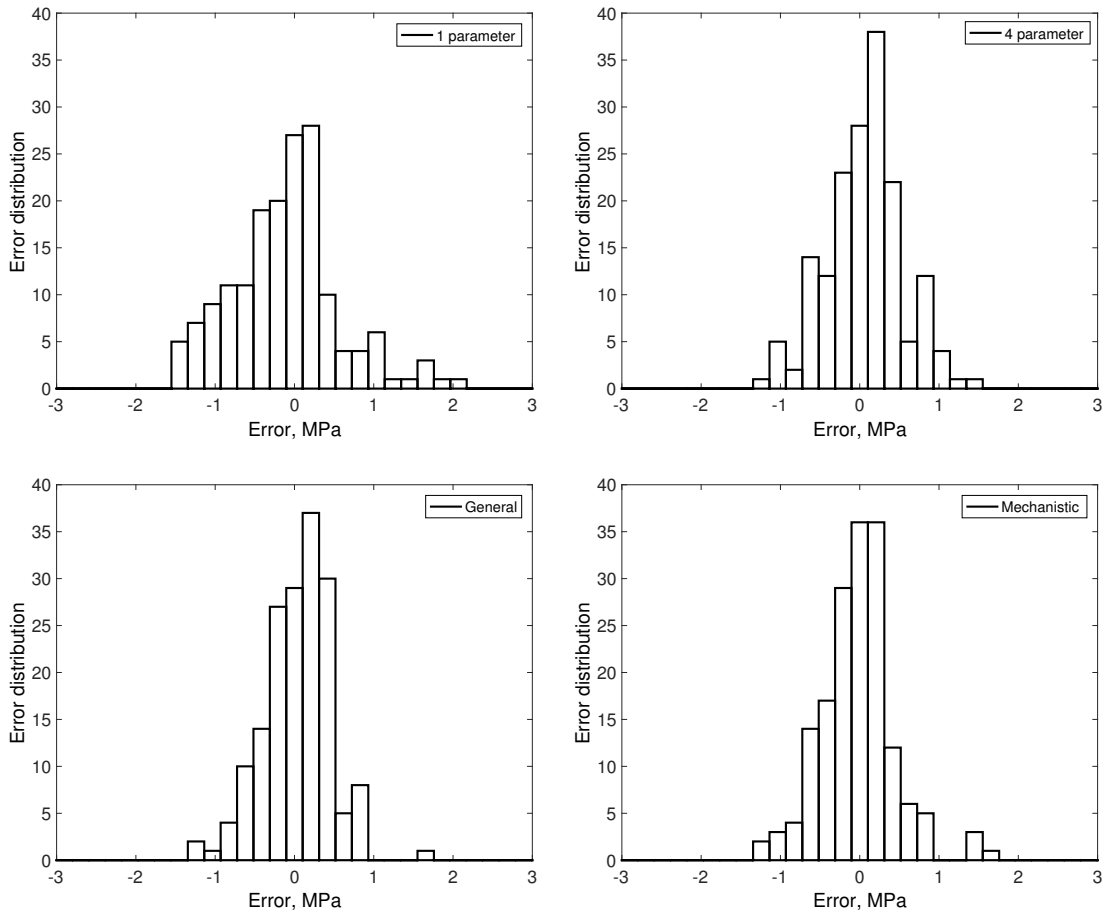

Figure 2.7: Error distribution plots for 1-parameter, 4-parameter, general, and mechanistic models.

t/D and W/D, and a combination thereof. Based on such assumptions, the function Q can be determined from experimental results by solving an optimization problem that minimizes a figure of merit of choice. We have postulated that this figure of merit has to be based on the assumption that a flat faced tablet and doubly curved tablet have the same tensile strength if they have the same relative density and are made of the same powder, under equivalent manufacturing conditions.

We have specifically investigated three different figures of merit, which we referred to as σ-norm, Q-norm and $Q\sigma$-norm, and we have proposed three new optimal tensile strength relationships, which we referred to as *general model*, *2-parameter model* and *mechanistic model*. The general model captures the leading order behavior of Q on the geometric parameters, it has the exact limiting behavior for flat faced tablets, and it

has four optimal parameters to be determined. The 2-parameter model simplifies the general model by assuming that Q is linear on the geometric parameters, and thus the number of parameters is reduced to two while the correct limiting behavior is retained. The mechanistic model is based on an effective cross-sectional surface area associated with strength (i.e., in contrast to previous models, it has a well-defined mechanistic interpretation), it exhibits the exact limiting behavior for flat geometries, and it only has two optimal parameters.

Here, we present guidelines for assessing the performance of optimal tensile strength relationships. Under this framework, other expressions for the non-linear function Q can be explored and the assumption that Q only depends on geometric parameters can even be relaxed. Similarly, figures of merit other than those studied here (i.e., σ-norm, Q-norm and $Q\sigma$-norm) can be examined. It bears emphasis that, regardless of the choice of Q and the optimization procedure, the performance of a new model can be assessed following the same procedure presented here. A desirable model needs to have a small number of optimal parameters to make it less computationally expensive. It has to have the correct analytical limiting behavior for flat tablets (i.e., Hertz solution), so that the tensile strength can be obtained from a small number of flat faced tablets. It has to be predictive, i.e., the optimization has to result in a narrow and symmetric distribution of errors around zero, for a given figure of merit. This figure of merit in turn has to render the optimization problem stable, i.e., it has to provide optimal parameters with tight confidence bounds.

Table 2.7: A systematic comparison of the proposed and existing models based on four different performance criteria.

Model	Equation	Number of Parameters	Limiting Behavior	Stability (1:best–5:worst)	Predictability (1:best–5:worst)
1-parameter	(2.3)	1	✓	1(σ-norm)	5
2-parameter	(4.5)	2	✓	3 (σ, Qσ-norm)	4
4-parameter	(2.2)	4	×	4 (σ, Qσ-norm)	3
general	(2.9)	4	✓	5 (σ-norm)	1
mechanistic	(2.13)	2	✓	2 (σ-norm)	2

We have assessed the performance of the proposed new models together with two models previously proposed in the literature, i.e., Shang's model (a 1-parameter model introduced in [2]) and a 4-parameter model (based on the model introduced by Pitt et al. [52] which is widely used in the pharmaceutical industry [35]), as shown in Table 2.7. It shows that the general model and the mechanistic model are more predictive than previously proposed tensile strength relationships. Both models automatically exhibit the correct limit for flat geometries, thus only a small number of flat faced tablets has to be tested in order to accurately capture the strength-relative density relationship. Our analysis also indicates that the mechanistic model is the most stable among the predictive models. This is in sharp contrast to the 4-parameter model, i.e., a re-calibration of Pitt's equation, that leads to an unstable optimization problem which, in addition, requires a large number of flat faced tablets in order to remain predictive in the limit of shallow/flat tablets.

It is interesting to note that stability and predictability are generally inversely correlated, with a Spearman's rank correlation coefficient, of -0.7 for the five models studied in this work. Spearman's rank correlation coefficient measures the monotonic relationship between two variables. However, the mechanistic model exhibits the opposite behavior, i.e., it is highly stable and predictive. The predictability characteristic of the mechanistic model is a consequence of a simple mechanical concept which mathematically turned out more complicated. Moreover, the stability characteristic is due to the small number of fitting parameters in this model.

It bears emphasis that experimental errors and uncertainty in the functionality of the geometric function Q may render the problem ill-posed. Therefore, these guidelines have to be followed with caution to resolve ambiguities in the results.

These observations suggest that both general and mechanistic models are cost- and time-effective, predictive alternatives to the tensile strength relationship currently used in the pharmaceutical industry. Furthermore, our analysis showcases the benefits of adopting a general framework for developing and evaluating the performance of optimal relationships for tensile strength of doubly convex tablets under diametrical compression.

We close by pointing out some limitations of our analysis and possible avenues for extensions of the general framework.

First, it is clear that the proposed parametric approximations for Q are not the only non-linear functions of geometric parameters that exhibit the correct limit for flat faced tablets. In addition, tensile strength of flat faced tablets may not be optimally described by an exponential function of the relative density. It is also possible that the function Q has to depend on powder properties or manufacturing variables in some cases of industrial relevance. The systematic investigation of functions Q of the type proposed here, the elucidation of their properties and the determination of the best optimal relationships in each area of application, are worthwhile directions of future research.

Second, our general framework relies on the assumption that, for given powder and manufacturing conditions, a flat faced tablet and doubly curved tablet have the same tensile strength if they have the same relative density. This is indeed a good first order approximation for the case study presented here (i.e., pure microcrystalline cellulose pressed at low compaction speeds). There are experimental techniques that can assess the density distribution of a tablet such as gamma-ray attenuation, x-ray micro computed tomography, or solid-state nuclear magnetic resonance. However, there is a lack of experimental technique that can test directly the point-to-point strength of the material. Most techniques perform indirect measurements of effective properties, with the exception of a beam-bending test that suffers from the difficulty of requiring ad-hoc geometries for the specimen. Thus, particle mechanics simulations capable of describing strength formation and evolution during the compaction process are desirable [65, 66, 67], but are beyond the scope of this work.

Chapter 3

Toward Predicting Tensile Strength of Pharmaceutical Tablets by Ultrasound Measurement in Continuous Manufacturing

3.1 Introduction

3.1.1 Batch vs. Continuous Manufacturing

Batch manufacturing consists of multiple discrete steps, which typically involves "hold times" between steps. On the other hand, in continuous manufacturing (CM) the material is processed in one step and sent directly and continuously to the next one [68]. There are many advantages to CM, including: (i) integrated processing with fewer steps, which results in minimal manual handling and increased safety; (ii) smaller facilities (i.e., reduced cost); and (iii) on-line monitoring and control for enhanced product quality assurance in real-time [69]. Many industries, such as petrochemical, household goods, and food technologies, have shifted to CM. In the pharmaceutical industry, CM has been introduced [68], but products are still manufactured mainly in batches due to heavy regulations. The major barriers to CM are replacing old equipment with new technology, which requires extensive training and employing reliable sensors for quality assurance and control [70].

In an attempt to explore and address the manufacturing issues in the pharmaceutical industry, the U.S. Food and Drug Administration (FDA) has released the Process Analytical Technology (PAT) initiative [71]. Designing and developing rapid techniques and ultimately improving the quality of pharmaceutical products are the goals of the PAT initiative. Quality by Design (QbD) initiative is a more recent attempt [72] to have a

better control on the critical quality attributes (CQAs) by understanding and exploring the effects of critical material attributes (CMAs) or/and critical process parameters (CPPs) [73]. Real time release testing (RTRT) is another terminology defined as "the ability to evaluate and ensure the quality of in-process and/or final product based on process data, typically include a valid combination of measured material attributes and process controls" [74]. All these initiatives gear toward measuring techniques to be rapid, robust, and preferably non-invasive. Just recently, FDA has approved two continuously manufactured products [75].

Many researchers have explored and studied utilizing non-destructive techniques (e.g., Near Infrared (NIR) spectroscopy [76], NIR chemical imaging [77], Raman spectroscopy [78], ultrasound and photoacoustic measurements [79, 80], and terahertz pulsed imaging [81, 82, 83]) to predict or measure CQAs.

As discussed in the previous chapter, the mechanical strength of tablets is typically measured by traditional destructive tests. The time spent to test the tablets destructively is in the order of minutes, which is not suitable for an on-line monitoring process. Perhaps, the biggest drawback of these destructive tests is that they damage the tablet structure and cause loss of product, not allowing measurement of final attribute - tablet dissolution, which is also destructive. Moreover, they also provide limited information about the mechanical state of a tablet. In recent past, ultrasound (US) testing has been introduced as a fast, non-invasive technique to measure tablet strength [80, 84, 85]. In the following section the fundamentals of ultrasonics are provided.

3.1.2 Principle of Ultrasonics

Ultrasound is sound waves pitched above human range with frequencies beyond 20 kHz. Sound waves are transmitted through any substance, solid, liquid, or gas having elastic properties [86] and travel through the material by vibrating the molecules. Based on the motion pattern, ultrasound waves are classified into four groups: longitudinal/compressional, transverse/shear, surface/Rayleigh, and plate/Lamb waves [87]. In ultrasound testing, longitudinal and shear waves are the two modes of propagation most widely used. The direction of particle motion is the same as the wave traveling

through the medium in longitudinal wave, whereas in shear wave the particle motion is perpendicular to the direction of propogation, shown in Fig. 3.1.

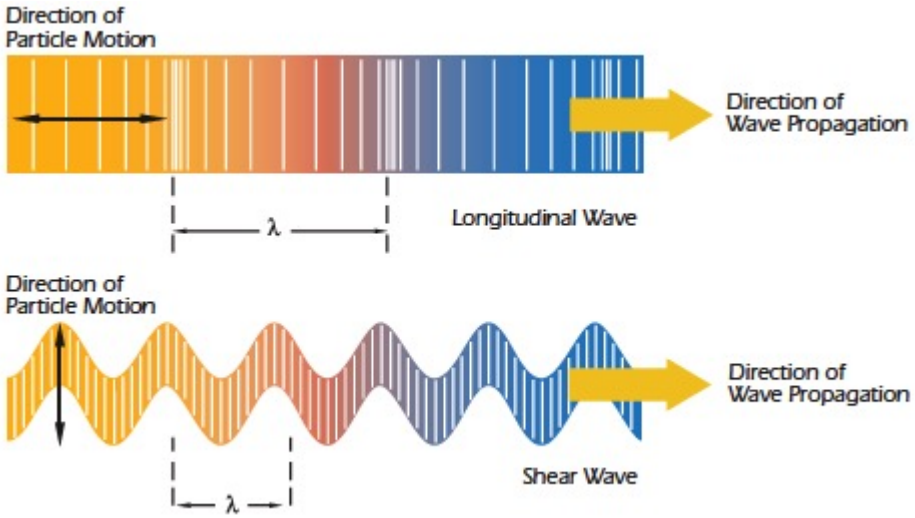

Figure 3.1: Particle motion vs. the direction of ultrasound wave propogation [3].

An ultrasonic wave displaces the particles of a medium from their equilibrium positions and as a result elastic restoring forces arise. Inertial and elastic restoring forces between the particles lead to the oscillatory motions of the medium [88].

There are two modes of ultrasound setup: pulse-echo (PE) and through-tranmission (TT). In PE, the sound wave is sent and received with the same transducer. In TT setup, two transducers are used and placed on two opposite sides of the sample, one tranmitting and the other receiving.

3.1.3 Ultrasonics in Pharmaceutics

US testing has been introduced as a non-invasive technique to gain information about the microstructure and mechanical state of tablets (e.g., capping tendency) [89, 80, 84, 85, 90, 91]. Amongst its other applications, we focus on the measurement of the elastic properties of tablets. This requires measuring time of flight (TOF) of a low intensity mechanical wave propagating in a medium. Elastic modulus, E, can be extracted by measuring the longitudinal speed of sound (SOS) of this transmitted US signal for a known sample size [80]. Hakulinen et al. [92] have observed that SOS decreases as the porosity of the tablet increases. In addition, the SOS in a tablet was found to increase

with its tensile strength [93, 85]. The ease of implementation, fast computing time, and low cost of this method make it possible to be placed on-line for real-time mechanical characterization of tablets.

Akseli et al. [94] evaluated the potential of a real-time acoustic technique as an on-line compaction monitoring tool. Good correlation between elastic properties, determined using US, and compaction profiles was observed. Leskinen et al. [84] introduced an in-die US measurement system by incorporating US transducers inside the upper and lower punches. US attenuation was found to be a good approach to detect defective tablets. In a later study, they measured the SOS in binary mixtures (i.e., mixtures of an active ingredient with an excipient) during tableting using the same system. They found that SOS is sensitive to the mixing time of magnesium stearate and the dwell time of the compaction cycle [95]. The in-die real-time tablet monitoring system has also been used by Liu et al. [96] to determine the thickness and integrity of the coating layer of dry-coated tablets and by Stephens et al. [97] to evaluate the tablet mechanical integrity and the presence of defects, and validate its applicability as a control system. Although the in-die measurement provides valuable information, the mechanical strength of a tablet is different if measured out-of-die. After compaction and in-die unloading the tablet experiences ejection forces, as well as radial and axial elastic relaxation, which might siginificantly affect the mechanical integrity of the tablet [12, 98, 99]. Only recently, Akseli et al. [100] presented a novel methodology to predict the breaking force and disintegration time of pharmaceutical tablets using US and machine learning tools.

In this study, we focused on evaluating the mechanical integrity of tablets after compaction via US testing. Cylindrical tablets were prepared either continuously or in batch. The formulation was kept constant (90% lactose monohydrate, 9% acetaminophen (APAP), and 1% MgSt), while the compaction force and level of shear strain varied. US testing was used to evaluate the strength of tablets by measuring the TOF. The tensile strength of the same tablets was then determined using a mechanical hardness tester. It was observed that, as the blend was exposed to an increasing level of total shear strain, the speed of sound decreased and the tablets became both softer and mechanically

weaker. It is also noticed that in order to predict the hardness of a tablet, two properties should be taken into account: elastic modulus and relative density. A strategy for tensile strength prediction is proposed that uses the existing theoretical/semi-empirical models for elastic modulus and tensile strength of porous materials. Overall, US testing is found to be a reliable technique to predict the variation of tablet strength with processing conditions.

3.2 Materials and Methods

3.2.1 Materials

α-Lactose (monohydrate N.F., crystalline, 310, Regular, Foremost Farms USA, Rothschild, Wisconsin, USA), acetaminophen (semi-fine, USP/paracetamol PhEur, Mallinckrodt, Raleigh, North Carolina, USA), and magnesium stearate N.F. (non-Bovine, Tyco Healthcare/Mallinckrodt, St. Louis, Missouri, USA) were used as purchased. A formulation containing 90% lactose, 9% acetaminophen (APAP), and 1% magnesium stearate (MgSt) was prepared on a weight basis and kept constant in both batch and continuous production.

The true density was measured with five parallel measurements with a pycnometer (AccuPyc 1340, Micromeritics) using helium as the measuring gas, shown in Fig. 3.2. The nominal particle sizes reported by the manufacturer and the measured true densities of the powders are listed in Table 3.1.

Table 3.1: Blend constituents, nominal mean particle size, and true density.

Material	Mean particle size (μm)	True density (g/cm^3)
Lactose	180	1.56
Acetaminophen (APAP)	45	1.30
Magnesium Stearate	10	1.04

Figure 3.2: Accupyc II 1340 Pycnometer, which uses the gas displacement method to measure volume/density accurately.

3.2.2 Continuous Manufacturing

The pilot plant employed for continuous direction compaction is situated at the Engineering Research Center for Structured Organic Particulate Systems (ERC-SOPS), Rutgers University (Fig. 3.3). A detailed description of this plant can be found in [101]. There are four main unit operations when tablets are produced by direct powder compression: feeding, delumping, blending, and compacting. We will present a brief overview of each of these operations next.

Feeding and delumping: First, gravimetric feeders from Coperion-KTron (Sewell, NJ), KT20 for APAP and KT35 for lactose were used for feeding. The powders were separately fed into a Quadro S197 Comil, which was used to delump the powders. MgSt was added using an MT12 feeder after the mill to prevent overlubrication of the formulation.

Blending: The blend was then sent to a continuous blender (Glatt GCG-70) with a speed set at 200 rpm. The blade configuration is described in [102, 4]. Chemical composition of the powder was monitored using a Bruker Matrix near-infrared (NIR) spectrometer.

Compaction: The desired formulation was sent through a hopper into the fill-o-matic with a speed set at 25 rpm. Finally, the blend was compressed using a 36-station Kikusui Libra-2 double layer tablet press with a 10 mm tooling at a compaction speed

of 20 rpm.

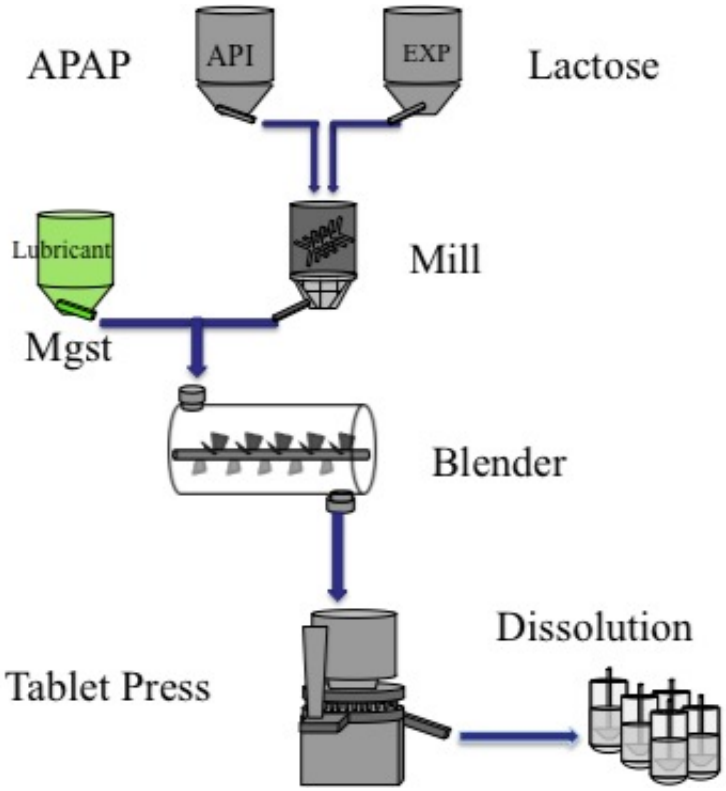

Figure 3.3: Continuous direct compaction manufacturing line [4].

The overall flow rate and the tablet mass were set to 20 kg/h and 350 mg, respectively. The tablets made in the continuous line will be referred to as *continuous* tablets. The compaction force (F_c) was varied during the run by changing the distance between punches. Since the individual F_c values are not recorded for each tablet, we categorize the tablets based on their nominal compaction force values (F_n). Tablets were collected after all the processing parameters reached steady state. 6 different F_n settings were selected ranging from 8 to 28 kN. 12 tablets for each of 8, 20, and 28 kN and 18 tablets for each of 12, 16, and 24 kN F_n conditions were analyzed.

3.2.3 Batch Production

Blend Preparation

Two different powder mixing equipments were used in the batch production of tablets: a V-blender (Patterson-Kelley Co., East Stroudsburg, PA) and a laboratory scale resonant acoustic mixer (labRAM) (Resodyn Acoustic Mixers, Butte, Montana, USA).

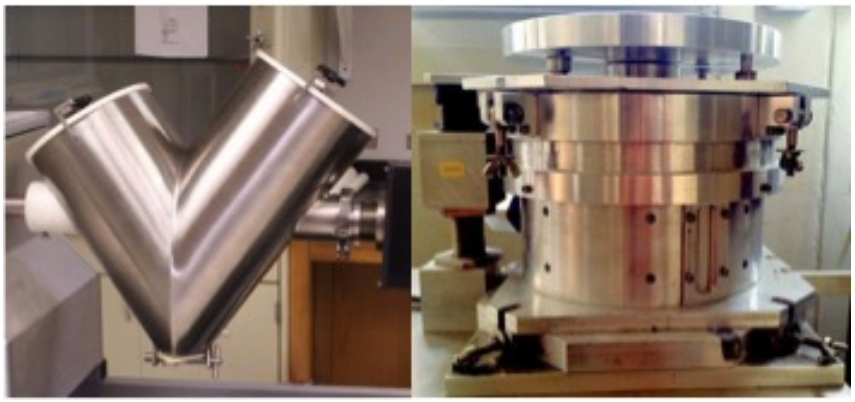

Figure 3.4: V-blender, a tumbling mixer and shearing device used to impart uniform shear to the blend.

In the V-blender mixer, a 15-minute pre-blending step was applied at a rotation rate of 15 rpm to reduce the stickiness of APAP and improve its flowability. MgSt was added and mixed with the blend for 2 additional minutes. The blended powder was then unloaded from the V-blender and subjected to a controlled shear environment in a modified Couette cell at a shear rate of 80 rpm (Fig. 3.4). For additional information about this instrument, the reader is referred to [103, 104]. Three different shear strain environments were selected in this study: 0, 160 and 640 revolutions, corresponding to 0, 2, and 8 minutes in the shear device. As we increase the number of revolutions in the shear cell, the degree of MgSt coverage on the particles increases. The effect of lubricant on powder properties is highlighted in more detail in the following chapter. The tablets made using this mixing method will be named according to the strain level experienced by the blend in the shear cell i.e., 0 *rev*, 160 *rev*, and 640 *rev* tablets.

Figure 3.5: Laboratory scale resonant acoustic mixer (LabRAM).

The low frequency and high intensity acoustic field in labRAM facilitate the movement of the loose powder mass to induce mixing. In the labRAM mixer (Fig. 3.5), 80% fill level was selected. Lactose and APAP were first blended for 2 minutes at an acceleration of 40 g, followed by the lubrication stage, where MgSt was added and the blend was mixed for an additional 1 minute at an acceleration of 60 g. These tablets will be referred to as *labRAM* tablets.

Tablet Compaction

The blends were compacted using a Presster tablet press simulator equipped with a 10 mm flat-face, B-type tooling. A Kikusui Libra-2 tablet press was emulated at a press speed of 20 rpm. A dwell time of 22.2 ms, corresponding to a production speed of 43,100 tablets per hour, was used. No pre-compression force was applied. These parameters in the Presster (e.g., tooling type and dwell time) were selected based on those employed in the tablet press of the continuous line. A total of 36 tablets for 0 rev, 160 rev, and 640 rev conditions and 25 labRAM tablets were analyzed.

3.2.4 Tablet Characterization

All the compacted tablets were stored at ambient room temperature and inside a sealed, clear plastic bag and kept for at least one week to allow for elastic relaxation prior to any characterization.

Density

All the tablets (made in batch or continuous) were weighed with a precision balance (±0.001 g, Adventurer Ohaus). Their thickness was carefully measured by a digital caliper (±0.01 mm, Absolute digimatic Caliper). The relative density of the tablets was calculated using Eq. (2.4). The true density of the blend was determined by

$$\frac{1}{\rho_t} = \sum_{i=1}^{3} \frac{n_i}{\rho_{t,i}} \tag{3.1}$$

n and ρ_t represent the concentration and true density of each ingredient. The thickness, mass, and relative density of all the batch tablets are listed in Tables 3.2 and 3.3. For continuous tablets, the mean values and standard deviations of all the measured parameters are provided in Table 3.4. It can be seen that some of the continuous tablets have masses significantly different from the targeted value (350mg) which resulted in deviations in their relative density. Detailed information about each individual continuous tablet is provided in the appendix.

Table 3.2: Compaction force (F_c), mass (m), thickness (t), relative density ($\bar{\rho}$), speed of sound (SOS), tensile strength (σ_t), and elastic modulus (E) of the labRAM tablets.

F_c (kN)	m (mg)	t (mm)	$\bar{\rho}$ (%)	SOS (m/s)	σ_t (MPa)	E (GPa)
5.2	359.2	3.67	81.7	614	0.24	0.47
6.1	352.8	3.55	83	677	0.28	0.58
6.6	344.6	3.43	83.9	681	0.33	0.59
10.6	349.5	3.34	87.4	823	0.64	0.9
8.3	354.4	3.46	85.5	783	0.43	0.8
8.6	349.6	3.4	85.9	787	0.48	0.81
6.6	348.5	3.46	84.1	721	0.32	0.67
10.3	343.3	3.28	87.4	808	0.61	0.87
13.5	355.3	3.34	88.8	831	0.88	0.93
12.1	353.2	3.33	88.6	816	0.81	0.9
11	345	3.28	87.8	812	0.72	0.88
15.6	350.7	3.24	90.4	920	1.06	1.17
15.6	345.4	3.21	89.8	907	1.13	1.13
21	350.4	3.17	92.3	955	1.48	1.28
22.9	348.9	3.15	92.5	972	1.66	1.33
29.5	354.3	3.14	94.2	1006	2.09	1.45
23.6	352.9	3.18	92.7	1013	1.83	1.45
23.1	357.7	3.22	92.7	1006	1.74	1.43
24.8	353.7	3.17	93.2	991	1.99	1.39
19.5	351.1	3.2	91.6	958	1.44	1.28
17.5	353.7	3.26	90.6	931	1.26	1.2
15.9	359.7	3.35	89.6	936	1.06	1.2
9.5	336.5	3.26	86.2	799	0.55	0.84
23.2	340.7	3.06	93	974	1.77	1.35
25.3	346.2	3.11	92.9	972	1.85	1.34

Table 3.3: Compaction force (F_c), mass (m), thickness (t), relative density ($\bar{\rho}$), speed of sound (SOS), tensile strength (σ_t), and elastic modulus (E) of the batch tablets mixed in the V-blender and then experienced different shear strain environments.

	F_c (kN)	m (mg)	t (mm)	$\bar{\rho}$ (%)	SOS (m/s)	σ_t (MPa)	E (GPa)
0rev	8.2	318.4	3.14	84.7	969	0.74	1.21
	10.7	343.1	3.32	86.3	1012	1.01	1.35
	14.3	347	3.28	88.3	1116	1.43	1.68
	17.1	363.2	3.37	90	1138	1.74	1.78
	16	351	3.28	89.3	1131	1.71	1.74
	18.6	354.2	3.25	91	1169	1.96	1.9
	21.4	359.1	3.26	92	1216	2.41	2.07
	23.1	351.3	3.18	92.2	1252	2.59	2.2
	23.8	346.4	3.12	92.7	1200	2.62	2.04
	13.7	348.2	3.28	88.6	1108	1.37	1.66
	6.2	327.1	3.32	82.3	878	0.49	0.97
	9.3	334.5	3.28	85.1	1000	0.84	1.3
160rev	17.3	383.2	3.54	90.4	1066	1.46	1.57
	14.4	367.2	3.45	88.9	975	1.25	1.29
	13	360.4	3.4	88.5	971	1.08	1.27
	8.2	325.6	3.22	84.4	852	0.54	0.93
	14	346.9	3.27	88.6	962	1.18	1.25
	16.6	352.6	3.27	90	1035	1.47	1.47
	22.9	352.5	3.19	92.3	1139	2.07	1.83
	25.4	347.8	3.14	92.5	1113	2.25	1.75
	23.2	346.8	3.15	91.9	1064	2.2	1.59
	9.5	342.4	3.35	85.3	872	0.67	0.99
	6	343.7	3.48	82.4	756	0.39	0.72
	16.5	343.6	3.2	89.6	1039	1.4	1.48
640rev	24.4	382.5	3.46	92.3	925	1.55	1.2
	22.2	371.8	3.39	91.6	897	1.29	1.12
	18.9	353.8	3.26	90.6	867	1.11	1.04
	9.1	350	3.41	85.7	682	0.42	0.61
	7	339.9	3.38	84	663	0.26	0.56
	12.1	350.5	3.35	87.3	761	0.6	0.77
	16.8	349.8	3.24	90.1	853	0.96	1
	13.4	336.6	3.18	88.4	799	0.69	0.86
	17.2	332.7	3.08	90.2	865	0.97	1.03
	22.1	355.3	3.23	91.8	892	1.28	1.11
	25.9	356.7	3.22	92.5	894	1.61	1.13
	8	354.9	3.49	84.9	712	0.34	0.66

Table 3.4: Mean values and standard deviations of mass (m), thickness (t), relative density ($\bar{\rho}$), speed of sound (SOS), tensile strength (σ_t), and elastic modulus (E) of the continuously manufactured tablets compacted at various nominal compaction forces (F_n).

F_n (kN)	m (mg)	t (mm)	$\bar{\rho}$ (%)	SOS (m/s)	σ_t (MPa)	E (GPa)
8	343.9±8	3.35±0.03	85.6±1.3	1147±50	1±0.16	1.72±0.17
12	350.5±14	3.31±0.07	88.4±1.9	1222±82	1.34±0.44	2.03±0.34
16	347.8±11.6	3.21±0.07	90.5±1.1	1330±39	1.83±0.28	2.45±0.17
20	345.8±8.3	3.13±0.04	92.4±1	1378±27	2.43±0.31	2.68±0.13
24	344.9±10.1	3.11±0.06	92.7±0.8	1389±28	2.5±0.31	2.73±0.13
28	342.9±5.4	3.05±0.03	94±0.6	1407±26	3.12±0.19	2.84±0.12

Acoustic Measurements

The experimental setup for the US measurements consisted of a pulser/receiver unit (Panametrics, 5077PR), a pair of protected-face longitudinal wave contact transducers (Panametrics, V606-RB) with a central frequency and diameter of 2.25 MHz and 13 mm, respectively, a digitizing oscilloscope (Tektronix TDS3052), and a computer controlling the data acquisition (Fig. 3.6). During experiments, the pulser/receiver unit was set to a pulse repetition frequency (PRF) of 500 Hz, a pulser voltage of 100 V, an amplification gain of +10, a central frequency of 2-2.25 MHz, and the entire frequency spectrum of the transducers was allowed to pass through the tablets.

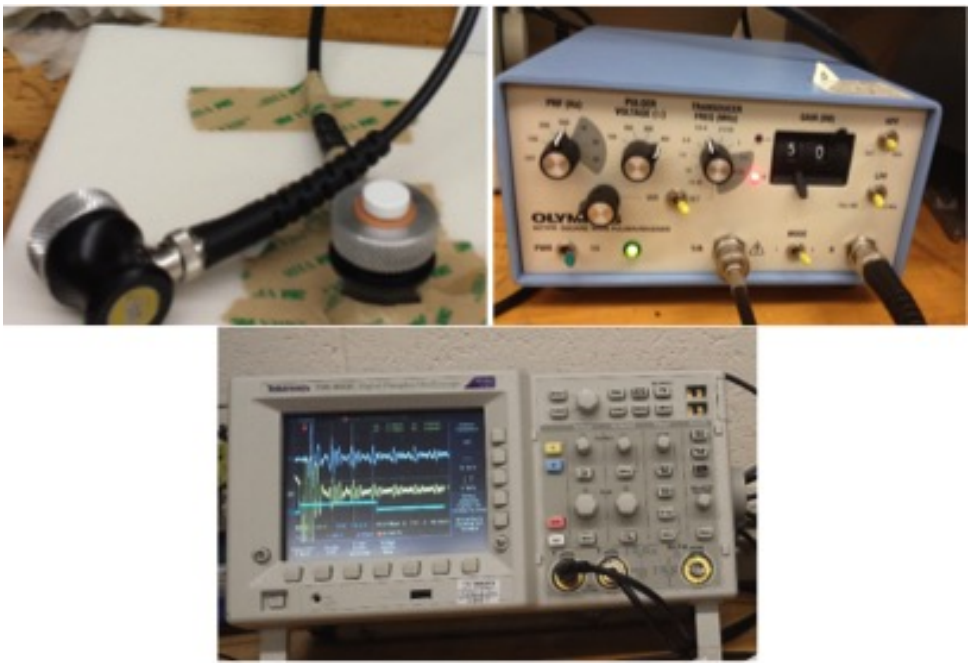

Figure 3.6: The acoustic experimental setup showing ultrasound transducers, pulser/receiver unit, and a digitizing oscilloscope.

In this method, the tablet is placed in direct contact between two piezoelectric transducers (TT geometry). A square electrical pulse from the pulser/receiver unit is launched into the transmitting transducer. Electrical signal is converted into ultrasound and propagates through the tablet as mechanical waves and is captured by the receiving transducer at the other end and digitized as a waveform by the oscilloscope. The time that it takes for the high frequency pressure pulses to pass through the tablet will be measured (i.e., TOF). From the acquired data, the TOF was obtained using the first peak of the received US signal, according to Fig. 3.7. The SOS was calculated as follows:

$$\mathrm{SOS} = \frac{t}{\mathrm{TOF}} \tag{3.2}$$

where t is the tablet thickness. The US transmission measurement system was tested using steel and aluminum samples with four different thicknesses for each case, as shown in Fig. 3.8. A delay time of 1.1 μs was measured for the setup independent of the material used. Subsequently, this delay time was subtracted from the measured TOF in this study.

The elastic modulus (E) of each tablet was then calculated from the SOS assuming the material is isotropic [90, 91]:

$$\mathrm{E} = \mathrm{SOS}^2 \rho_b. \tag{3.3}$$

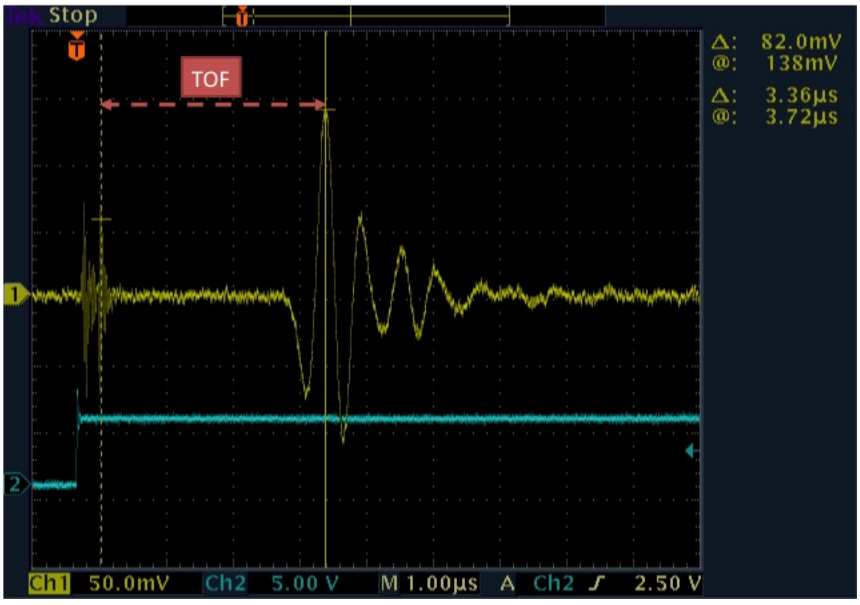

Figure 3.7: Time of flight measurement of a US waveform.

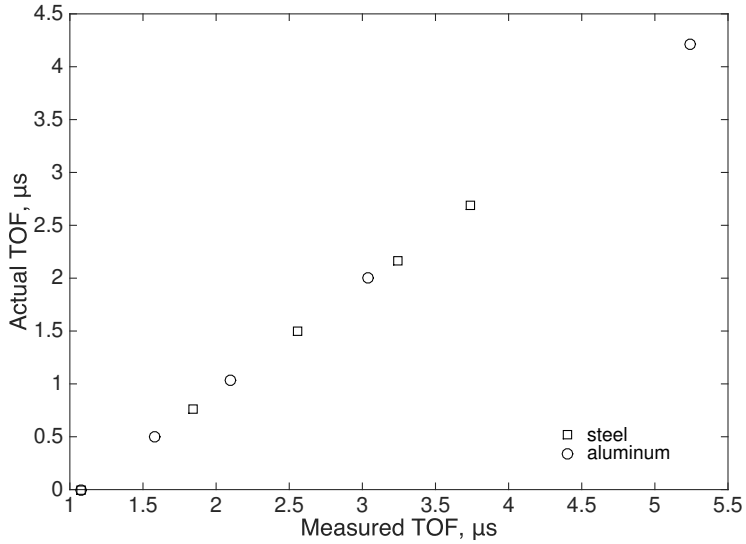

Figure 3.8: Calibration of the ultrasound testing using steel and aluminum samples.

We note that in this study, the US measurements of the continuous tablets were conducted off-line. However, the micro-second TOF of the US signal shows that in principle the US methodology is sufficiently fast to be placed as an in-line measurement.

Tensile Strength Measurements

The diametrical compression test was performed using a standard mechanical hardness tester (Dr. Schleuniger, Pharmatron, model 6D) (Fig. 3.9). The tensile strength of tablets, σ_t, is calculated using Eq. (1.5). Diameter of the tablets are assumed to be constant and equal to 10 mm as radial relaxation was minimal.

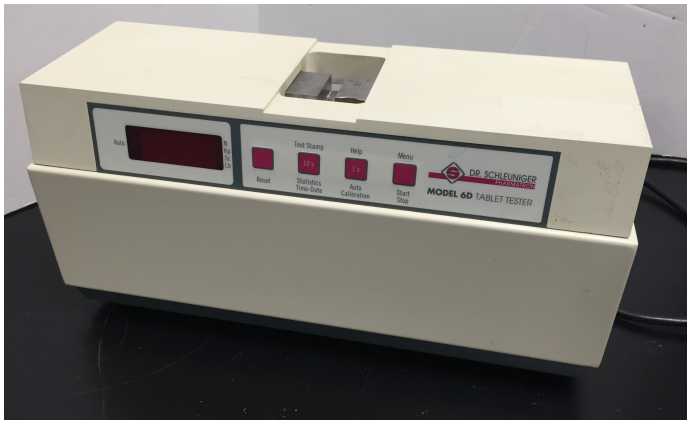

Figure 3.9: Standard hardness tester used to measure the breaking force of tablets.

3.3 A Strategy for Tensile Strength Prediction of Tablets

The mechanical properties of a pharmaceutical tablet not only depend on the material but also on the porosity of the compact. Finding these properties at zero porosity would make it possible to compare blends and predict their maximum strength in compact form. In this study, the fundamental assumption is the existence of a correlation between the elastic modulus and tensile strength at zero porosity of the powder, E_0 and σ_0, respectively. US testing enables us to indirectly measure E_0 and, analogously diametrical compression testing allows us to indirectly measure σ_0. These two parameters serve as mechanical characteristics of tablets, which are a function of material properties and processing history. Once we find the relationship between E_0 and σ_0, we can predict hardness, using US measurements alone.

In the following sections, the existing theoretical/semi-empirical models to determine E_0 and σ_0 are summarized.

3.3.1 Elastic Modulus-Porosity Correlation

The relationship between E and porosity, ϕ, is well established in the literature, and both empirical correlations as well as analytical results have been reported. The porosity is defined as $\phi = 1 - \bar{\rho}$, and Phani and Niyogi [105] derived a semi-empirical relation with the elastic modulus:

$$\frac{E}{E_0} = (1 - a\phi)^n = f(\phi), \tag{3.4}$$

where a and n are material constants, providing information about the packing geometry and pore structure of the material. The constant a is equal to $1/\phi_{c,E}$, where $\phi_{c,E}$ is defined as the porosity of which E vanishes. The minimum value that a can take is 1 corresponding to the maximum value of $\phi_{c,E} = 1$.

Bassam et al. [106] explored the elastic modulus of fifteen representative tableting excipient powders for different porosities using a four-point beam bending technique and analyzed the data following an empirical function proposed by Spinner et al. [107]:

$$E = E_0(1 - B\phi + C\phi^2), \tag{3.5}$$

where B and C are fitting coefficients. Note that Eq. (3.5) is equivalent to a second-order Taylor series approximation of Eq. (3.4) around zero porosity, with $B = an$ and $C = \frac{a^2}{2}n(n-1)$. The model can be further approximated by a linear regression ($C = 0$):

$$E = E_0(1 - m\phi), \tag{3.6}$$

where $m = an$. According to Rossi [108], m accounts for the stress concentration factor around pores in the material and depends on pore geometry and orientation, which is consistent with the description by Phani and Niyogi [105].

3.3.2 Tensile Strength-Porosity Correlation

We considered a theoretical model based on percolation theory proposed by Kuentz and Leuenberger [5] to relate σ_t and $\bar{\rho}$:

$$\ln(1 - \frac{\sigma_t}{\sigma_0}) = \bar{\rho} - \bar{\rho}_{c,\sigma_t} + \ln(\frac{1 - \bar{\rho}}{1 - \bar{\rho}_{c,\sigma_t}}), \tag{3.7}$$

Eq. (3.7) can be rewritten as follows

$$\sigma_t = \sigma_0 \left[1 - (\frac{\phi}{\phi_{c,\sigma_t}}) e^{(\phi_{c,\sigma_t} - \phi)}\right], \tag{3.8}$$

where ϕ_{c,σ_t} is the porosity at which σ_t goes to zero.

The relationship between σ_t and $\bar{\rho}$ is generally presented by an exponential form [49, 109, 44, 110]. Although this relationship usually provides a good fit to the data, it is empirical and does not provide the limiting values (i.e., ϕ_{c,σ_t} and σ_0) needed to implement the strategy discussed above.

3.4 Results and Discussion

The calculated SOS, σ_t, and E values for continuous and batch tablets are listed in Tables 3.2, 3.3, and 3.4.

In Fig. 3.10, we present the relationship between $\bar{\rho}$ and σ_t for all the continuous and batch tablets. The diametrical compression test results were fitted to Eq. (3.8) using the nonlinear regression method based on the Trust-Region algorithm [111]. Table 3.5 lists the fitted parameters and R^2 values. We found a reasonable agreement between the model and the experimental results as shown by the R^2 values. Blends with the same formulation but experiencing different level of shear strain resulted in different mechanical properties. As expected, the strength of tablets decreased with the level of shear strain.

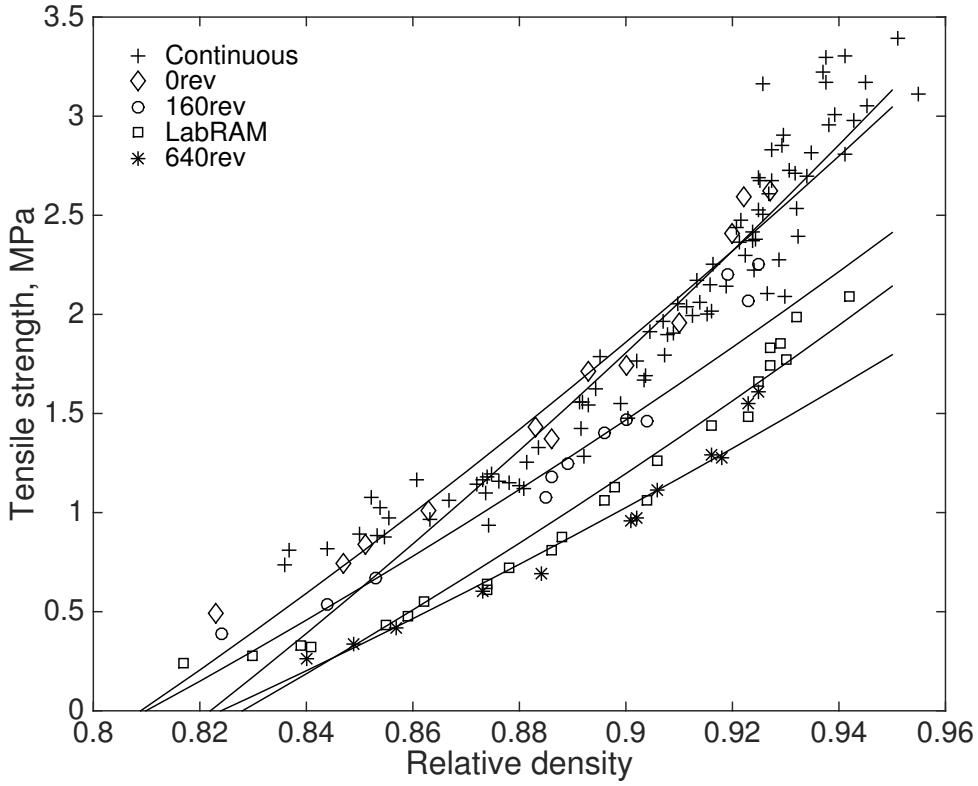

Figure 3.10: The relationship between relative density and tensile strength following the Kuentz and Leuenberger [5] model.

Table 3.5: Tensile strength at zero porosity (σ_0) and critical relative density ($\bar{\rho}_{c,\sigma_t}$) found from Eq. (3.8) for all the differently produced tablets.

cases	σ_0 (MPa)	$\bar{\rho}_{c,\sigma_t}$ (%)	R^2
continuous	4.60	82.2	0.911
0rev	4.36	80.9	0.966
160rev	3.46	81.0	0.921
640rev	2.65	82.4	0.954
labRAM	3.19	82.8	0.944

Fig. 3.11 shows a linear relationship between $\bar{\rho}$ and E in agreement with Eq. (3.6). We also fitted the experimental data to Eqs. (3.4) and (3.5). Table 3.6 lists the fitted coefficients and R^2 values of all the tablets. Bassam et al. [106] reported that lactose monohydrate resulted in a linear regression in terms of porosity, with a vanishing quadratic term (i.e., $C = 0$ in Eq. (3.5)). However, in our study the C values are not negligibly small and change noticeably from one case to the other. The E_0 values

are almost the same for all the three models. It is worthwhile to note that the fitting coefficients are dependent on many parameters selected in the optimization process, and for the same R^2 values we can find a different set of fitting parameters. In addition, we are considering a relatively small range of relative densities and thus, it is acceptable to use a linear regression to estimate E_0. It bears emphasis that these results might change for a wider range of relative densities but the methodology would still hold.

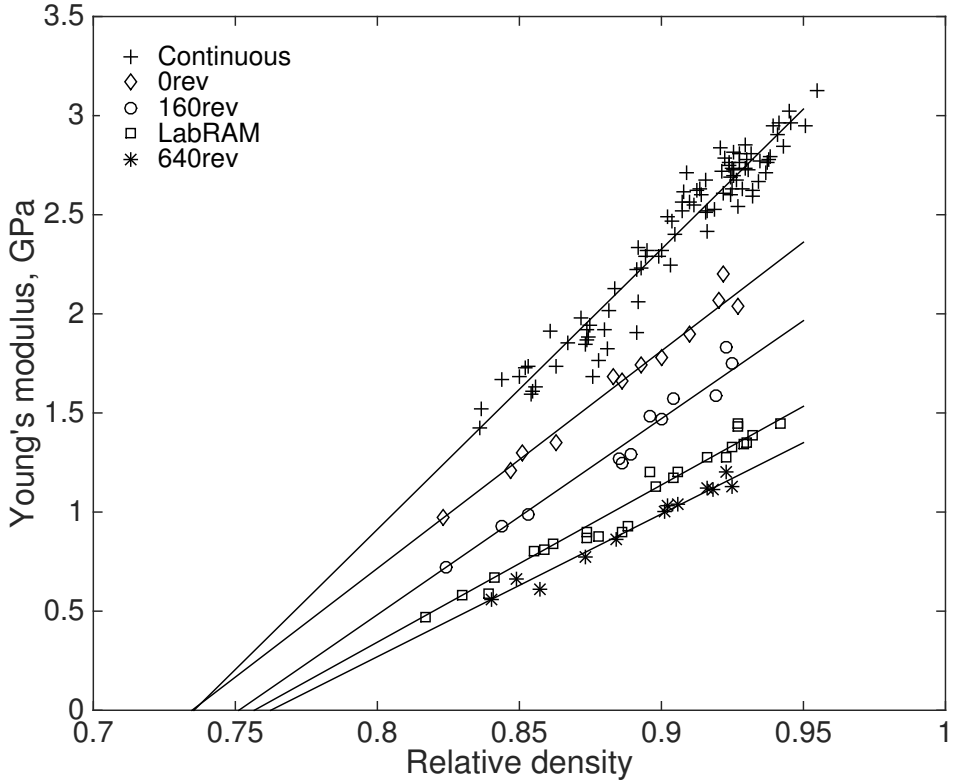

Figure 3.11: Elastic modulus as a function of relative density.

It is worth to mention that ϕ_{c,σ_t} and $\phi_{c,E}$ describe two different phenomena, and can be different for the same material and processing conditions. For the material studied here, at a certain relative density we can start to see tensile stiffness in the blend without forming a bond between the particles.

Figs. 3.10 and 3.11 allow us to estimate the effective shear strain level corresponding to labRAM and continuous tablets. The selected parameters in labRAM mixer make the hardness of labRAM tablets fall between the 160 rev and 640 rev tablets, indicating

that labRAM is a fast and efficient mixing technique [28]. On the other hand, the continuous manufacturing process resulted in a low effective shear strain, even below the 0 rev tablets.

Table 3.6: Elastic modulus at zero porosity (E_0) and other fitting coefficients according to Eqs. (3.4), (3.5), and (3.6) for all the group of tablets.

	Phani					Spinner					Rossi			
cases	E_0 (GPa)	a	n	R^2	$\bar{\rho}_{c,E}$ (%)	E_0 (GPa)	B	C	R^2	$\bar{\rho}_{c,E}$ (%)	E_0 (GPa)	m	R^2	$\bar{\rho}_{c,E}$ (%)
continuous	3.73	3.81	0.98	0.935	73.7	3.71	3.61	-1.06	0.935	74.2	3.74	3.78	0.935	73.5
0rev	3.04	3.44	1.22	0.978	70.9	3.06	4.28	2.40	0.978	72.4	2.91	3.77	0.977	73.5
160rev	2.68	3.37	1.46	0.971	70.3	2.70	5.08	5.22	0.971	72.6	2.46	4.02	0.965	75.1
640rev	1.96	2.93	1.98	0.978	65.9	1.95	5.77	8.18	0.978	69.3	1.71	4.21	0.978	76.2
labRAM	1.90	4.25	0.93	0.97	74.0	1.90	3.91	-1.13	0.967	0.76	1.93	4.11	0.967	75.7

It is clear that the total shear strain had an effect on E values. As shear strain increased the SOS values decreased and the tablets became both softer and mechanically weaker. The decrease in E_0 values with shear strain (Table 3.6) is also an indication of weaker bonding stiffness between particles.

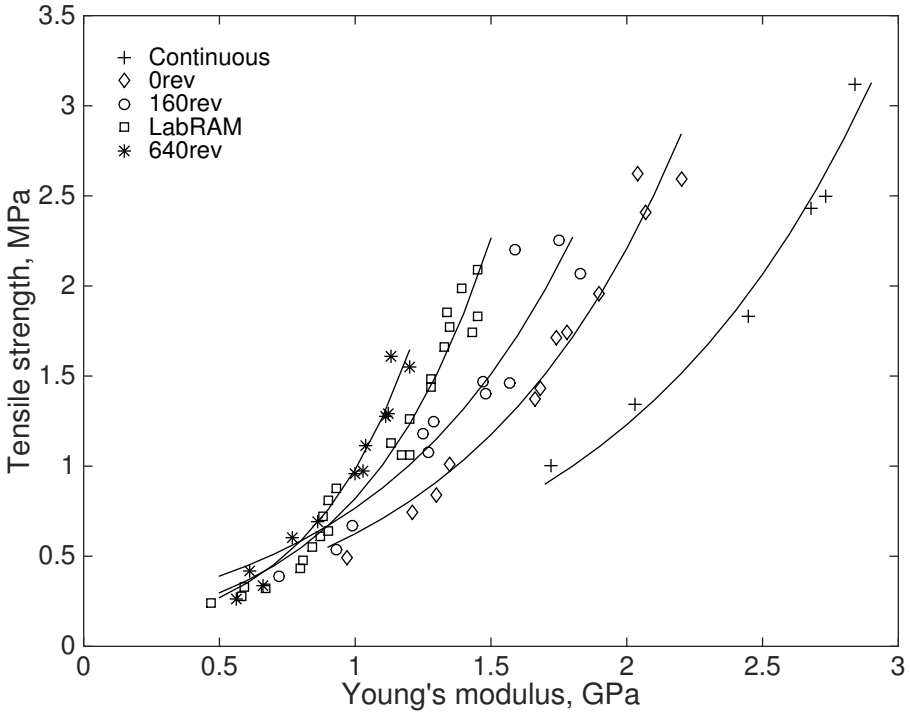

Figure 3.12: Tensile strength as a function of elastic modulus. Mean values are shown for the continuous tablets.

Based on Figs. 3.10 and 3.11, US testing seems to be more sensitive than the hardness tester in differentiating tablets. Comparing the continuous and 0 rev tablets, for the same $\bar{\rho}$, σ_t values are very similar. However, their E values are noticeably different. Fig. 3.12 shows that we can associate different σ_t values for one value of E. However, $\bar{\rho}$ values are different for those tablets with the same E and different σ_t. Therefore, knowing both $\bar{\rho}$ and E it is possible to predict tablet hardness. Fig. 3.13 shows that by considering $\bar{\rho}$ and E simultaneously we are able to distinguish the differently produced tablets.

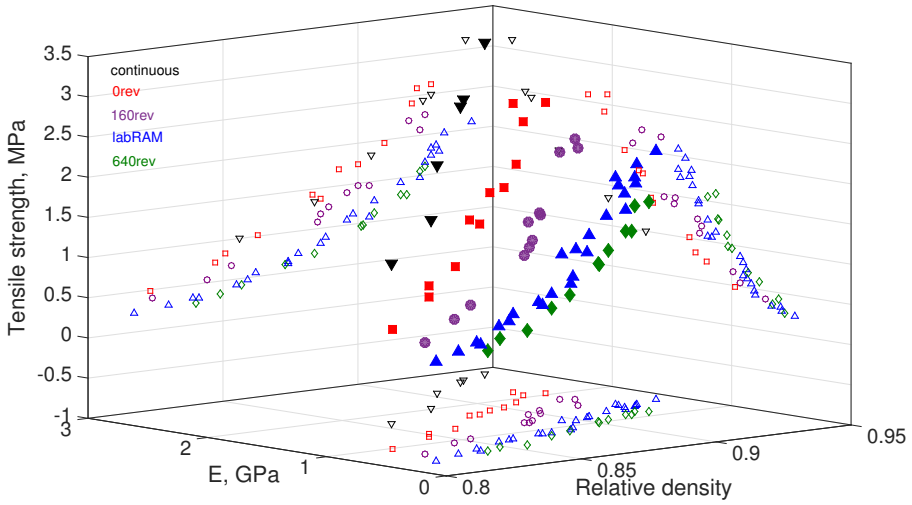

Figure 3.13: σ_t as a function of $\bar{\rho}$ and E and the projection of datapoints on each plane.

Following our proposed strategy, we examine the correlation between the tensile strength and elastic modulus at zero porosity. Fig. 3.14 shows a one-to-one relationship between E_0 and σ_0. Once this relationship is found for a certain blend formulation, we can use US testing only to predict the tensile strength of tablets adopting Eq. (3.8). This is possible when we know the relative density of tablets prior to US testing.

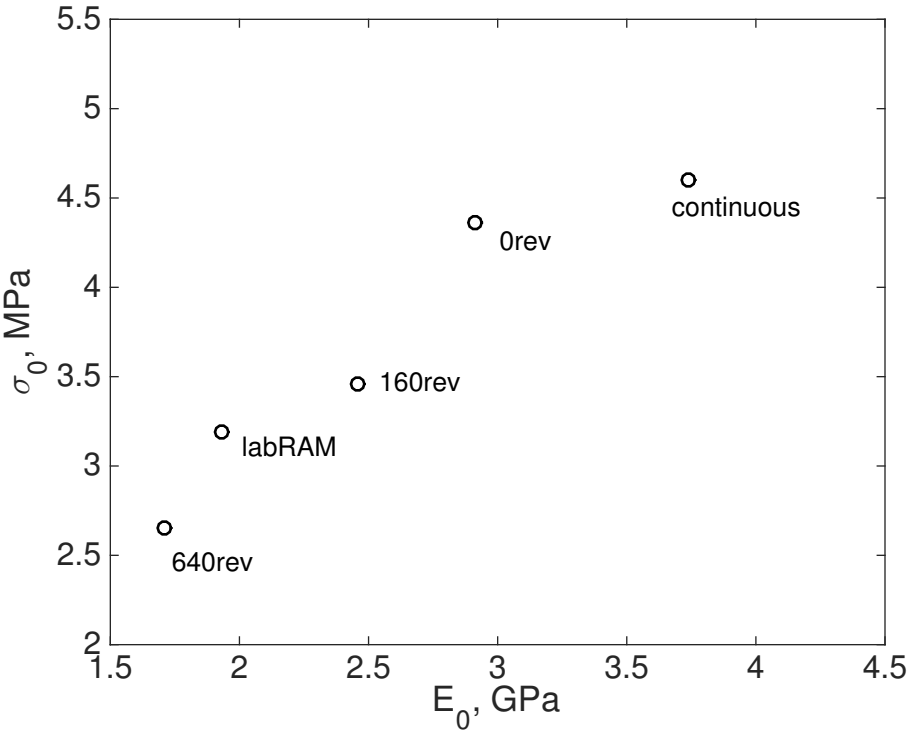

Figure 3.14: A one-to-one relationship between E_0 and σ_0 for tablets with the same formulation but different processing history. E_0 values are derived from Eq. (3.6). Note that 0 rev, 160 rev, and 640 rev tablets have experienced a 2-minute mixing with MgSt in the V-blender.

3.5 Conclusion

We successfully used ultrasound (US) measurement system on tablets. The effect of two processing parameters, compaction force and level of shear strain were examined. US speed of sound was found to be sensitive to the relative density and the level of shear strain. US testing could detect even small differences between tablets that a hardness tester failed to do so. This is an added advantage of using this technique to monitor mechanical properties, because a slight change could have a significant consequence on dissolution.

A strategy for hardness prediction is proposed that uses the existing models for elastic modulus and tensile strength of porous materials. A clear correlation between elastic modulus and tensile strength at zero porosity is presented. Thus, US testing is a good candidate to be placed on/at-line to measure the mechanical integrity of tablets

non-destructively. These results provide information about the behavior of processing parameters on the performance of tablets and the ability to engineer product properties.

3.6 Appendix

Table 3.7: Mass (m), thickness (t), relative density ($\bar{\rho}$), speed of sound (SOS), tensile strength (σ_t), and elastic modulus (E) of each individual continuously manufactured tablet compacted at a nominal compaction force (F_n).

F_n (kN)	m (mg)	t (mm)	$\bar{\rho}$ (%)	SOS (m/s)	σ_t (MPa)	E (GPa)
8	344	3.37	85.23	1154	1.07	1.73
	341.2	3.33	85.55	1117	0.97	1.63
	332.7	3.32	83.67	1092	0.81	1.52
	352.4	3.37	87.31	1178	1.17	1.85
	341	3.35	84.99	1139	0.89	1.68
	346.3	3.35	86.31	1147	0.97	1.73
	341.6	3.34	85.40	1106	1.03	1.59
	330.4	3.3	83.60	1058	0.74	1.43
	338.6	3.35	84.39	1139	0.82	1.67
	348.4	3.38	86.06	1207	1.16	1.91
	354	3.39	87.19	1219	1.14	1.98
	356.2	3.4	87.47	1206	1.19	1.94
12	351.3	3.29	89.15	1183	1.42	1.90
	376	3.41	92.07	1421	2.43	2.83
	342.8	3.26	87.80	1148	1.15	1.76
	338.9	3.23	87.61	1122	1.16	1.68
	341.8	3.24	88.08	1165	1.12	1.82
	366.5	3.34	91.62	1315	2.02	2.42
	342	3.28	87.41	1188	0.93	1.88
	331.8	3.26	85.32	1156	0.88	1.74
	343.6	3.29	87.38	1183	1.10	1.87
	346.4	3.3	88.00	1196	1.14	1.92
	343.7	3.29	87.40	1201	1.18	1.92
	340.2	3.29	86.68	1183	1.06	1.85
	350.8	3.33	88.13	1224	1.26	2.01
	371.6	3.43	90.46	1319	1.91	2.40
	352.8	3.34	88.37	1256	1.33	2.12
	357.2	3.35	89.21	1232	1.29	2.06
	334.1	3.27	85.48	1112	0.88	1.61
	377.7	3.47	90.88	1399	1.91	2.71
16	340.1	3.13	90.72	1249	1.80	2.52
	330.1	3.09	89.20	1309	1.56	2.33
	340.3	3.15	90.20	1346	1.76	2.49
	343.6	3.16	90.79	1374	1.90	2.61
	354.6	3.21	92.23	1408	2.29	2.79
	345.3	3.16	91.24	1374	2.0	2.63
	340.2	3.18	89.5	1303	1.79	2.32
	341.8	3.17	90.03	1299	1.48	2.32
	337.7	3.17	89.13	1278	1.56	2.22
	369.7	3.34	92.42	1358	2.22	2.6
	352	3.24	90.71	1361	1.97	2.56

Table 3.7 Continued

	347.4	3.21	90.36	1338	1.69	2.47
	347.1	3.23	89.90	1292	1.55	2.29
	342.2	3.2	89.29	1280	1.54	2.23
	341	3.19	89.43	1297	1.63	2.29
	347.7	3.22	90.34	1278	1.67	2.25
	364.7	3.33	91.63	1343	2.25	2.52
	375.2	3.38	92.87	1363	2.27	2.63
20	344.1	3.11	92.38	1401	2.37	2.76
	334	3.06	91.14	1354	2.04	2.55
	336.9	3.08	91.33	1375	2.17	2.63
	363	3.22	94.13	1438	2.81	2.97
	337.8	3.1	90.98	1360	2.05	2.56
	351.6	3.15	93.20	1358	2.54	2.62
	351.5	3.15	93.17	1406	2.72	2.81
	341.1	3.11	91.58	1341	2.15	2.51
	348.1	3.14	92.56	1389	2.51	2.72
	352.2	3.16	93.06	1386	2.73	2.73
	340	3.09	91.87	1343	2.14	2.53
	349.6	3.14	92.96	1389	2.90	2.74
24	378.6	3.31	95.50	1465	3.11	3.12
	339	3.06	92.50	1366	2.69	2.63
	352.7	3.15	93.49	1394	2.81	2.77
	327.8	2.99	91.54	1384	2.0	2.67
	347.6	3.13	92.72	1410	2.83	2.81
	341.3	3.08	92.52	1413	2.68	2.82
	341	3.09	92.14	1392	2.36	2.72
	343	3.08	92.98	1400	2.09	2.78
	341.8	3.08	92.66	1375	2.11	2.67
	343.9	3.08	93.23	1351	2.39	2.59
	342.3	3.09	92.49	1392	2.53	2.73
	340	3.08	92.17	1363	2.47	2.61
	345.2	3.11	92.68	1341	2.61	2.54
	350.6	3.15	92.23	1419	2.85	2.85
	347.6	3.13	92.72	1397	2.67	2.76
	345.4	3.12	92.43	1381	2.38	2.69
	334.9	3.06	91.38	1366	2.06	2.60
	346.3	3.13	92.38	1397	2.41	2.75
28	354.2	3.11	95.09	1427	3.39	2.95
	340.2	3.03	93.75	1390	3.17	2.76
	347.5	3.07	94.51	1448	3.17	3.02
	340.8	3.01	94.54	1433	3.05	2.96
	345.3	3.07	93.91	1435	3.01	2.95
	338	3.01	93.76	1394	3.30	2.78
	339.3	3.02	93.81	1398	2.96	2.80
	337	3.04	92.56	1382	3.16	2.70
	349.4	3.1	94.11	1422	3.30	2.90
	343.3	3.04	94.29	1407	2.98	2.85
	343.4	3.06	93.70	1378	3.22	2.71
	336.7	3.01	93.40	1368	2.70	2.67

Chapter 4

Quantification of Lubrication and Particle Size Distribution Effects on Tensile Strength and Stiffness of Tablets

4.1 Introduction

Lubricants are one of the key ingredients in the pharmaceutical formulations to improve flowability, increase bulk powder density, and reduce die wall friction and ejection forces [112, 113, 114, 115, 116, 117, 118, 119]. Magnesium stearate (MgSt) is the most frequently used lubricant [9]; typically added to the formulation in small amounts ($0.25\% - 1.0\%$ (w/w)) [120, 116]. It has been shown that MgSt can adversely affect the physical and chemical properties of tablets [121, 122]. Hypothetically, MgSt forms a layer on the host particles weakening the interparticle bonding [123, 124, 125]. The lubricant type and concentration, type of mixer and its operation method, and mixing time are all important processing variables that affect the tablet compactibility, interparticle bonding and thus, final mechanical properties [126, 127, 128, 115, 129, 130, 131]. However, the deformation mechanism of host particles also play a role [123]. For example, brittle materials that undergo fragmentation are said to be unaffected by MgSt due to the creation of unexposed surfaces during compression [124, 132]. In contrast, plastically deformable powders are significantly impacted by lubricant mixing [133, 134, 135]. Mollan and Çelik [136] ascribed the reduction in the total work of compaction by increasing the lubricant concentration to decreased particle cohesiveness. Zuurman et al. [137] argued that the decrease in tablet strength of pharmaceutical powders such as microcrystalline cellulose mixed with MgSt is caused by a more extensive relaxation of the lubricated tablets corresponding to a weaker interparticle bonding.

There has been growing interest in quantifying what the powder experiences in mixing with lubricant to enable a more robust prediction of tablet quality attributes. Over a decade ago, the blender parameters were translated to a more relevant and fundamental variables, strain and shear rate, using a modified Couette shear cell to better quantify lubrication effect [103, 138]. Shear rate is proportional to the energy input rate per unit mass and total strain is proportional to the total energy input per unit mass.

Narang et al. [139] derived a dimensionless equation to quantify total shear imparted by the force feeder on the granulation in terms of a shear number, which provides guidance to the scale-up and interchangeability of tablet presses. Kushner and Moore [140] proposed an empirical model, which can describe the impact of both formulation and process parameters on the extent of lubrication in a pharmaceutical powder blend. Just recently, Nakamura et al. [141] suggested to use Carr's flowaibility index (FI), which showed a strong correlation with MgSt mixing time, as an effective index to control physical properties of tablets like friability and hardness.

Particle size distribution (PSD) also plays an important role on the compaction and tablet properties [142]. A decrease in particle size of the powdered material has been shown to increase tablet porosity [43, 143]. Smaller particles are inclined to be more cohesive since the interparticle cohesive forces are comparable to the weight of the particles making them more compressible [144, 145]. Reduction in particle size typically results in an increase in the mechanical strength of tablets [146, 147, 43, 148]. This is attributed to a greater packing density after the particle rearrangement and an increase in the surface area available for interparticulate attractions [149, 150, 143]. Attempts were made to correlate specific surface area to the mechanical strength of tablets and a linear relationship was found for different types of lactose [150, 143]. However, Nyström et al. [10] suggested that the intermolecular forces are the dominating mechanism in the compactibility of powders and only in some cases the available surface area could be used to establish a model to correlate with mechanical strength of tablets. On the contrary, sodium chloride tablets have been reported to become stronger as their particle size increased associated to more bonding between particles through solid bridges [151].

Katikaneni et al. [152] investigated the tableting properties and predominant consolidation mechanism of ethylcellulose as lubricant concentration and particle size varied individually. The concurrent effect of lubrication and particle size on mechanical properties of pharmaceutical tablets during and after compaction has also been explored. Van der Watt [153] was the first to show that tablet properties change after the same MgSt mixing time for different particle sizes of Avicel PH 102. In more recent years, Almaya and Aburub [154] examined the effect of particle size on lubricant sensitivity for different types of materials (e.g., plastic, brittle, and viscoelastic). They concluded that for MCC (a plastically deforming material) particle size impacts tablet strength only in the presence of lubricant. For starch (a viscoelastic material) tablet strength is affected by the particle size with or without added lubricant. Finally, for dibasic calcium phosphate dihydrate (a brittle material) particle size has no effect on tablet strength with or without the lubricant. However, there is no previous work that goes beyond the qualitative predictions.

The primary goal of the present study is to quantify the lubrication effect combined with the particle size on the tensile strength and elastic modulus of tablets. To this end, the tablet strength envelope of two grades of lactose, lactose α-monohydrate (LM) and spray-dried lactose (SDL), caused by different PSD and lubrication conditions was explored. Creating this tablet strength (i.e., stiffness and tensile strength) spectrum allows for optimal selection of lubricant concentration, mixing time, and particle size range with respect to the resources available. Tablets were compressed to different relative densities ranging from 0.8 to 0.94 using an instrumented compactor simulator. We have introduced a new parameter in the existing optimal tensile strength and elastic modulus relationships that accounts for the PSD, lubricant concentration and its mixing time with the host particles. The new model is predictive and effective and can be expanded to include other blend properties or processing parameters effects. Moreover, it can be explored for other quality attributes of tablets as well.

4.2 Material and Methods

4.2.1 Materials

The materials used in this study include α-lactose monohydrate (Foremost Farms, Wisconsin, USA), spray-dried Fast-Flo lactose monohydrate N.F. (Foremost Farms, Wisconsin, USA) and magnesium stearate N.F. non-Bovine (Mallinckrodt, Missouri, USA) as lubricant. Lactose monohydrate (LM) exhibits relatively poor binding properties. Spray drying is a method used to enhance its binding properties [14]. Spray-dried lactose (SDL) (i.e., Fast-Flo lactose) is a mixture of crystalline and amorphous lactose, which is a more common direct compression ingredient compared to LM.

The true density of LM, SDL, and MgSt powders was measured using the AccuPyc Pycnometer (Accupyc II 1340, Micromeritics) with helium as density medium (Fig. 3.2). The powders were dried at 50°C for 24 hours before the test.

4.2.2 Blend Preparation

Each powder was sieved through a vibrational sieve shaker (Octagon 2000, Endecotts Ltd., England) into different particle size distributions (Fig. 4.1). LM was divided into three particle size fractions 0-75, 75-106, and 106-150 μm. SDL was divided into four particle size fractions 0-75, 75-106, 106-150, and 150-212 μm. The sieve shaker was operated at amplitude of 8. The as-received powder was poured in the top pan of the clamped sieve stack. The powders on the lower pan (corresponding to 0-75 μm) were collected at an interval of approximately 15 min. This procedure was repeated until the powder in the lower pan was a negligible amount.

Figure 4.1: Endecotts sieve shaker with multiple pans stacked and clamped.

The particle size distribution (PSD) was measured using a Beckman Coulter LS 13 320 laser diffraction particle size analyzer (Fig. 4.2) to ensure if the desired distribution was achieved. The measurement is based on the principles of light scattering [155]. The instrument measures particle size over the range of 0.017 μm to 2000 μm.

MgSt was pre-sieved through a #50 mesh (300 μm opening) prior to mixing with powders using a LabRAM. As discussed in section 1.4, the mixing intensity $(0-100\%)$ is the parameter that can be controlled in the LabRAM, which determines the amplitude of the mechanical vibration, translating into acceleration values $(0-100$ g's) depending on the load mass [28]. In all the experimental work presented here the acceleration of 40 g was used. In other words, for each blending condition, based on the powder mass and powder properties, the mixing intensity was adjusted to give the same a_{peak} (cf. Eq. (1.1)). Regardless, the variations in powder mass were kept minimal.

Overall, MgSt concentration and mixing time varied from 0.25% to 2% and 30 sec to 2400 sec, respectively, aiming to produce tablets with a wide range of mechanical properties. Samples were stored in airtight plastic bags until used.

Figure 4.2: Beckman Coulter LS 13320 laser diffraction particle size analyzer.

4.2.3 Tablet Compaction

The samples were compacted using a Presster tablet press simulator equipped with an 8 mm flat round face, B-type tooling. A Fette 1200 tablet press was emulated at a constant speed of 25 rpm. A dwell time of 26 ms, corresponding to a production speed of 36,000 tablets per hour, was used. Compression force and punch displacement are measured via strain gauges placed on the compression roll pins and a linear variable displacement transducer connected to each punch, respectively. No pre-compression force was applied. The total number of tablets per case varied from 8 to 17. All the compacted tablets were stored at ambient room temperature and inside a sealed plastic bag and kept for at least 24 hours prior to any characterization.

4.2.4 Tablet Characterization

The mass of tablets was measured with a precision balance (± 0.001 g, Adventurer Ohaus). The thickness and diameter of tablets were measured using a MultiTest 50 (MT50) tablet hardness tester (± 0.01 mm, Sotax, Allschwil, Switzerland) (Fig. 4.3).

From these measurements, the relative density of the tablets was calculated

$$\bar{\rho} = \frac{\frac{4m}{\pi D^2 t}}{\rho_t} \tag{4.1}$$

where m, D, and t are the mass, diameter, and thickness of the tablet and ρ_t is the true density of the blend.

Figure 4.3: MultiTest 50 - manual tablet hardness tester.

Ultrasound measurements were conducted followed by the instructions explained in Chapter 3, except the protected layer on the transducers were replaced by Parafilm tape to improve the contact between transducers and tablets, as suggested by Hakulinen et al. [92]. A delay time of 0.8μs was measured for the setup independent of the material used. The elastic modulus of tablets were determined by Eq. (3.3). The tablets were then diametrically compressed using an MT50 tablet hardness tester. The tensile strength of tablets, σ_t, is calculated using Eq. (1.5).

4.3 Results and discussion

The average true density of LM, SDL, and MgSt was measured to be 1.555, 1.546, and 1.040 gcm^{-3}, respectively. According to Yohannes et al. [156], the true density of lactose and MCC particles was found to be independent of the PSD. Thus, the density measurements were only conducted on the as-received samples and the changes in the true density of powders with different PSD were assumed negligible. A total of 19

blends of LM and 23 blends of SDL were prepared varying in lubricant concentration (c_l), mixing time (t_m), and PSD, listed in Table 4.1.

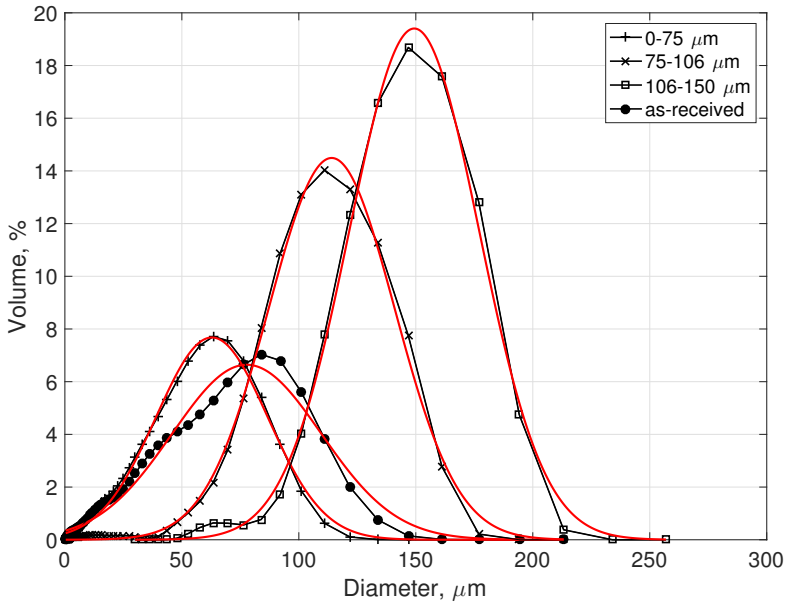

(a)

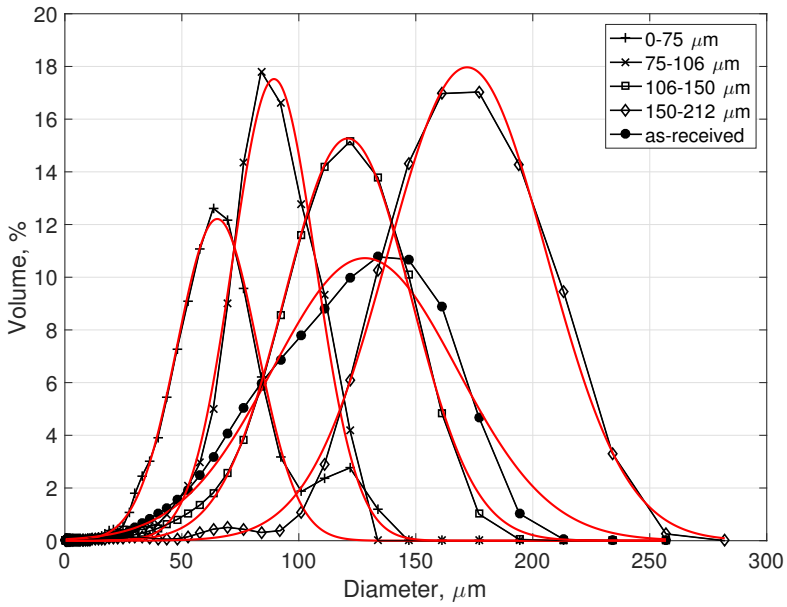

(b)

Figure 4.4: Particle size distribution of (a) lactose monohydrate and (b) spray-dried lactose. Red lines show the Gaussian fitting for each distribution.

Table 4.1: Mean (μ) and standard deviation (σ) for each particle size distribution, MgSt concentration, and the mixing time for all the cases studied.

Powder	Cases	PSD (μm)	μ (μm)	σ (μm)	c_l (%)	t_m (sec)
Lactose monohydrate	1	0-75	62.83	22.87	0.5	30
	2	0-75	62.83	22.87	0.25	120
	3	0-75	62.83	22.87	0.5	120
	4	0-75	62.83	22.87	1	120
	5	0-75	62.83	22.87	2	120
	6	0-75	62.83	22.87	2	300
	7	0-75	62.83	22.87	0.25	1200
	8	0-75	62.83	22.87	0.25	2400
	9	0-75	62.83	22.87	2	1200
	10	75-106	114	26.89	0.25	120
	11	75-106	114	26.89	0.25	1200
	12	75-106	114	26.89	2	1200
	13	106-150	149.3	25.6	0.25	120
	14	106-150	149.3	25.6	0.5	120
	15	106-150	149.3	25.6	0.25	1200
	16	106-150	149.3	25.6	2	1200
	17	as-received	77.72	31.85	0.25	120
	18	as-received	77.72	31.85	0.25	1200
	19	as-received	77.72	31.85	2	1200
Spray-dried lactose	20	0-75	65.14	17.15	0.5	30
	21	0-75	65.14	17.15	2	30
	22	0-75	65.14	17.15	1	120
	23	0-75	65.14	17.15	0.5	600
	24	0-75	65.14	17.15	2	600
	25	0-75	65.14	17.15	2	1200
	26	75-106	89.39	17.74	1	30
	27	75-106	89.39	17.74	0.5	120
	28	75-106	89.39	17.74	2	120
	29	75-106	89.39	17.74	1	600
	30	106-150	120.9	27.04	0.5	30
	31	106-150	120.9	27.04	2	30
	32	106-150	120.9	27.04	1	120
	33	106-150	120.9	27.04	0.5	600
	34	106-150	120.9	27.04	2	600
	35	106-150	120.9	27.04	2	1200
	36	150-212	171.9	33.91	0.5	30
	37	150-212	171.9	33.91	2	30
	38	150-212	171.9	33.91	1	120
	39	150-212	171.9	33.91	0.5	600
	40	150-212	171.9	33.91	2	600
	41	as-received	128.3	39.5	0.25	120
	42	as-received	128.3	39.5	2	1200

Figs. 4.4(a) and 4.4(b) show PSD measured for the sieved and as-received samples of

LM and SDL, respectively. A Gaussian or normal distribution (Eq. (4.2)) was fitted to all the curves using Matlab 2016a and the mean (μ) and standard deviation (σ) for each PSD are reported in Table 4.1.

$$y = \frac{1}{\sigma\sqrt{(2\pi)}} \exp\left(\frac{-(x-\mu)^2}{2\sigma^2}\right) \tag{4.2}$$

In our case, y is the Volume (%) and x is the particle diameter (μm). There is a clear difference between the as-received powders. As-received LM contains mainly of fine particles with average particle size close to the smallest PSD (0-75 μm), whereas as-received SDL has larger particles. This justifies the addition of the fourth PSD (150-212 μm) selected for SDL. For each PSD sample, there are particles smaller (except for 0-75 μm) and larger than the target PSD. Possible reasons were mentioned in Yohannes et al. [156]. Optical microscopy on samples with different PSD showed insignificant change in particle shape. Thus, particle shape was assumed to be a constraint in this study. PSD was shown to be affected by the RAM mixing time [29]. However, our goal is to be able to correlate the mechanical strength of tablets to the initial properties of the powder. Thus, the PSD measurement was only done on the unlubricated samples.

4.3.1 Effect of Particle Size and Lubrication on Compaction Properties

Compaction pressure is calculated by dividing the compaction force over the cross sectional area of the tooling used. The in-die relative density is determined by Eq. (4.1), but t varies as the gap between the upper and lower punches changes during loading and unloading. During loading the punches get closer and the thickness of the powder bed decreases until it reaches its minimum, where the maximum compaction pressure is applied. When the force is released, the unloading stage starts and some of the energy is recovered and the tablet expands axially. The total work input during the compaction process is the area under the loading curve of a force-displacement profile. In this study, instead of force-displacement, we used compaction pressure vs. in-die relative density profiles, which allows for a fair comparison between the samples.

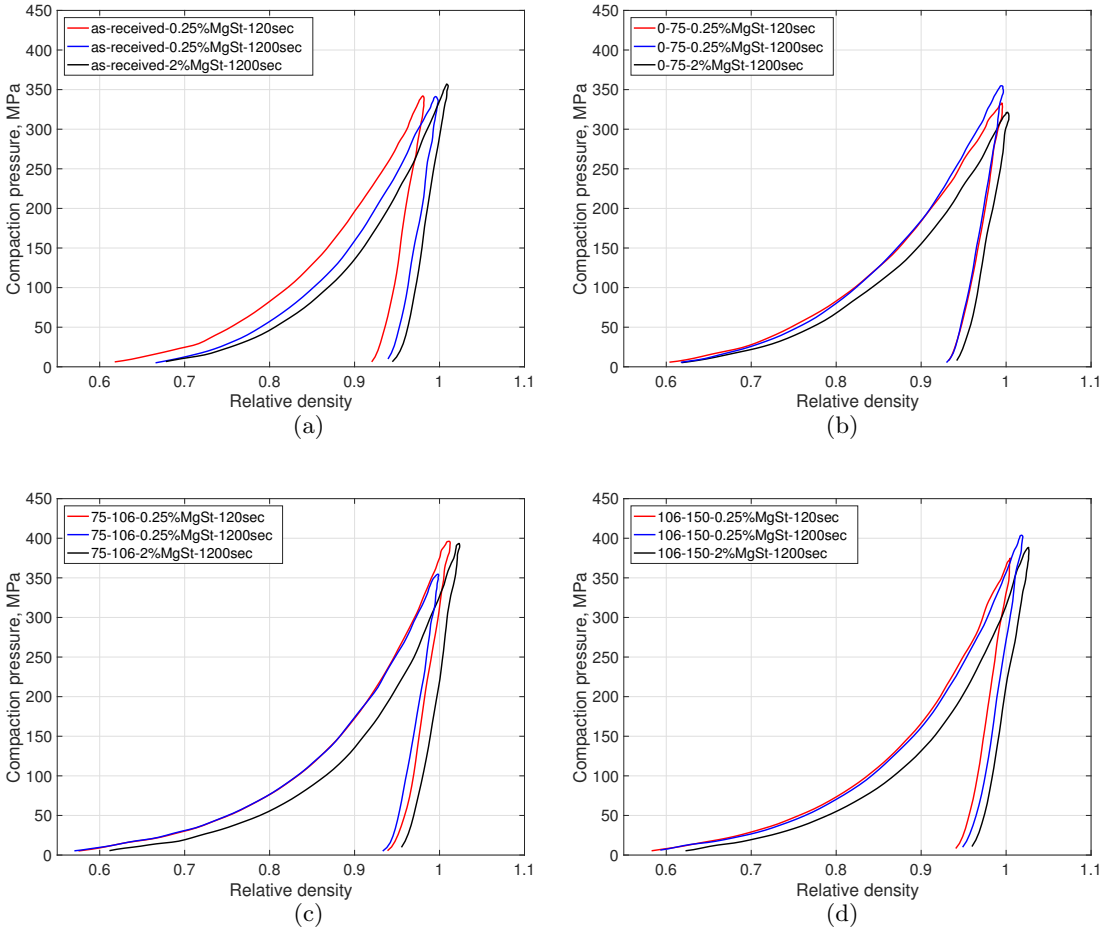

Figure 4.5: Lubrication effect on compaction pressure vs. in-die relative density of lactose monohydrate for different particle size distributions: (a) as-recieved, (b) 0-75 μm, (c) 75-106 μm, and (d) 106-150 μm.

Fig. 4.5 compares the axial compaction pressure vs. in-die relative density profiles of three similar lubrication conditions for the as-received and sieved LM powders. It has been reported that better packing can be achieved during die filling, in particles exposed to higher shear strain levels causing higher initial relative densities (i.e., the die-fill relative density) [103, 157]. In this study, this phenomenon was noticeably observed in the as-received LM. For the sieved samples, by keeping the MgSt concentration constant, the mixing time did hardly affect the loading and unloading path as a function of relative density. On the other hand, in all the cases, the increase in MgSt concentration results in a different compaction profile, moving toward the right-hand side. This shift is partially caused by the decrease in the true density of the blend. Fig. 4.5(b) discernibly shows

that the forces evolved during compression are slightly lower when more lubrication was used, i.e. less work was needed. It has been reported that with increase in lubricant level lower input work is expected attributing it to reduced particle cohesiveness and decreased frictional effects at the punch faces and die wall [136, 158].

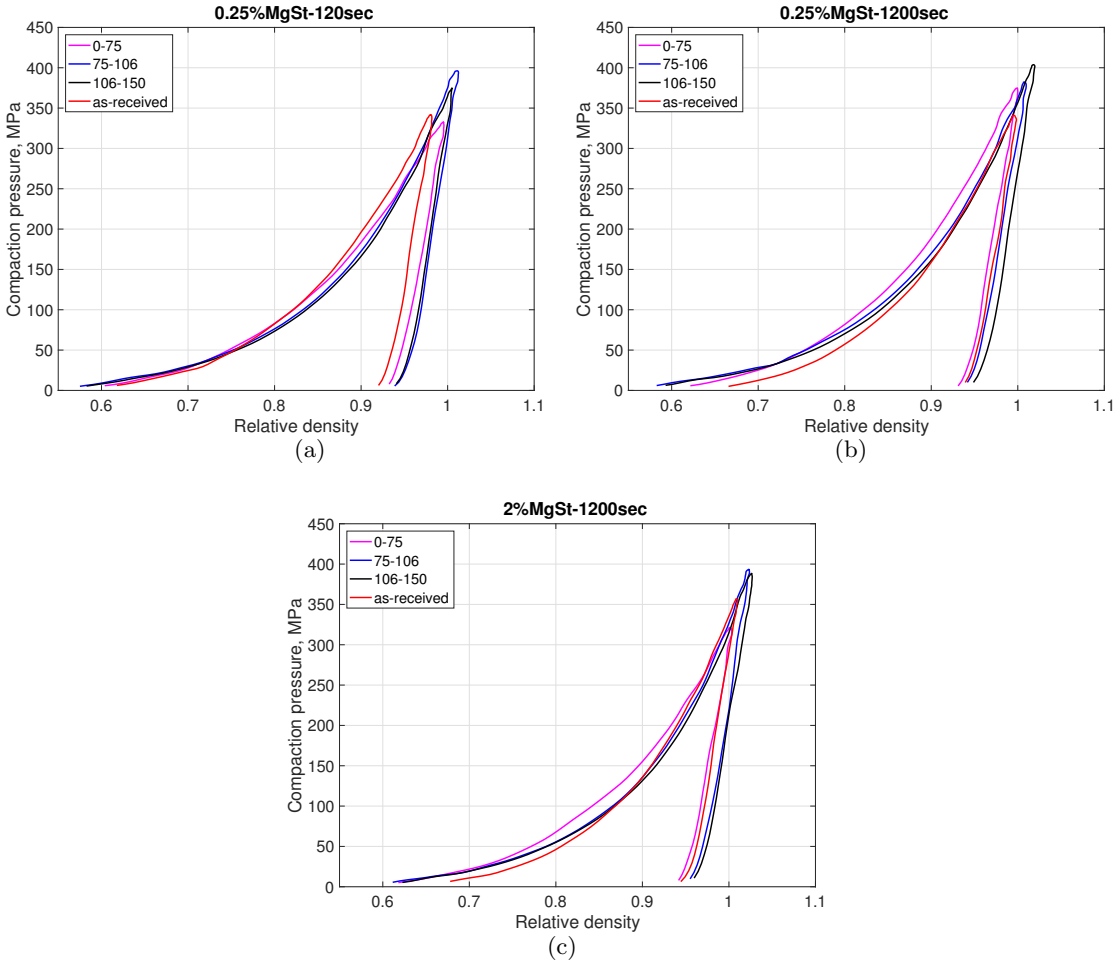

Figure 4.6: Particle size effect on compaction pressure vs. in-die relative density of lactose monohydrate for different lubrication parameters: (a) 0.25%MgSt-120sec, (b) 0.25%MgSt-1200sec, and (c) 2%MgSt-1200sec.

Fig. 4.6 was plotted to better compare the compaction profiles for different PSD with the same lubrication history. There is no significant difference among the compaction profiles for each condition, indicating that PSD does not affect the deformation behavior of LM with the presence of lubrication. The high initial relative density in the as-received sample compared to the sieved samples, may be explained by its relatively

larger standard deviation in PSD (31.85 μm) (Table 4.1). The fine particles fill the voids in between the large particles increasing the bulk density of the powder [156].

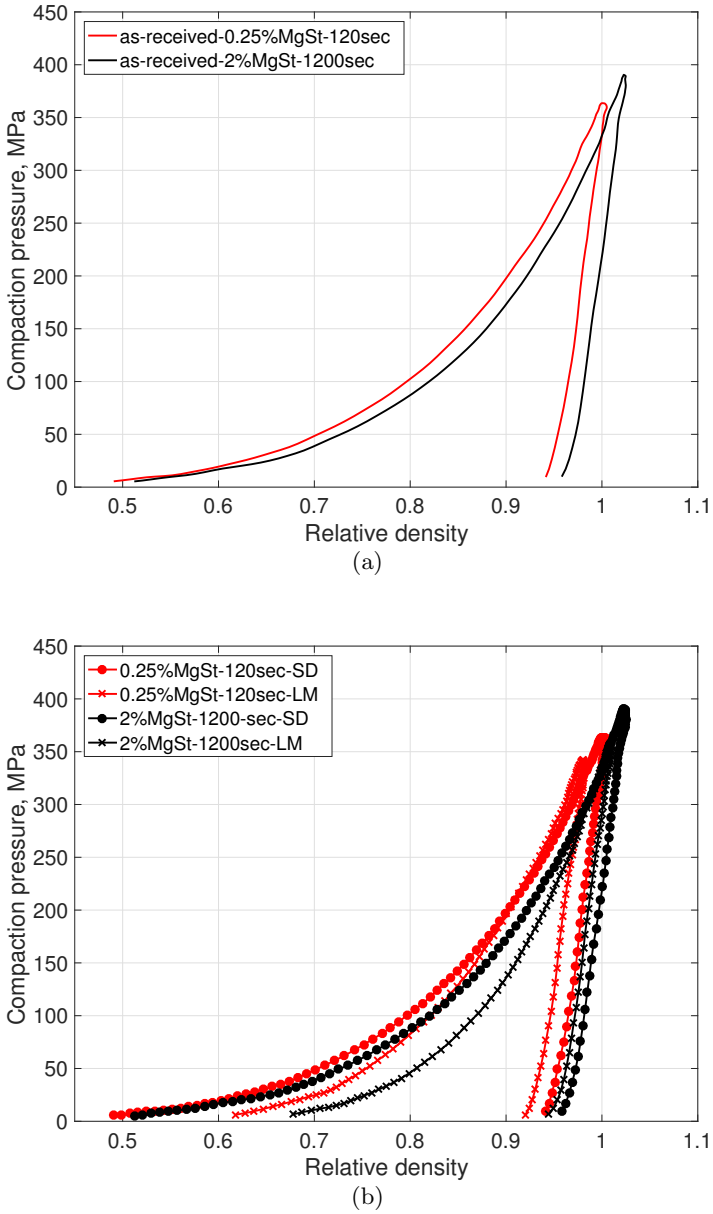

Figure 4.7: (a) Compaction pressure vs. in-die relative density for as-received spray-dried lactose. (b) Comparison of compaction curves of as-received lactose monohydrate and spray-dried lactose for two extreme lubrication conditions.

The compaction pressure- in-die relative density profiles of as-received SDL for two extreme lubrication conditions ascertained little lubricant sensitivity of SDL, as depicted

in Fig. 4.7(a). Fig. 4.7(b) compares the compaction behavior between the two as-received powders. The total work input during the compaction process is much higher for SDL. Mollan and Çelik [136] argued that as the total work input increases, the compacted powder is expected to be stronger as a result of higher energies used to form bonds between particles. If this hypothesis holds, we expect SDL tablets to be much stronger than LM tablets. We should be mindful that the energy of a tablet formation that affects the bond strength, according to the first law of thermodynamics, is associated with both the work done on the powder to form a tablet and the heat released by the system [159].

It is also interesting to mention that for the same lubrication condition the difference in the compaction profiles between the two powders almost disappears when it reaches its maximum. This happens at relative densities beyond 0.9, where the area of true contact between particles is large.

Figs. 4.5 and 4.7(a) suggest that for the two materials studied, PSD and lubrication history have no impact on the unloading curve. One way to characterize the decompression phase is to measure the axial elastic recovery ($ER\%$) [160], which is computed by $\frac{\bar{\rho}_{max}-\bar{\rho}_f}{\bar{\rho}_f} \times 100\%$, where $\bar{\rho}_{max}$ is the relative density at maximum compaction force and $\bar{\rho}_f$ is the final in-die relative density. According to Table 4.2, the computed values were in agreement with the observations and showed no trend. Fig. 4.8 is depicted to ease the comparison between the cases. Clearly, more data points should probably be used to determine if such a trend exists or not. Moreover, determining $ER\%$ alone is not sufficient for comparing the unloading curves.

It bears emphasis that the upper punch force-displacement curves were used to characterize the powder compaction behavior under the assumption that the die wall friction was negligible. Since in this work the lubrication of the powder has been changed considerably it may have resulted in different die wall frictions. To investigate the effect of die wall friction the lower punch force readings should be studied. Therefore, in order to better understand and characterize the compaction behavior of powders more information needs to be extracted from the compaction profiles, which is outside the

scope of this dissertation.

Table 4.2: Percentage elastic recovery and the maximum relative density for different particle size distribution and three lubrication conditions (in consecutive order: 0.25%MgSt-2min, 0.25%MgSt-20min, and 2%MgSt-20min) of lactose monohydrate.

PSD	Cases (cf. Table 4.1)	$ER\%$	$\bar{\rho}_{max}$
0-75 μm	2	0.995	6.72
	7	0.9997	7.37
	9	1.002	6.36
75-106 μm	10	1.0113	7.73
	11	0.9983	6.99
	12	1.023	7.09
106-150 μm	13	1.005	6.83
	15	1.018	7.29
	16	1.026	6.95
as-received	17	0.9802	6.52
	18	0.9955	5.97
	19	1.0084	6.8

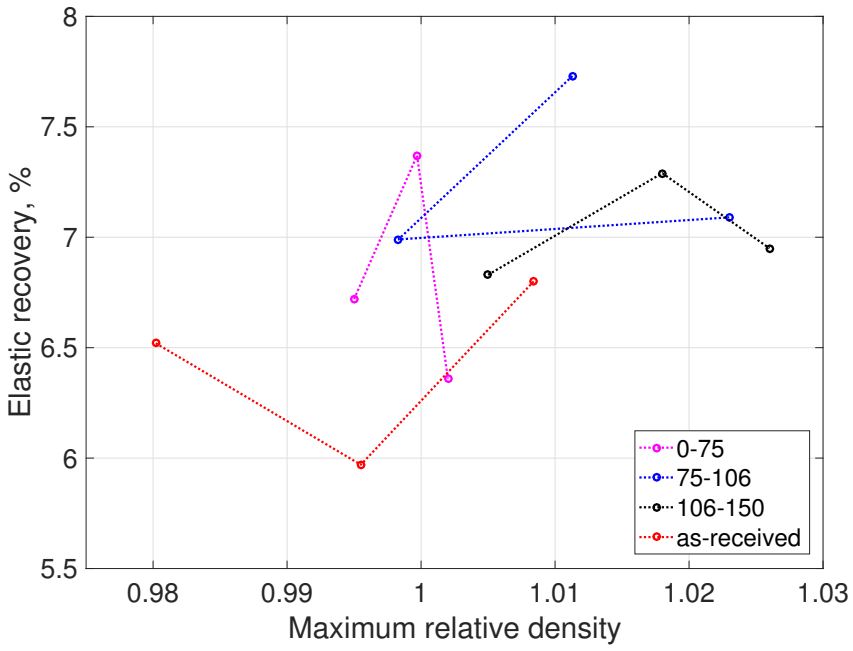

Figure 4.8: Elastic recovery vs. in-die maximum relative density for different particle size distributions of lactose monohydrate.

4.3.2 Effect of Particle Size and Lubrication on Tensile Strength and Stiffness of Tablets

Elastic modulus and tensile strength vs. out-of-die relative density for different PSDs of LM tablets are depicted in Figs. 4.9 and 4.10. Since there were more cases studied for 0-75 μm, the results are plotted separately.

As was expected, both the elastic modulus and tensile strength decreased by adding more lubricant and/or mixing time. Although, the effect is more significant in smaller PSD compared to large PSD. This can be attributed to smaller particles having more available surface area to be covered by MgSt coating. For all the PSD levels, the lubrication affects the strength and stiffness level until it reaches a saturation regime, where the powder would no longer be affected with the addition of lubricant concentration or mixing time, in accordance with Kikuta and Kitamori [130]. It should be noted that the lubricant concentration and mixing time do not affect the tensile strength and elastic modulus of tablets by the same rate. The results demonstrate an envelope for tensile strength and elastic modulus obtainable for tablets with relative densities ranging between 0.8 and 0.94 considering different PSDs and lubricant conditions.

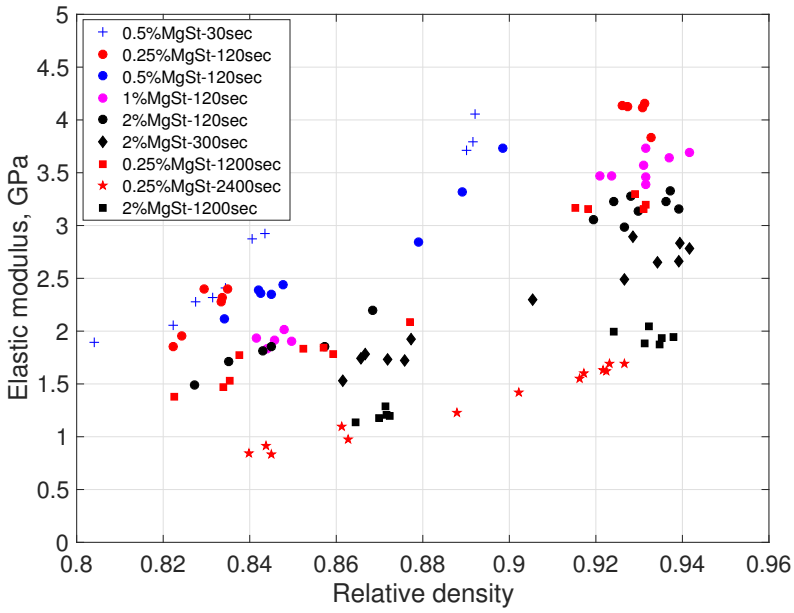

(a)

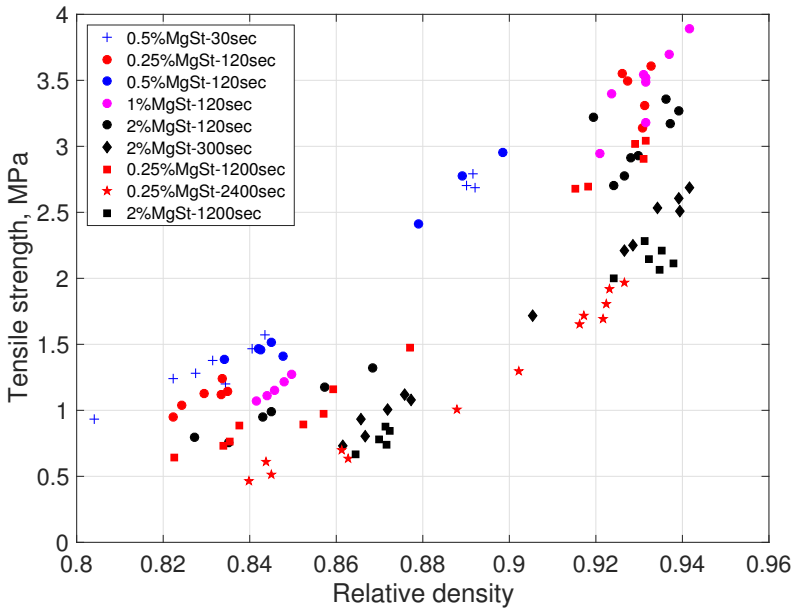

(b)

Figure 4.9: Elastic modulus and tensile strength vs. out-of-die relative density of all the lactose monohydrate tablets with PSD of 0-75 μm.

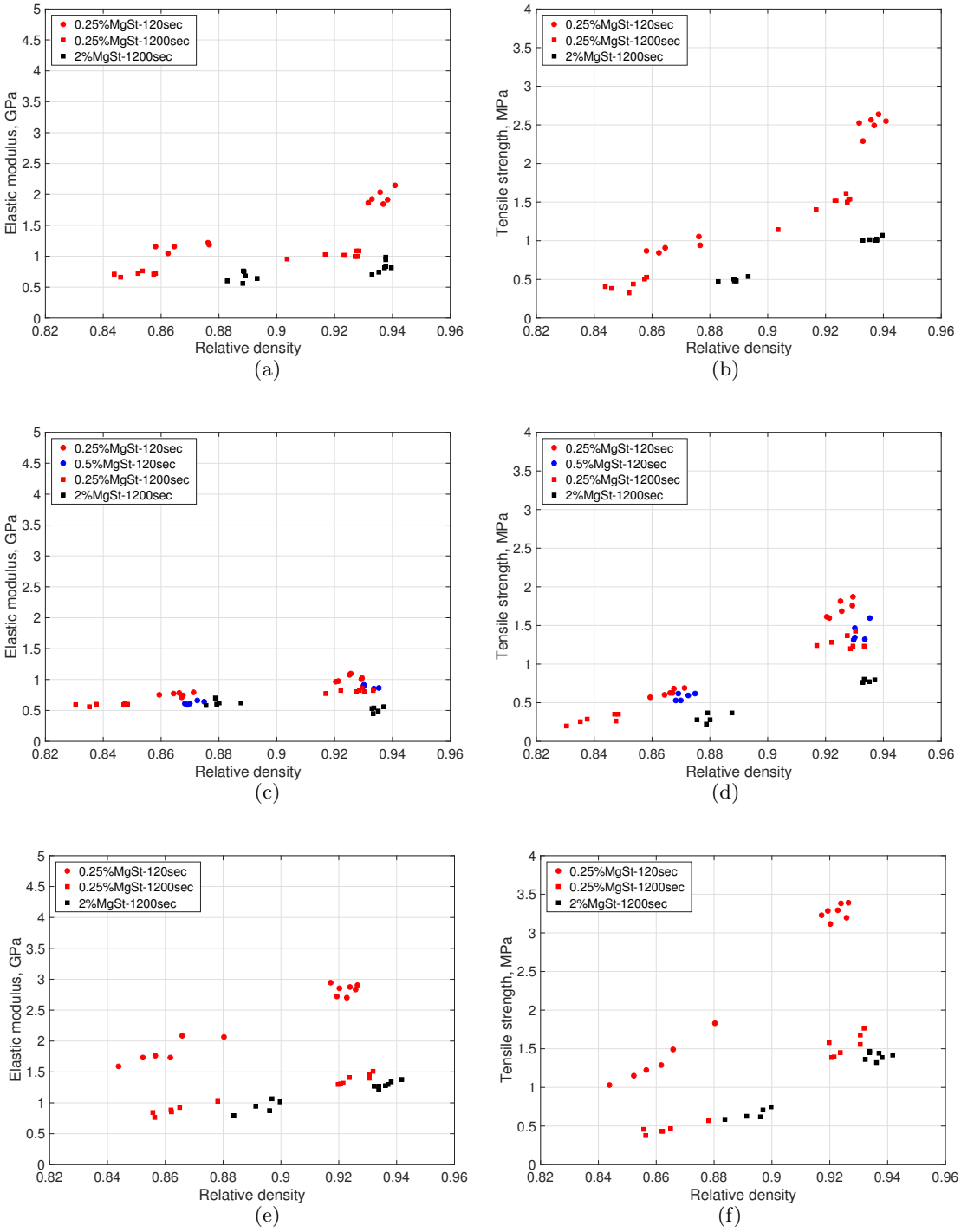

Figure 4.10: Elastic modulus and tensile strength vs. out-of-die relative density for different PSDs of lactose monohydrate; (a,b) 75-106 μm, (c,d) 106-150 μm, and (e,f) as-received.

The reduction in strength of large particles (106-150 μm), even for the least lubricated

tablets (case 13), was to a degree that hardly particles formed a solid and the tablets were extremely weak. In fact, the elastic modulus measurements of highly lubricated tablets with high relative densities (case 16) failed, indicating that there was not sufficient bonding stiffness to pass the ultrasound wave. Obviously, in practical purposes this level of strength is not desirable but since our goal is to have a model based on lubrication sensitivity we created a vast collection of data.

The initial particle size of LM affects the mechanical strength of tablets, as depicted in Fig. 4.11. Large mean particle sizes exhibited faster response to tablet strength saturation by increasing lubricant concentration and/or mixing time. For 0.25%MgSt-2min case, the difference between each PSD is noticeable. This may be due to the more available surface area in smaller particles requiring more mixing time to fully be coated by MgSt. The as-received tablets in the low lubrication condition show high elastic modulus and tensile strength because of having a large population of small particles. However, as the shear strain increases, the larger particles are overlubricated causing a significant drop in the elastic modulus and tensile strength. Altogether, we have observed that the lubricant and PSD sensitivity of LM are more pronounced in the tablet properties than in its deformation behavior during compaction.

The elastic modulus and tensile strength of all the SDL tablets are plotted against their relative densities for different PSD levels in Fig. 4.12. SDL shows a non-negligible sensitivity to lubrication. As expected by the compaction profiles, SDL tablets showed higher values of elastic modulus and tensile strength compared to LM tablets. This difference is more remarkable between the stiffness of tablets compared to the their tensile strength.

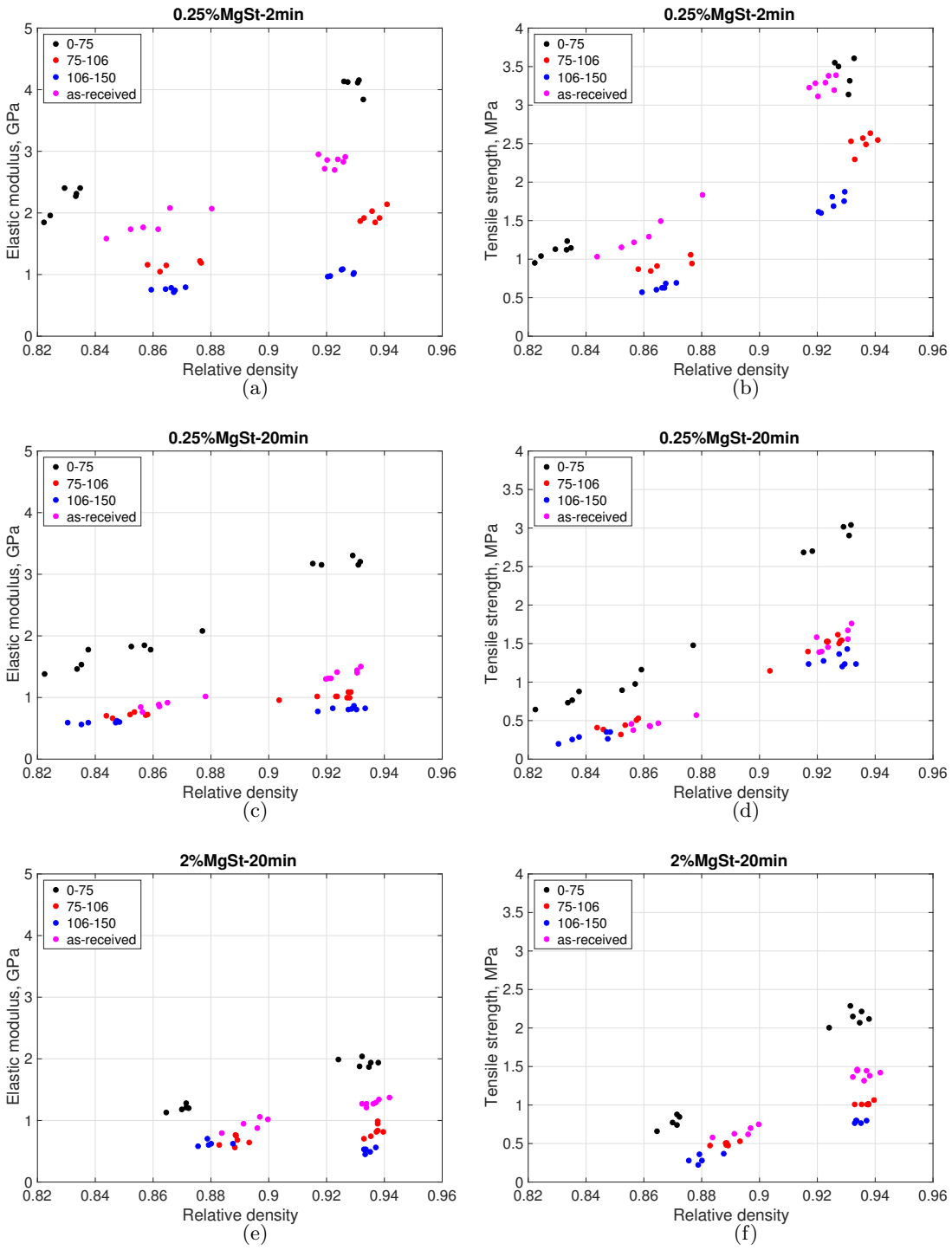

Figure 4.11: Particle size effect on elastic modulus and tensile strength of lactose monohydrate tablets at different lubrication conditions (a,b) 0.25%MgSt-2min, (c,d) 0.25%MgSt-20min, and (e,f) 2%MgSt-20min.

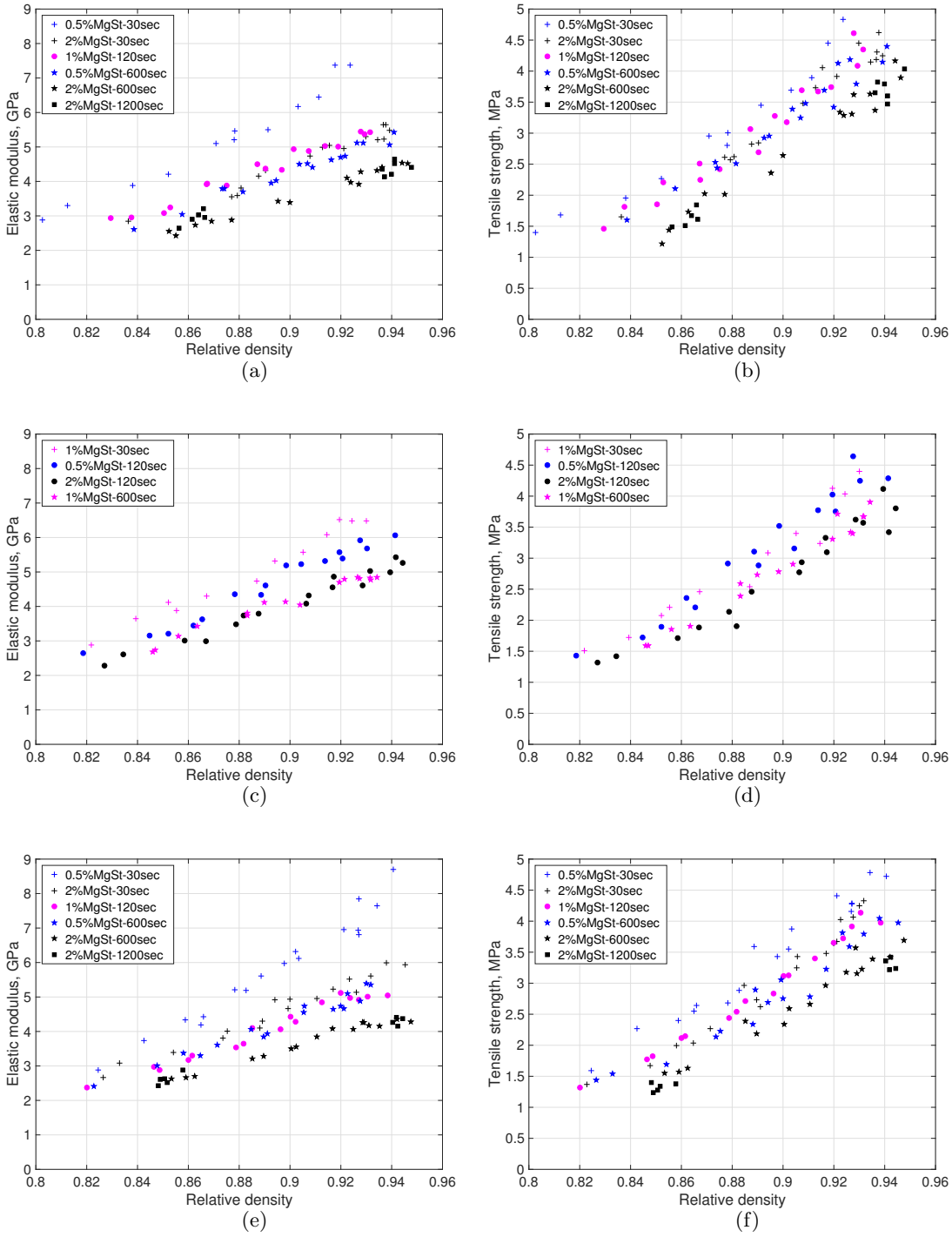

Figure 4.12: Elastic modulus and tensile strength vs. out-of-die relative density for different PSDs of spray-dried lactose; (a,b) 0-75 μm, (c,d) 75-106 μm, (e,f) 106-150 μm, (g,h) 150-212 μm, and (i,j) as-received.

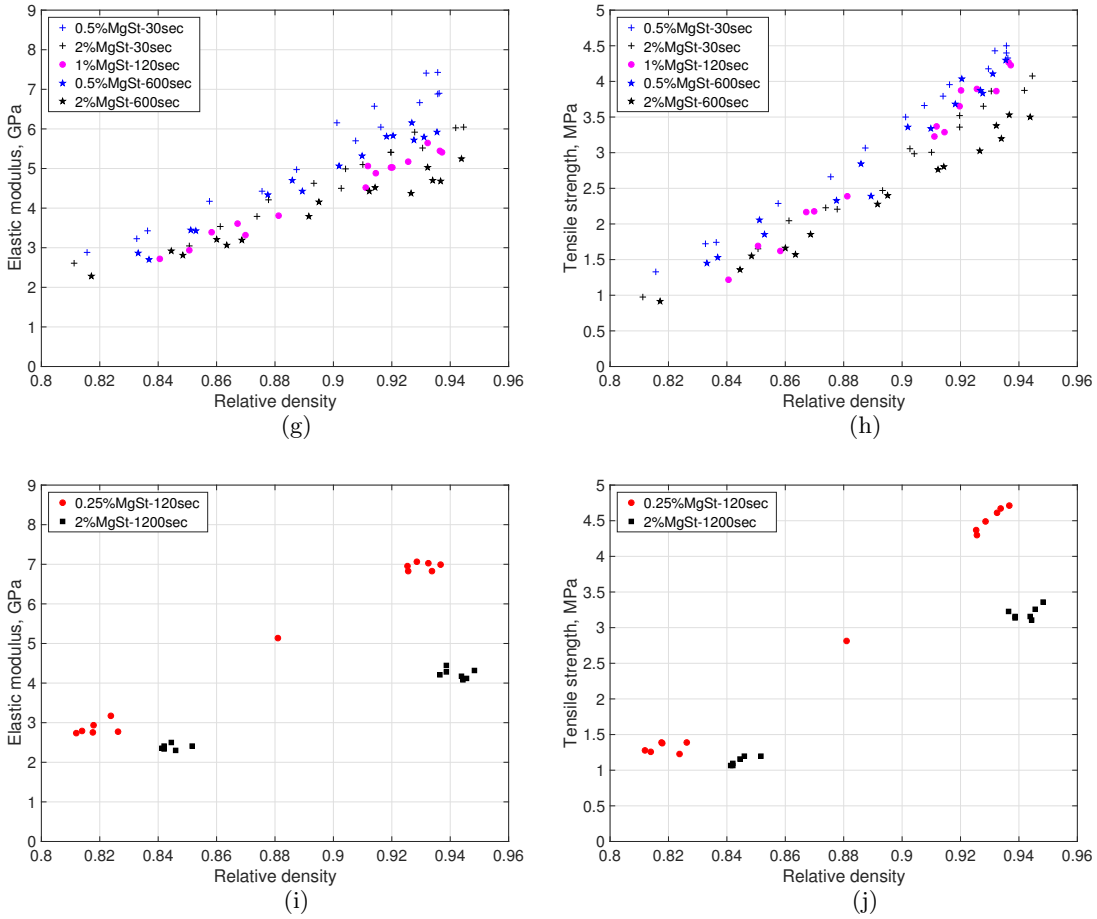

Figure (4.12 Cont.): Elastic modulus and tensile strength vs. out-of-die relative density for different PSDs of spray-dried lactose; (a,b) 0-75 μm, (c,d) 75-106 μm, (e,f) 106-150 μm, (g,h) 150-212 μm, and (i,j) as-received.

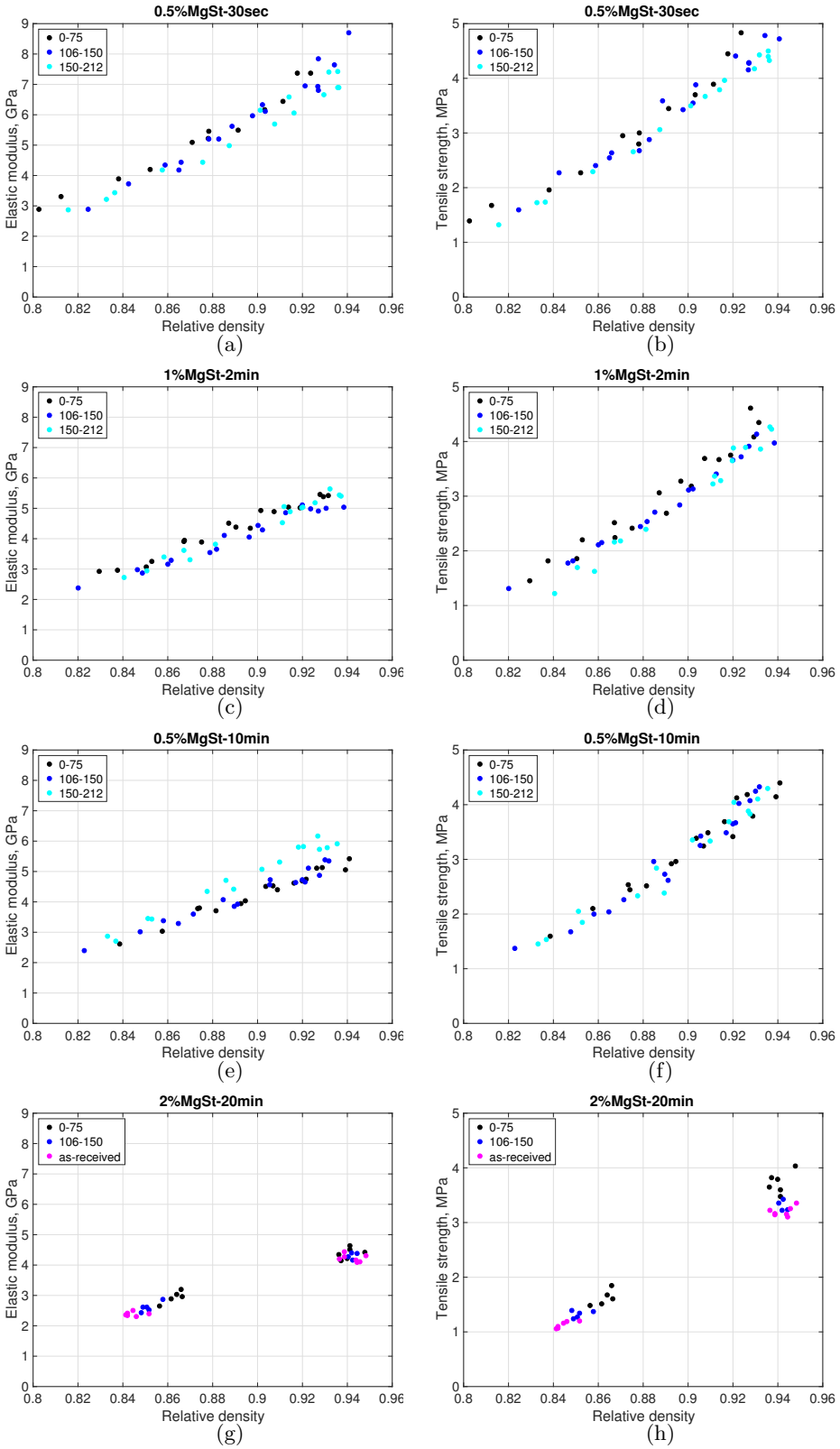

Figure 4.13: Particle size effect on elastic modulus and tensile strength of spray-dried lactose tablets at different lubrication conditions (a, b) 0.5%MgSt-30sec, (c, d) 1%MgSt-2min, (e, f) 0.5%MgSt-10min, and (g, h) 2%MgSt-20min.

Four different lubrication conditions were selected to compare the PSD effect on the tensile strength and elastic modulus of SDL tablets. According to Fig. 4.13, unlike LM, particle size does not affect the tensile strength and elastic modulus of SDL tablets, taking into account different lubrication conditions.

All the 42 cases (cf. Table 4.1) were individually fitted to Eq. (4.3) [108] and Eq. (4.4) [5], thoroughly explained in subsections 3.3.1 and 3.3.2.

$$\mathrm{E} = \mathrm{E}_0 \left(1 - \left(\frac{1-\bar{\rho}}{1-\rho_{c,\mathrm{E}}}\right)\right) \tag{4.3}$$

$$\sigma_t = \sigma_0 \left[1 - \left(\frac{1-\bar{\rho}}{1-\rho_{c,\sigma_t}}\right) e^{(\bar{\rho}-\rho_{c,\sigma_t})}\right] \tag{4.4}$$

where E_0 and σ_0 are the elastic modulus and tensile strength at zero-porosity, respectively and $\rho_{c,\mathrm{E}}$ and ρ_{c,σ_t} are the relative density at which E and σ_t go to zero, respectively. Table 4.3 lists all the fitted parameters and R^2_{adj} values. A good fit was shown for all the cases ($R^2_{adj} \geq 0.92$), except the elastic modulus fitting of cases 12 and 16, due to the implications of acquiring data from these tablets exhibiting low elasticity using the already selected settings on the ultrasound testing.

Table 4.3: σ_0, $\bar{\rho}_{c,\sigma_t}$, E_0, and $\bar{\rho}_{c,E}$ together with their R^2_{adj} values for all the cases.

Powder	Cases	σ_0 (MPa)	$\bar{\rho}_{c,\sigma_t}$ (%)	R^2_{adj}(%)	E_0 (GPa)	$\bar{\rho}_{c,E}$ (%)	R^2_{adj}(%)
Lactose monohydrate	1	5.6	76.16	97.83	6.47	72.93	95.84
	2	5.36	77.27	98.41	5.4	71.29	97.36
	3	6.19	78.07	97.88	5.77	73.7	93.82
	4	5.64	79.61	98.81	4.86	74.42	98.5
	5	4.99	79.7	97.12	4.28	73.14	97.98
	6	4.21	82.47	99.42	3.69	75.3	94.9
	7	4.92	80.08	98.13	4.52	75.12	96.93
	8	3.31	81.26	96.7	2.4	75.68	98.22
	9	3.79	82.9	98.28	2.73	76.68	95.89
	10	4.18	82.13	98.22	2.69	76.82	95.98
	11	2.81	81.9	99.03	1.36	68.71	95.95
	12	1.78	83.72	99.37	1.06	70.27	48.36
	13	3.3	82.78	99.29	1.36	69.58	92.44
	14	2.47	82.34	96.89	1.16	72.02	96.32
	15	2.26	81.22	97.63	1.01	61.14	97.06
	16	1.45	84.28	97.78	-	-	-
	17	6.01	81.05	98.94	4.07	74.52	96.29
	18	3.02	83.38	97.65	2	75.6	97.87
	19	2.62	85.1	96.59	1.84	78.37	92.92
Spray-dried lactose	20	6.91	74.65	95.83	9.8	72.78	96.16
	21	6.49	77.13	96.11	7.23	74.09	95.58
	22	6.56	76.89	95.42	7.29	72.45	97.03
	23	6.23	76.76	95.56	6.85	73.55	96.77
	24	5.7	79.32	97.22	5.76	74.42	98.2
	25	5.58	79.22	98.29	5.48	70.42	95.82
	26	6.15	75.09	94.81	8.74	72.71	97.22
	27	6.49	76.39	94.75	7.98	74.2	96.82
	28	5.39	76.86	94.56	6.7	74.06	96.99
	29	5.67	76.87	97.63	6.54	72.75	97.13
	30	6.71	75.2	96.37	10.66	76.53	95.92
	31	5.6	76.17	94.33	7.5	72.96	96.45
	32	5.97	76.19	98.65	6.85	73.25	96.55
	33	6.42	77.87	96.53	6.94	73.27	95.9
	34	5.13	77.73	96.27	5.57	72.62	96.86
	35	4.77	77.87	99.11	5.39	71.23	98.53
	36	6.47	75.51	99.59	9.43	74.48	96.17
	37	5.66	76.74	98.12	7.65	73.37	96.05
	38	6.44	79.05	98.41	7.37	74.81	97.31
	39	6.29	77.22	96.35	8.27	74.77	97.6
	40	4.95	76.83	98.75	6.31	71.99	96.39
	41	6.91	76.36	99.5	9.47	73.97	99.24
	42	4.63	78.08	99.49	5.3	71.68	97.89

4.3.3 Proposed Model

Toward quantifying the PSD and lubricant sensitivity effects on mechanical properties of tablets, we introduce a parameter "C" into the tensile strength and elastic modulus relationships with relative density. For the sake of simplicity and generality, we assume a form for C that captures the leading order term of the variables, that is

$$C = \frac{{c_l}^{x_1}\ {t_m}^{x_2}\ \mu^{x_3}}{x_4} \tag{4.5}$$

where $\{x_1,\, x_2,\, x_3,\, x_4\}$ are the fitting coefficients. The coefficient x_4 serves as a "normalization" parameter to make C dimensionless. C will depend on the response variable (i.e., tensile strength and elastic modulus) and material properties. Thus, we define four distinct C parameters, referred to as $C_{\mathrm{E},LM}$ and $C_{\sigma,LM}$ for lactose monohydrate and $C_{\mathrm{E},SPD}$ and $C_{\sigma,SPD}$ for spray-dried lactose.

In order to introduce C into the Eqs. (4.3) and (4.4), we need to find the relationships between C and E_0, σ_0, $\rho_{c,\mathrm{E}}$, and ρ_{c,σ_t} (the fitting parameters in those relationships). Figs. 4.9, 4.10 and 4.12 show that the data points converge as $\bar{\rho}$ decreases, in agreement with what authors observed in Razavi et al. [161]. Thus, to keep the optimization problem simpler and mathematically less complex, we assume constant $\rho_{c,\mathrm{E}}$ and ρ_{c,σ_t} for each powder, regardless of its PSD, lubricant concentration or/and mixing time. Thus, as a first order approximation only E_0 and σ_0 were considered as functions of C. We parameterize E_0 and σ_0 as follows:

$$\mathrm{E}_0 = \frac{\mathrm{E}_{0,\emptyset} - \mathrm{E}_{0,\infty}}{1 + C_{\mathrm{E}}} + \mathrm{E}_{0,\infty}, \quad \text{where} \;\; C_{\mathrm{E}} = \frac{{c_l}^{b_1}\ {t_m}^{b_2}\ \mu^{b_3}}{b_4} \tag{4.6}$$

$$\sigma_0 = \frac{\sigma_{0,\emptyset} - \sigma_{0,\infty}}{1 + C_{\sigma}} + \sigma_{0,\infty}, \quad \text{where} \;\; C_{\sigma} = \frac{{c_l}^{d_1}\ {t_m}^{d_2}\ \mu^{d_3}}{d_4} \tag{4.7}$$

where $\{b_1,\, b_2,\, b_3,\, b_4\}$ and $\{d_1,\, d_2,\, d_3,\, d_4\}$ are the fitting parameters presented in function C for E_0 and σ_0, respectively. ($\mathrm{E}_{0,\emptyset}$ and $\mathrm{E}_{0,\infty}$) and ($\sigma_{0,\emptyset}$ and $\sigma_{0,\infty}$) correspond to properties for when $C = 0$ and $C = \infty$, respectively. Thus, $\mathrm{E}_{0,\emptyset}$ and $\mathrm{E}_{0,\infty}$ are the maximum and minimum values E_0 can obtain, which are determined by fitting the

experimental data to the above equation. The same holds for σ_0. For most materials, $\mathrm{E}_{0,\infty}$ (or $\sigma_{0,\infty}$) will go to zero. However, it has been reported that materials, which experience significant fracture may develop some tablet strength even if they are fully lubricated [153, 130]. Therefore, the limit of infinite lubrication does not necessarily need to be zero strength and stiffness.

The functionality of E_0 and σ_0 is in fact unknown. In this study, we parameterized these two functions only in the interest of simplicity and generality. Other functionalities may be explored, which falls outside the scope of this dissertation.

E_0 and σ_0 were predicted from experimental results by solving the following general optimization problems

$$\min_{\{b_1,\ldots,\mathrm{E}_{0,\infty},\rho_{c,\mathrm{E}}\}} \left[\sum_{i\in\mathcal{P}} \left(\mathrm{E}(\bar{\rho}_i) - \mathrm{E}_{0\{b_1,\ldots,b_4,\mathrm{E}_{0,\emptyset},\mathrm{E}_{0,\infty}\}} \left(1 - \frac{1-\bar{\rho}_i}{1-\rho_{c,\mathrm{E}}}\right)\right)^2\right]^{1/2}$$

$$\min_{\{d_1,\ldots,\sigma_{0,\infty},\rho_{c,\sigma_t}\}} \left[\sum_{i\in\mathcal{Q}} \left(\sigma_t(\bar{\rho}_i) - \sigma_{0\{d_1,\ldots,d_4,\sigma_{0,\emptyset},\sigma_{0,\infty}\}} \left(1 - \frac{1-\bar{\rho}_i}{1-\rho_{c,\sigma_t}}\right) e^{(\bar{\rho}i-\rho_{c,\sigma_t})}\right)^2\right]^{1/2}$$

where $\mathcal{P}$ and $\mathcal{Q}$ are a set of experimental points obtained from ultrasound and diametrical compression tests, respectively. In this study, $\mathcal{P}$ and $\mathcal{Q}$ consisted of 316 points for SPD and 204 and 214 points for LM, respectively. It is noted that those 10 observations that were removed from the set for the elastic modulus optimization correspond to case 16 in Table 4.3. Case 5 from LM dataset and cases 24 and 33 from SDL dataset were randomly taken out and adopted later to evaluate the validity of the model.

The solution to the optimization problems forced $\mathrm{E}_{0,\infty}$ and $\sigma_{0,\infty}$ to go to zero for both materials. Thus, Eqs. (4.6) and (4.7) were reduced to

$$\mathrm{E}_0 = \frac{\mathrm{E}_{0,\emptyset}}{1 + \frac{{c_l}^{b_1}\ {t_m}^{b_2}\ \mu^{b_3}}{b_4}}$$

$$\sigma_0 = \frac{\sigma_{0,\emptyset}}{1 + \frac{{c_l}^{d_1}\ {t_m}^{d_2}\ \mu^{d_3}}{d_4}}$$

Table 4.4: Optimal coefficients and their residual error of elastic modulus optimization problem for lactose monohydrate and spray-dried lactose.

Powder	$E_{0,\emptyset}$ (GPa)	b_1	b_2	b_3	b_4	$\rho_{c,E}$	E-norm (GPa)
Lactose monohydrate	28.1221	0.1491	0.2645	1.7082	841.377	0.7316	3.31
Spray-dried lactose	390932.897	0.1654	0.0859	-0.0179	0.0000266	0.7354	5.529

Table 4.5: Optimal coefficients and their residual error of tensile strength optimization problem for lactose monohydrate and spray-dried lactose.

Powder	$\sigma_{0,\emptyset}$ (MPa)	d_1	d_2	d_3	d_4	ρ_{c,σ_t}	σ-norm (MPa)
Lactose monohydrate	14.9186	0.1982	0.301	1.2984	498.924	0.7924	3.739
Spray-dried lactose	10.0276	0.3342	0.1237	0.2154	7.5374	0.7653	3.31

The optimal values together with the residual errors for the optimization problems are in Tables 4.4 and 4.5. For LM, b_3 and d_3 values indicate that changes in PSD result in more drastic changes in elastic modulus and tensile strength of tablets compared to c_l and t_m. On the other hand, c_l seems to be the most influential variable on the mechanical properties of SDL (see, b_1 and d_1 values in Tables 4.4 and 4.5). $E_{0,\emptyset}$ of SDL resulted in an unrealistic prediction. Hence, we attempted to produce tablets of SDL with no lubrication, but the compaction was not successful due to extremely high frictional and ejection forces. Overall, caution must be taken in interpreting $E_{0,\emptyset}$ and $\sigma_{0,\emptyset}$.

In summary, our proposed strategy shows that elastic modulus (or, tensile strength) not only depends on the relative density of tablets, it is also inversely proportional to a non-linear function of material and blending properties and can be presented as follows:

$$E = \frac{E_{0,\emptyset}}{1 + \frac{{c_l}^{b_1}\ {t_m}^{b_2}\ \mu^{b_3}}{b_4}} \left(1 - \frac{1-\bar{\rho}}{1-\rho_{c,E}}\right) \tag{4.8}$$

$$\sigma_t = \frac{\sigma_{0,\emptyset}}{1 + \frac{{c_l}^{d_1}\ {t_m}^{d_2}\ \mu^{d_3}}{d_4}} \left(1 - \frac{1-\bar{\rho}}{1-\rho_{c,\sigma_t}}\right) e^{(\bar{\rho}-\rho_{c,\sigma_t})} \tag{4.9}$$

The groundwork of our model was to relate the variables that contribute to parameter C, to E_0 and σ_0. Figs. 4.14 and 4.15 demonstrate the functionality of the proposed relationship. The model fitted the data well for both materials. The validation points were in good agreement with the predicted curves. It should be noted that our optimization problems were constructed to minimize the experimental and predicted values of elastic modulus and tensile strength of tablets. Thereby, the fitting coefficients presented in Tables 4.4 and 4.5 are not the optimal values for predicting E_0 and σ_0.

The measured and predicted elastic modulus and tensile strength as a function of relative density for all the LM and SDL tablets are plotted in Figs. 4.16 and 4.17, respectively. The colorbar represents a normalized parameter C. The model well captured the lubrication trend with respect to PSD in the elastic modulus and tensile strength for the two compacted powders.

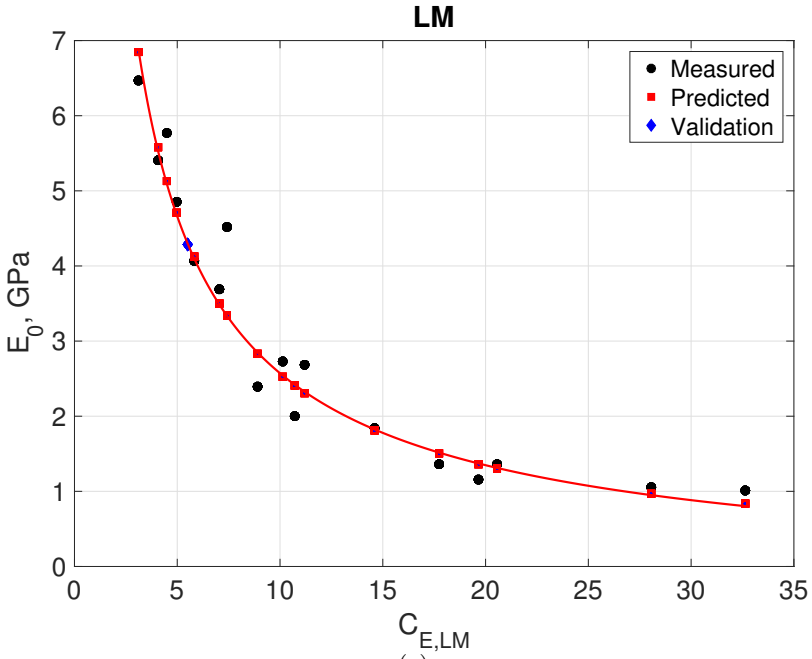

(a)

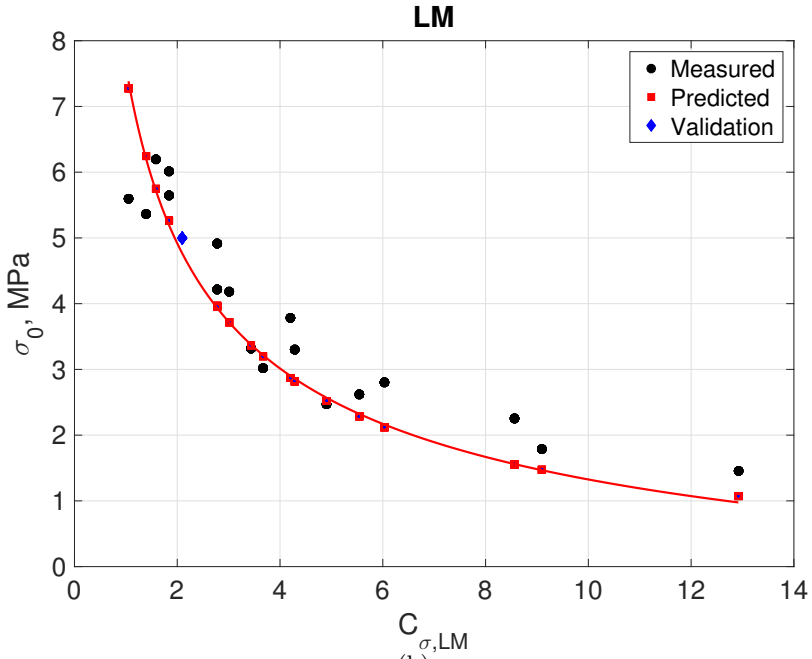

(b)

Figure 4.14: The measured and predicted values of E_0 and σ_0 as a function of parameter "C" for lactose monohydrate. A validation point, in blue, is also provided.

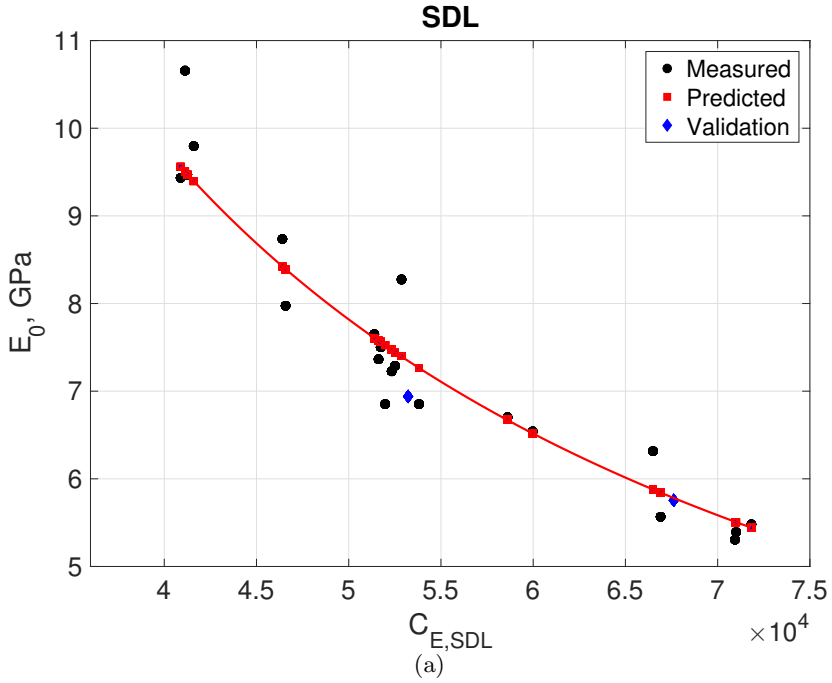

Figure 4.15: The measured and predicted values of E_0 and σ_0 as a function of parameter "C" for spray-dried lactose. Two validation points, in blue, are provided.

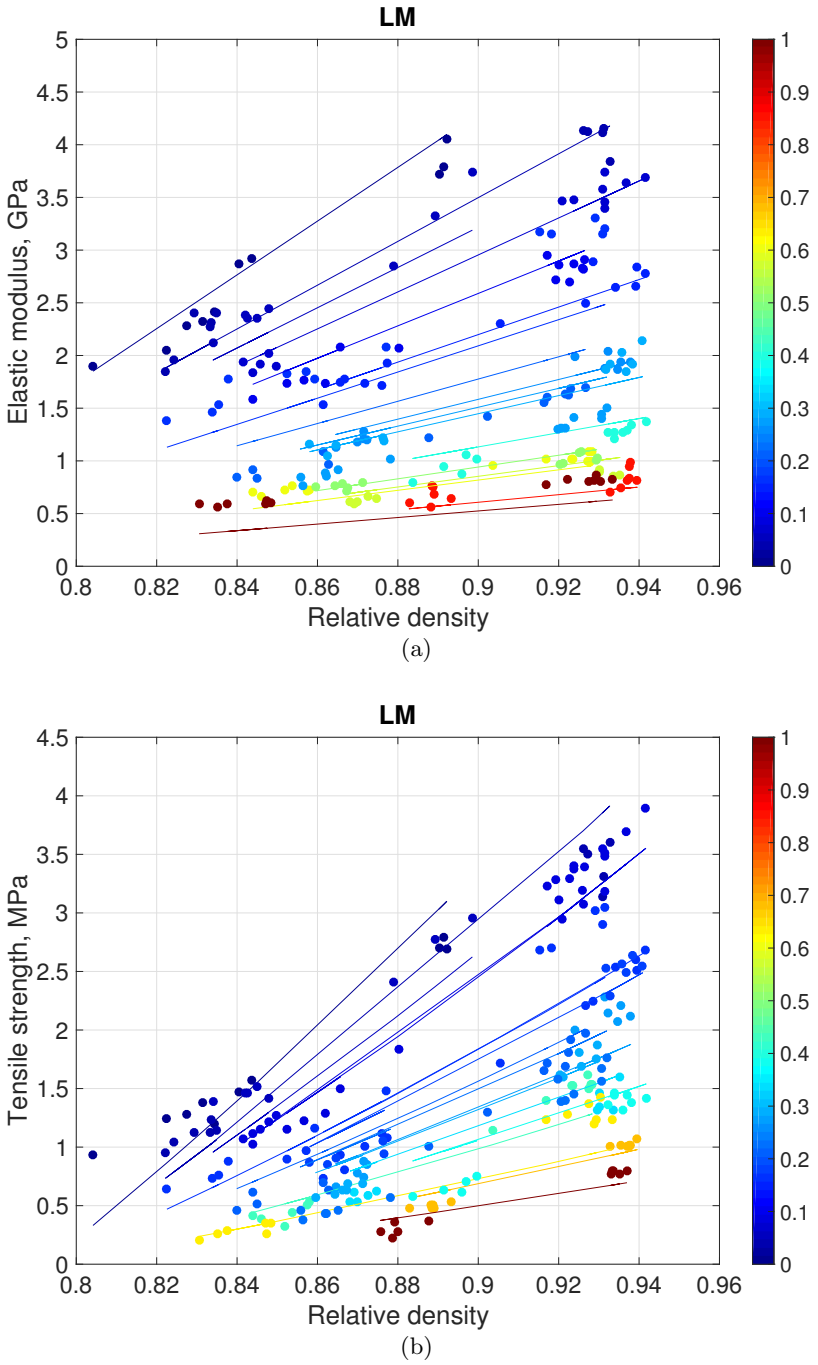

Figure 4.16: (a) Elastic modulus and (b) tensile strength of lactose monohydrate tablets as a function of the relative density capturing the lubrication and PSD effect. The colorbar represents a normalized C parameter. 0: least lubricated+smallest PSD and 1: most lubricated+largest PSD.

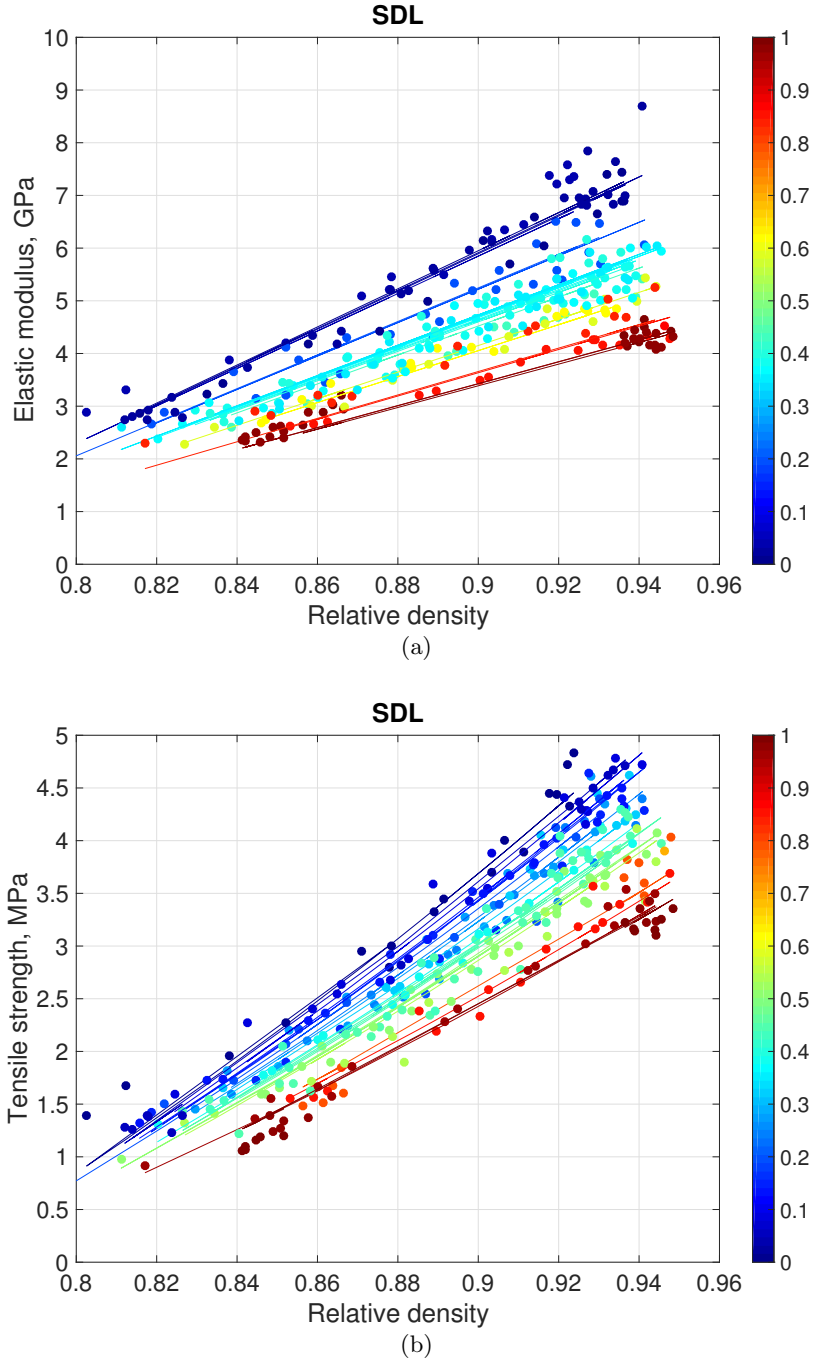

Figure 4.17: (a) Elastic modulus and (b) tensile strength of spray-dried lactose tablets as a function of relative density capturing the lubrication and PSD effect. The colorbar represents a normalized C parameter. 0: least lubricated and 1: most lubricated.

Figs. 4.18 and 4.19 compare the validation measurements with predicted lines for elastic modulus and tensile strength of LM and SDL tablets, respectively (case 5 for LM and

cases 24 and 33 for SDL). The agreement between the validations and model predictions are very promising.

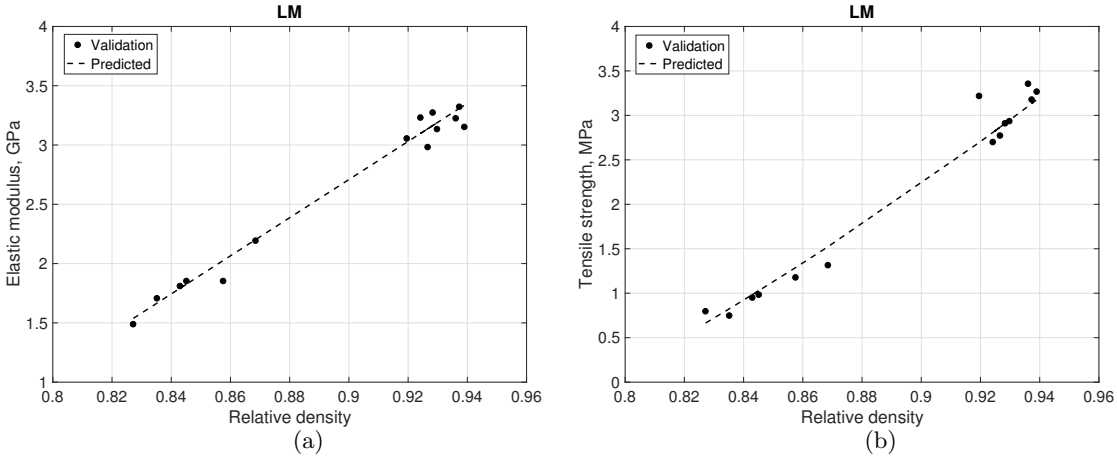

Figure 4.18: Comparsion of the validation experiments to the model prediction for (a) elastic modulus and (b) tensile strength of lactose monohydrate tablets as a function of relative density (case 5 in Table 4.1).

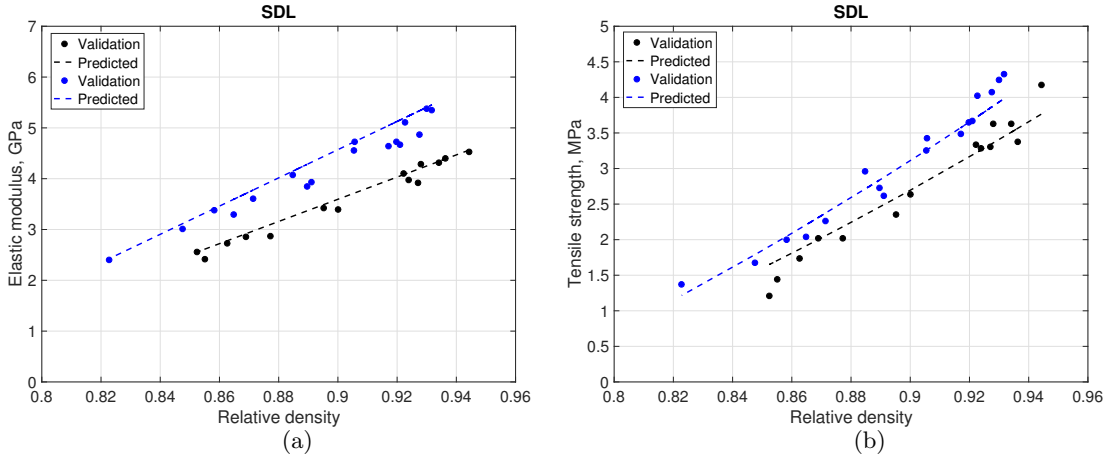

Figure 4.19: Comparsion of the validation experiments to the model predictions for (a) elastic modulus and (b) tensile strength of spray-dried lactose tablets as a function of relative density (cases 24 and 33 in Table 4.1).

Figs. 4.20(a) and 4.20(b) show the relationship between actual (measured) and predicted elastic modulus and tensile strength for all the LM and SDL tablets. Good correlations were observed between the predicted and actual values. For elastic modulus predictions, R^2 of 0.94 for both powders was found and for tensile strength predictions R^2 was 0.96 and 0.91 for SDL and LM, respectively.

Therefore, our proposed model can be successfully adopted to predict the mechanical strength of tablets capturing the lubricant sensitivity and PSD effects.

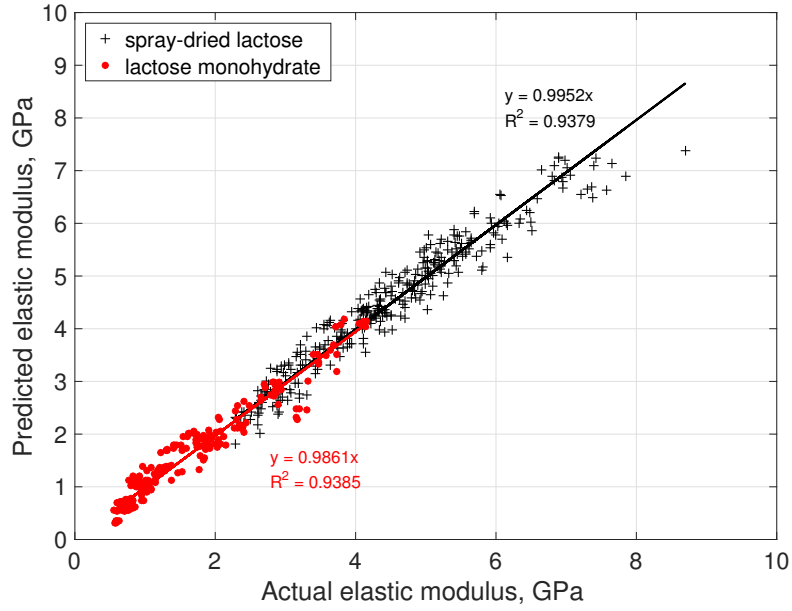

(a)

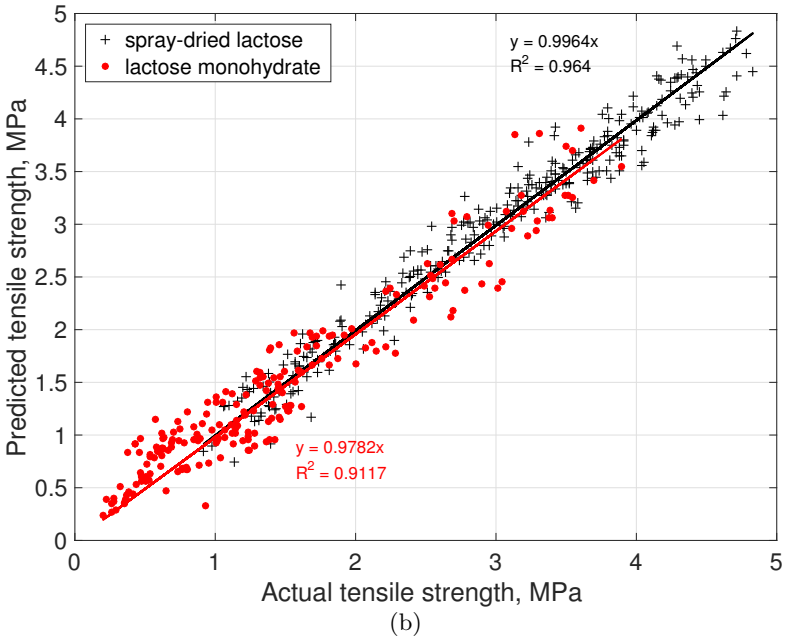

(b)

Figure 4.20: Predicted vs. actual values of (a) elastic modulus, where the R^2 was 0.94 for both powders and (b) tensile strength, where R^2 was 0.96 and 0.91 for spray-dried lactose and lactose monohydrate, respectively.

4.4 Summary and Conclusion

We have proposed a general framework for predicting a wide range of elastic modulus and tensile strength that a specific powder can attain based on its lubricant sensitivity and considering different particle size distributions. This was possible by introducing a new parameter in the existing tensile strength and elastic modulus models of porous materials. The model showed a good predictability for two grades of lactose. Our model can be extended to all the powders that undergo different deformation mechanisms and explored for ternary or more complex mixtures.

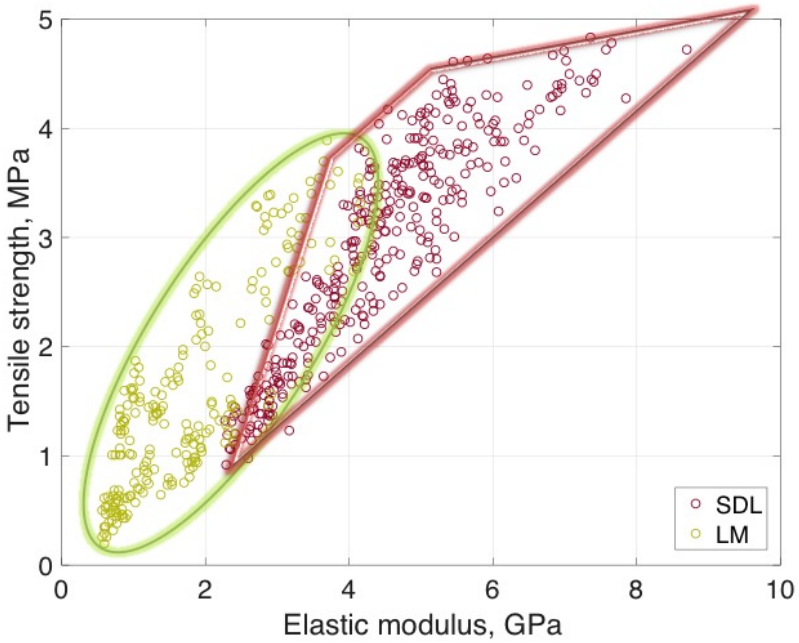

Figure 4.21: Elastic modulus and tensile strength regime for lactose monohydrate and spray-dried lactose tablets. Relative density of tablets ranged from 0.8 to 0.94.

We have covered a wide, if not the widest, strength level of lactose monohydrate and spray-dried lactose tablets with respect to particle size distributions and lubrication conditions. Fig. 4.21 depicts the measured tensile strength vs. elastic modulus of all the lactose monohydrate and spray-dried lactose tablets. The data points show a pattern, which can be identified by zones. An elliptic zone for LM and a trapezoidal zone for SPD are sketched. These zones provide an "accessible" regime, which is ideal for

design strategies. For a certain formulation, creating such a zone will help to optimize the processing variables for the desirable mechanical properties of tablets and to keep away from the boundaries.

As a validation of the proposed strategy in the previous chapter, we plotted σ_0 vs. E_0 (Fig. 4.22). The correlation is still clear with more number of observations and it seems to follow a nonlinear behavior.

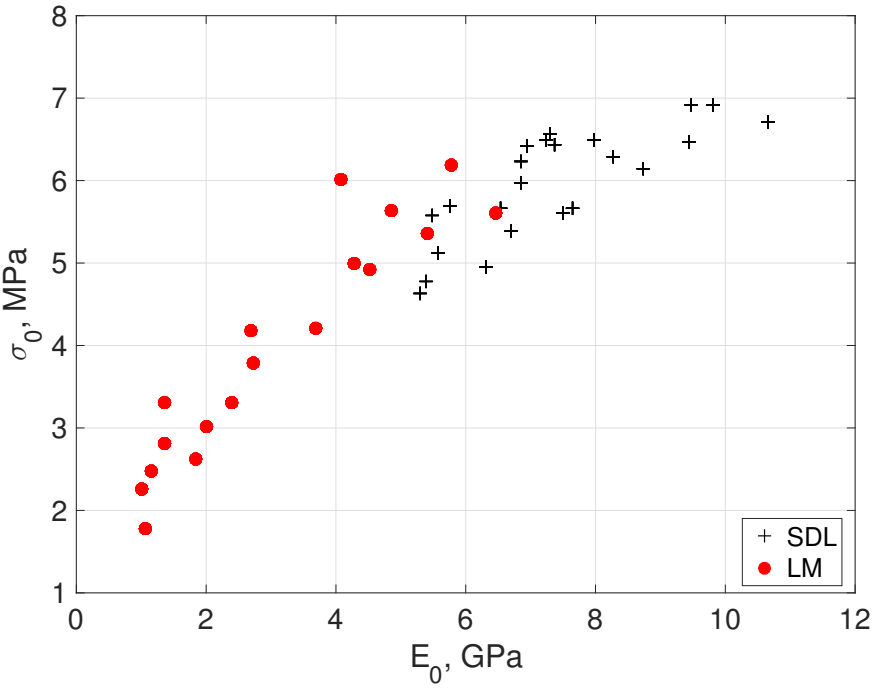

Figure 4.22: E_0 and σ_0 relationship for lactose monohydrate and spray-dried lactose tablets.

Chapter 5

Conclusions and Recommendations

5.1 Remarks

In Chapter 2, we proposed a general framework for determining optimal relationships for tensile strength from the breaking force of doubly convex tablets under diametrical compression. The approach is based on the observation that tensile strength is directly proportional to the breaking force and inversely proportional to Q, a nonlinear function of geometric parameters and materials properties.

We have proposed three new optimal tensile strength relationships, which we referred to as *general model*, *2-parameter model* and *mechanistic model*. The general model captures the leading order behavior of Q on the geometric parameters, it has the exact limiting behavior for flat faced tablets, and it has four optimal parameters to be determined. The 2-parameter model simplifies the general model by assuming that Q is linear on the geometric parameters, and thus the number of parameters is reduced to two while the correct limiting behavior is retained. The mechanistic model is based on an effective cross-sectional surface area associated with strength and exhibits the exact limiting behavior for flat geometries with only two optimal parameters.

We provided a set of recommendations on how to compare the models based on their number of parameters, stability, predictability, and having the correct limiting behavior. Our observations suggest that both general and mechanistic models are cost- and time-effective, predictive alternatives to the tensile strength relationship currently used in the pharmaceutical industry. Furthermore, our analysis showcases the benefits of adopting a general framework for developing and evaluating the performance of optimal relationships for tensile strength of doubly convex tablets under diametrical compression.

Chapter 3 demonstrated that ultrasound (US) measurement system can be successfully used to attain information about the mechanical integrity of pharmaceutical tablets. The effect of two processing parameters, compaction force and level of shear strain were examined. US speed of sound was found to be sensitive to the relative density and the level of shear strain. US testing could detect even small differences between tablets that a hardness tester failed to do so. This is an added advantage of using this technique to monitor mechanical properties, because a slight change could have a significant consequence on dissolution.

A strategy for hardness prediction was proposed that uses the existing models for elastic modulus and tensile strength of porous materials. A clear correlation between elastic modulus and tensile strength at zero porosity was presented. Thus, US testing was found to be a good candidate to be placed on/at-line to measure the mechanical integrity of tablets non-destructively. These results provide information about the behavior of processing parameters on the performance of tablets and the ability to engineer product properties. The extension of this work was continued in Chapter 4, where a general methodology was proposed for predicting a wide range of elastic modulus and tensile strength that a specific powder can attain based on its lubricant sensitivity and considering different particle size distributions. This was possible by introducing a new parameter in the existing tensile strength and elastic modulus models of porous materials. The empirical model showed a good predictability for two grades of lactose. Our model can be extended to all the powders that undergo different deformation mechanisms and explored for ternary or more complex mixtures. This quantitative strategy will enable formulators to better understand the formulation compaction behavior and select optimal processing parameters.

5.2 Future Work

Based on the work presented in this dissertation, several potential areas are discussed here for future study.

1. Chapters 3 and 4 demonstrated the efficacy of ultrasound measuring system to

analyze the mechanical integrity of tablets in a fast and non-destructive fashion. As a future plan, building a tablet testing toolbox is pursued, which consists of weight, hardness using ultrasound, thickness, diameter or length, chemical composition using NIR or Raman testing stations. This toolbox will ensure quick, automated, non-destructive testing to ensure all the critical quality attributes are measured for individual tablets.

2. To cut the amount of experimental work needed to characterize every new pharmaceutical formulation, it is necessary to study the effect of material properties on the tablet press performance. Thus, a general methodoloy for hardness model needs to be developed considering material properties and tablet press variables.

3. In this dissertation we have only tested flat faced cylindrical tablets for ultrasound testing. It would be of interest to study the stiffness of doubly convex tablets and investigate if the framework presented in Chapter 2 can be applied for the ultrasound measurements.

4. The particle size effect on lubrication sensitivity of an excipient was explored in Chapter 4. The model can be extended and generalized for pharmaceutical formulations taking into account other powder properties (e.g., bulk density) and/or processing parameters (e.g., compaction speed). We can also use the Quette shearing device to impart uniform shear to the powders and replace the mixing time in the model to shear rate and mechanical strain.

5. In Chapter 4, we briefly presented the possible particle size effect and lubrication sensitivity of powders on compaction profiles. More rigorous studies on the final stage of the unloading curves are favorable, which is thought to have a good correlation with tablet strength and are areas worthy of further investigation.

Acknowledgement of Previous Publications

Portion of this thesis is based on previously published work of the student. Publications in support of this thesis have been summarized below.

Publications in support of this thesis

1. **Razavi, S. M.**, Gonzalez, M., & Cuitino, A. M. (2015). General and mechanistic optimal relationships for tensile strength of doubly convex tablets under diametrical compression. International journal of pharmaceutics, 484(1), 29-37.

2. **Razavi, S. M.**, Callegari, G., Drazer, G., & Cuitino, A. M. (2016). Toward predicting tensile strength of pharmaceutical tablets by ultrasound measurement in continuous manufacturing. International journal of pharmaceutics, 507(1), 83-89.

References

[1] A. Dévay. The theory and practice of pharmaceutical technology. *University of Pécs, Pécs*, 2013.

[2] C. Shang, I. C. Sinka, B. Jayaraman, and J. Pan. Break force and tensile strength relationships for curved faced tablets subject to diametrical compression. *International journal of pharmaceutics*, 442(1):57–64, 2013.

[3] NDT Olympus. Ultrasonic transducers technical notes. *Accessed on March*, 2006.

[4] P. Pawar, Y. Wang, G. Keyvan, G. Callegari, A. Cuitino, and F. J. Muzzio. Enabling real time release testing by nir prediction of dissolution of tablets made by continuous direct compression (cdc). *International Journal of Pharmaceutics*, 512(1):96–107, 2016.

[5] M. Kuentz and H. Leuenberger. A new model for the hardness of a compacted particle system, applied to tablets of pharmaceutical polymers. *Powder technology*, 111(1):145–153, 2000.

[6] F. J. Muzzio, T. Shinbrot, and B. J. Glasser. Powder technology in the pharmaceutical industry: the need to catch up fast. *Powder technology*, 124(1):1–7, 2002.

[7] M. H. Rubinstein and M. E. Aulton. Pharmaceutics, the science of dosage form design. *Edinburgh London Melbourne and New York: Churchill Livingstone*, 2000.

[8] M. K. Kottke and E. M. Rudnic. Tablet dosage forms. *Modern pharmaceutics*, 4: 291–333, 2002.

[9] R. F. Shangraw and D. A. Demarest. A survey of current industrial practices in the formulation and manufacture of tablets and capsules. *Pharmaceutical technology*, 17(1):32–32, 1993.

[10] C. Nyström, G. Alderborn, M. Duberg, and P. Karehill. Bonding surface area and bonding mechanism-two important factors fir the understanding of powder comparability. *Drug development and industrial pharmacy*, 19(17-18):2143–2196, 1993.

[11] M. Duberg and C. Nyström. Studies on direct compression of tablets xvii. porositypressure curves for the characterization of volume reduction mechanisms in powder compression. *Powder Technology*, 46(1):67–75, 1986.

[12] D. Train. An investigation into the compaction of powders. *Journal of Pharmacy and Pharmacology*, 8(1):745–761, 1956.

[13] C. Führer. Substance behaviour in direct compression. *Labo-Pharma Probi. Techn*, 25:759–762, 1977.

[14] G. Alderborn and C. Nystrom. Pharmaceutical powder compaction technology. *Drugs and the pharmaceutical sciences*, 71:71–71, 1996.

[15] R. J. Roberts, R. C. Rowe, and K. Kendall. Brittleductile trasitions in die compaction of sodium chloride. *Chemical engineering science*, 44(8):1647–1651, 1989.

[16] N. Rasenack and B. W. Müller. Crystal habit and tableting behavior. *International journal of pharmaceutics*, 244(1):45–57, 2002.

[17] R. J. Roberts and R. C. Rowe. The effect of punch velocity on the compaction of a variety of materials. *Journal of pharmacy and pharmacology*, 37(6):377–384, 1985.

[18] R. Ishino, H. Yoshino, Y. Hirakawa, and K. Noda. Influence of tabletting speed on compactibility and compressibility of two direct compressible powders under high speed compression. *RN*, 38(7), 1990.

[19] B. Van Veen, K. Van der Voort Maarschalk, G. K. Bolhuis, K. Zuurman, and H. W. Frijlink. Tensile strength of tablets containing two materials with a different compaction behaviour. *International journal of pharmaceutics*, 203(1):71–79, 2000.

[20] P. M. C. Lacey. Developments in the theory of particle mixing. *Journal of applied chemistry*, 4(5):257–268, 1954.

[21] J. Bridgwater. Fundamental powder mixing mechanisms. *Powder Technology*, 15 (2):215–236, 1976.

[22] L. T. Fan, Y. Chen, and F. S. Lai. Recent developments in solids mixing. *Powder Technology*, 61(3):255–287, 1990.

[23] T. Elperin and A. Vikhansky. Granular flow in a rotating cylindrical drum. *EPL (Europhysics Letters)*, 42(6):619, 1998.

[24] D. Brone, A. Alexander, and F. J. Muzzio. Quantitative characterization of mixing of dry powders in v-blenders. *AIChE Journal*, 44(2):271–278, 1998.

[25] A. Alexander, T. Shinbrot, B. Johnson, and F. J. Muzzio. V-blender segregation patterns for free-flowing materials: effects of blender capacity and fill level. *International journal of pharmaceutics*, 269(1):19–28, 2004.

[26] M. Lemieux, F. Bertrand, J. Chaouki, and P. Gosselin. Comparative study of the mixing of free-flowing particles in a v-blender and a bin-blender. *Chemical Engineering Science*, 62(6):1783–1802, 2007.

[27] Resonant Acoustic Mixer. Resonant acoustic® mixing. *URI: http://www.resodynmixers.com/wp-content/uploads/2009/05/ram-technical-white-paper1.pdf*, 2009.

[28] J. G. Osorio and F. J. Muzzio. Evaluation of resonant acoustic mixing performance. *Powder Technology*, 2015.

[29] Juan G Osorio, Koushik Sowrirajan, and Fernando J Muzzio. Effect of resonant acoustic mixing on pharmaceutical powder blends and tablets. *Advanced Powder Technology*, 27(4):1141–1148, 2016.

[30] C. F. Harwood, K. Walanski, E. Luebcke, and C. Swanstrom. The performance of continuous mixers for dry powders. *Powder Technology*, 11(3):289–296, 1975.

[31] R. Weinekötter and L. Reh. Continuous mixing of fine particles. *Particle & particle systems characterization*, 12(1):46–53, 1995.

[32] L. Pernenkil and C. L. Cooney. A review on the continuous blending of powders. *Chemical Engineering Science*, 61(2):720–742, 2006.

[33] S. Oka, A. Sahay, W. Meng, and F. J Muzzio. Diminished segregation in continuous powder mixing. *Powder Technology*, 309:79–88, 2017.

[34] M. Saravanan, K. S. Nataraj, and K. S. Ganesh. The effect of tablet formulation and hardness on in vitro release of cephalexin from eudragit l100 based extended release tablets. *Biological and Pharmaceutical Bulletin*, 25(4):541–545, 2002.

[35] USP. *The United States Pharmacopeia*. 34th ed. US Pharmacopeial Convention, Rockville, Maryland, 2011.

[36] J. T. Fell and J. M. Newton. Determination of tablet strength by the diametral-compression test. *Journal of Pharmaceutical Sciences*, 59(5):688–691, 1970.

[37] P. Stanley. Mechanical strength testing of compacted powders. *International journal of pharmaceutics*, 227(1):27–38, 2001.

[38] F. Podczeck. Methods for the practical determination of the mechanical strength of tabletsäîfrom empiricism to science. *International journal of pharmaceutics*, 436(1):214–232, 2012.

[39] C. Nyström, W. Alex, and K. Malmqvist. A new approach to tensile strength measurement of tablets. *Acta Pharmaceutica Suecica*, 14(3):317, 1977.

[40] F. Carneiro and A. Barcellos. Tensile strength of concrete. *Rilem Bulletin*, 13: 97–123, 1953.

[41] H. R. Hertz. Gesammelte werke, band iii: Die prinzipien der mechanik in neuem zusammenhange dargestellt. *Barth, Leipzig*, 1894.

[42] K. Ridgway, C. Lazarou, and E. E. Thorpe. The properties of tablets manufactured on an automatically-controlled rotary machine. *Journal of Pharmacy and Pharmacology*, 24(4):265–271, 1972.

[43] A. McKenna and D. F. McCafferty. Effect of particle size on the compaction mechanism and tensile strength of tablets. *Journal of Pharmacy and Pharmacology*, 34(6):347–351, 1982.

[44] C. K. Tye, C. C. Sun, and G. E. Amidon. Evaluation of the effects of tableting speed on the relationships between compaction pressure, tablet tensile strength, and tablet solid fraction. *Journal of pharmaceutical sciences*, 94(3):465–472, 2005.

[45] S. P. Timoshenko and J. N. Goodier. *Theory of Elasticity*. Mcgraw-hill, New York, 1970.

[46] M. M. Frocht. Vol. ii. *Wiley, New York*, 1:948, 1948.

[47] J. T. Fell and J._M. Newton. The tensile strength of lactose tablets. *Journal of Pharmacy and Pharmacology*, 20(8):657–659, 1968.

[48] A. T. Procopio, A. Zavaliangos, and J. C. Cunningham. Analysis of the diametrical compression test and the applicability to plastically deforming materials. *Journal of Materials Science*, 38(17):3629–3639, 2003.

[49] E. Ryshkewitch. Compression strength of porous sintered alumina and zirconia. *Journal of the American Ceramic Society*, 36, 1953.

[50] I. Haririan and M. Newton. Tensile strength of circular flat and convex-faced avicel ph102 tablets. *DARU Journal of Pharmaceutical Sciences*, 7(3):36–40, 1999.

[51] I. C. Sinka, F. Motazedian, A. C. F. Cocks, and K. G. Pitt. The effect of processing parameters on pharmaceutical tablet properties. *Powder Technology*, 189(2):276–284, 2009.

[52] K. G. Pitt, J. M. Newton, and P. Stanley. Stress distributions in doubly convex cylindrical discs under diametral loading. *Journal of Physics D: Applied Physics*, 22(8):1114, 1989.

[53] K. G. Pitt, J. M. Newton, and P. Stanley. Tensile fracture of doubly-convex cylindrical discs under diametral loading. *Journal of materials science*, 23(8): 2723–2728, 1988.

[54] K. G. Pitt and M. G. Heasley. Determination of the tensile strength of elongated tablets. *Powder Technology*, 238:169–175, 2013.

[55] C. Shang, I. C. Sinka, and J. Pan. Modelling of the break force of tablets under diametrical compression. *International journal of pharmaceutics*, 445(1):99–107, 2013.

[56] F. Podczeck, K. R. Drake, and J. M. Newton. Investigations into the tensile failure of doubly-convex cylindrical tablets under diametral loading using finite element methodology. *International journal of pharmaceutics*, 454(1):412–424, 2013.

[57] T. Tang. Effects of load-distributed width on split tension on unnotched and notched cylindrical specimens. *Journal of testing and Evaluation*, 22(5):401–409, 1994.

[58] G. Hondros. The evaluation of poissonäôs ratio and the modulus of materials of a low tensile resistance by the brazilian (indirect tensile) test with particular reference to concrete. *Australian Journal of Applied Science*, 10(3):243–268, 1959.

[59] S. K. Kourkoulis, C. F. Markides, and P. E. Chatzistergos. The brazilian disc under parabolically varying load: theoretical and experimental study of the displacement field. *International Journal of Solids and Structures*, 49(7):959–972, 2012.

[60] Q. Z. Wang, X. M. Jia, S. Q. Kou, Z. X. Zhang, and P. A. Lindqvist. The flattened brazilian disc specimen used for testing elastic modulus, tensile strength and fracture toughness of brittle rocks: analytical and numerical results. *International Journal of Rock Mechanics and Mining Sciences*, 41(2):245–253, 2004.

[61] C. Bagault, D. Nelias, M. Baietto, and T. C. Ovaert. Contact analyses for anisotropic half-space coated with an anisotropic layer: Effect of the anisotropy on the pressure distribution and contact area. *International Journal of Solids and Structures*, 50(5):743–754, 2013.

[62] R. Iyer, S. Hegde, Y. Zhang, J. Dinunzio, D. Singhal, A. Malick, and G. Amidon. The impact of hot melt extrusion and spray drying on mechanical properties and tableting indices of materials used in pharmaceutical development. *Journal of pharmaceutical sciences*, 102(10):3604–3613, 2013.

[63] J. W. Kennerley, J. M. Newton, and P. Stanley. A modified weibull treatment for the analysis of strength-test data from non-identical brittle specimens. *Journal of Materials Science*, 17(10):2947–2954, 1982.

[64] MATLAB. *Release 2012b*. The MathWorks Inc., Natick, Massachusetts, 2012.

[65] M. Gonzalez and A. M. Cuitiño. A nonlocal contact formulation for confined granular systems. *Journal of the Mechanics and Physics of Solids*, 60(2):333–350, 2012.

[66] M. Gonzalez and A. M. Cuitiño. Microstructure evolution of compressible granular systems under large deformations. *Journal of the Mechanics and Physics of Solids*, 93:44–56, 2016.

[67] B. Yohannes, M. Gonzalez, A. Abebe, O. Sprockel, F. Nikfar, S. Kiang, and A. M. Cuitiño. Evolution of the microstructure during the process of consolidation and bonding in soft granular solids. *International journal of pharmaceutics*, 503(1): 68–77, 2016.

[68] S. L. Lee, T. F. OConnor, X. Yang, C. N. Cruz, S. Chatterjee, R. D. Madurawe, C. M. V. Moore, X. Y. Lawrence, and J. Woodcock. Modernizing pharmaceutical manufacturing: from batch to continuous production. *Journal of Pharmaceutical Innovation*, 10(3):191–199, 2015.

[69] S. Chatterjee. FDA perspective on continuous manufacturing. In *IFPAC Annual Meeting, Baltimore, Baltimore*, 2012.

[70] S. Byrn, M. Futran, H. Thomas, E. Jayjock, N. Maron, R. F. Meyer, A. S. Myerson, M. P. Thien, and B. L. Trout. Achieving continuous manufacturing for final dosage formation: Challenges and how to meet them. may 20–21, 2014 continuous manufacturing symposium. *Journal of pharmaceutical sciences*, 104 (3):792–802, 2015.

[71] FDA. Guidance for industry: Pat-a framework for innovative pharmaceutical development, manufacturing, and quality assurance. *DHHS, Rockville, MD*, 2004.

[72] FDA. Guidance for industry: Q8(r2). *Pharmaceutical Development*, 2009.

[73] L. Yu. Pharmaceutical quality by design: product and process development, understanding, and control. *Pharmaceutical research*, 25(4):781–791, 2008.

[74] ICH Harmonised Tripartite Guideline. Pharmaceutical development q8 (r2). *Current step*, 4, 2009.

[75] Yu L. Continuous manufacturing has a strong impact on drug quality. *URI: https://blogs.fda.gov/fdavoice/index.php/2016/04/continuous-manufacturing- has-a-strong-impact-on-drug-quality*, 2016.

[76] J. D. Kirsch and J. K. Drennen. Near-infrared spectroscopy: applications in the analysis of tablets and solid pharmaceutical dosage forms. *Applied Spectroscopy Reviews*, 30(3):139–174, 1995.

[77] H. Ma and C. A. Anderson. Characterization of pharmaceutical powder blends by nir chemical imaging. *Journal of pharmaceutical sciences*, 97(8):3305–3320, 2008.

[78] T. Vankeirsbilck, A. Vercauteren, W. Baeyens, G. Van der Weken, F. Verpoort, G. Vergote, and J. P. Remon. Applications of raman spectroscopy in pharmaceutical analysis. *TrAC trends in analytical chemistry*, 21(12):869–877, 2002.

[79] J. Ketolainen, M. Oksanen, J. Rantala, J. Stor-Pellinen, M. Luukkala, and P. Paronen. Photoacoustic evaluation of elasticity and integrity of pharmaceutical tablets. *International journal of pharmaceutics*, 125(1):45–53, 1995.

[80] I. Akseli, B. C. Hancock, and C. Cetinkaya. Non-destructive determination of anisotropic mechanical properties of pharmaceutical solid dosage forms. *International journal of pharmaceutics*, 377(1):35–44, 2009.

[81] R. P. Cogdill, R. N. Forcht, Y. Shen, P. F. Taday, J. R. Creekmore, C. A. Anderson, and J. K. Drennen. Comparison of terahertz pulse imaging and near-infrared spectroscopy for rapid, non-destructive analysis of tablet coating thickness and uniformity. *Journal of Pharmaceutical Innovation*, 2(1):29–36, 2007.

[82] Y. C. Shen. Terahertz pulsed spectroscopy and imaging for pharmaceutical applications: a review. *International journal of pharmaceutics*, 417(1):48–60, 2011.

[83] R. K. May, K. Su, L. Han, S. Zhong, J. A Elliott, L. F. Gladden, M. Evans, Y. Shen, and J. A. Zeitler. Hardness and density distributions of pharmaceutical tablets measured by terahertz pulsed imaging. *Journal of pharmaceutical sciences*, 102(7):2179–2186, 2013.

[84] J. T. T. Leskinen, S. P. Simonaho, M. Hakulinen, and J. Ketolainen. In-line ultrasound measurement system for detecting tablet integrity. *International journal of pharmaceutics*, 400(1):104–113, 2010.

[85] S. P. Simonaho, T A. Takala, M. Kuosmanen, and J. Ketolainen. Ultrasound transmission measurements for tensile strength evaluation of tablets. *International journal of pharmaceutics*, 409(1):104–110, 2011.

[86] F. P. Capote and M. D. L. de Castro. *Analytical applications of ultrasound*, volume 26. Elsevier, 2007.

[87] B. Raj, V. Rajendran, and P. Palanichamy. *Science and technology of ultrasonics*. Alpha Science Int'l Ltd., 2004.

[88] B. A. Auld. *Acoustic fields and waves in solids*, volume 1. 1973.

[89] I. Akseli and C. Cetinkaya. Air-coupled non-contact mechanical property determination of drug tablets. *International journal of pharmaceutics*, 359(1):25–34, 2008.

[90] I. Akseli, N. Ladyzhynsky, J. Katz, and X. He. Development of predictive tools to assess capping tendency of tablet formulations. *Powder technology*, 236:139–148, 2013.

[91] I. Akseli, A. Stecuła, X. He, and N. Ladyzhynsky. Quantitative correlation of the effect of process conditions on the capping tendencies of tablet formulations. *Journal of pharmaceutical sciences*, 103(6):1652–1663, 2014.

[92] M. A. Hakulinen, J. Pajander, J. Leskinen, J. Ketolainen, B. Van Veen, K. Niinimäki, K. Pirskanen, A. Poso, and R. Lappalainen. Ultrasound transmission technique as a potential tool for physical evaluation of monolithic matrix tablets. *AAPS PharmSciTech*, 9(1):267–273, 2008.

[93] I. Akseli, S. Iyer, H. P. Lee, and A. M. Cuitiño. A quantitative correlation of the effect of density distributions in roller-compacted ribbons on the mechanical properties of tablets using ultrasonics and x-ray tomography. *AAPS PharmSciTech*, 12(3):834–853, 2011.

[94] I. Akseli, C. Libordi, and C. Cetinkaya. Real-time acoustic elastic property monitoring of compacts during compaction. *Journal of Pharmaceutical Innovation*, 3 (2):134–140, 2008.

[95] J. T. T. Leskinen, S. P. Simonaho, M. Hakulinen, and J. Ketolainen. Real-time tablet formation monitoring with ultrasound measurements in eccentric single station tablet press. *International journal of pharmaceutics*, 442(1):27–34, 2013.

[96] J. Liu, J. D. Stephens, B. R. Kowalczyk, and C. Cetinkaya. Real-time in-die compaction monitoring of dry-coated tablets. *International journal of pharmaceutics*, 414(1):171–178, 2011.

[97] J. D. Stephens, B. R. Kowalczyk, B. C. Hancock, G. Kaul, and C. Cetinkaya. Ultrasonic real-time in-die monitoring of the tablet compaction process. a proof of concept study. *International journal of pharmaceutics*, 442(1):20–26, 2013.

[98] W. M. Long. Radial pressures in powder compaction*. *Powder Metallurgy*, 3(6): 73–86, 1960.

[99] K. V. D. V. Maarschalk, H. Vromans, G. K. Bolhuis, and C. F. Lerk. Influence of plasticizers on tableting properties of polymers. *Drug development and industrial pharmacy*, 24(3):261–268, 1998.

[100] I. Akseli, J. Xie, L. Schultz, N. Ladyzhynsky, T. Bramante, X. He, R. Deanne, K. R. Horspool, and R. Schwabe. A practical framework toward prediction of breaking force and disintegration of tablet formulations using machine learning tools. *Journal of Pharmaceutical Sciences*, 106(1):234–247, 2017.

[101] R. Singh, A. Sahay, F. J. Muzzio, M. Ierapetritou, and R. Ramachandran. A systematic framework for onsite design and implementation of a control system in a continuous tablet manufacturing process. *Computers & Chemical Engineering*, 66:186–200, 2014.

[102] A. U. Vanarase and F. J. Muzzio. Effect of operating conditions and design parameters in a continuous powder mixer. *Powder Technology*, 208(1):26–36, 2011.

[103] A. Mehrotra, M. Llusa, A.l Faqih, M. Levin, and F. J. Muzzio. Influence of shear intensity and total shear on properties of blends and tablets of lactose and cellulose lubricated with magnesium stearate. *International journal of pharmaceutics*, 336 (2):284–291, 2007.

[104] K. Pingali, R. Mendez, D. Lewis, B. Michniak-Kohn, A. Cuitiño, and F. J. Muzzio. Mixing order of glidant and lubricant–influence on powder and tablet properties. *International journal of pharmaceutics*, 409(1):269–277, 2011.

[105] K. K. Phani and S. K. Niyogi. Young's modulus of porous brittle solids. *Journal of materials science*, 22(1):257–263, 1987.

[106] F. Bassam, P York, R. C. Rowe, and R. J. Roberts. Young's modulus of powders used as pharmaceutical excipients. *International journal of pharmaceutics*, 64(1): 55–60, 1990.

[107] S. Spinner, F. P. Knudson, and L. Stone. *Elastic Constant-Porosity Relation for Polycrystalline Thoria*. Defense Technical Information Center, 1964.

[108] R. C. Rossi. Prediction of the elastic moduli of composites. *Journal of the American Ceramic Society*, 51(8):433–440, 1968.

[109] F. P. Knudsen. Dependence of mechanical strength of brittle polycrystalline specimens on porosity and grain size. *Journal of the American Ceramic Society*, 42 (8):376–387, 1959.

[110] S. M. Razavi, M. Gonzalez, and A. M. Cuitiño. General and mechanistic optimal relationships for tensile strength of doubly convex tablets under diametrical compression. *International Journal of Pharmaceutics*, 2015.

[111] MATLAB. *version 8.4.0 (R2014b)*. The MathWorks Inc., Natick, Massachusetts, 2014.

[112] L. Lachman, H. A. Lieberman, J. L. Kanig, et al. *The theory and practice of industrial pharmacy*. Lea & Febiger Philadelphia, 1976.

[113] G. Moody, M. H. Rubinstein, and R. A. FitzSimmons. Tablet lubricants I. theory and modes of action. *International Journal of Pharmaceutics*, 9(2):75–80, 1981.

[114] Y. Hirai and J. Okada. Effect of lubricant on die wall friction during the compaction of pharmaceutical powders. *Chemical and Pharmaceutical Bulletin*, 30 (2):684–694, 1982.

[115] R. Dansereau and G. E. Peck. The effect of the variability in the physical and chemical properties of magnesium stearate on the properties of compressed tablets. *Drug Development and Industrial Pharmacy*, 13(6):975–999, 1987.

[116] T. A. Miller and P. York. Pharmaceutical tablet lubrication. *International journal of pharmaceutics*, 41(1-2):1–19, 1988.

[117] P. J. Sheskey, R. T. Robb, R. D. Moore, and B. M. Boyce. Effects of lubricant level, method of mixing, and duration of mixing on a controlled-release matrix tablet containing hydroxypropyl methylcellulose. *Drug development and industrial pharmacy*, 21(19):2151–2165, 1995.

[118] F. Podczeck and Y. Mia. The influence of particle size and shape on the angle of internal friction and the flow factor of unlubricated and lubricated powders. *International Journal of Pharmaceutics*, 144(2):187–194, 1996.

[119] A. M. N. Faqih, A. Mehrotra, S. V. Hammond, and F. J. Muzzio. Effect of moisture and magnesium stearate concentration on flow properties of cohesive granular materials. *International journal of pharmaceutics*, 336(2):338–345, 2007.

[120] N. O. Lindberg. Evaluation of some tablet lubricants. *Acta Pharmaceutica Suecica*, 9(3):207–214, 1972.

[121] M. E. Johansson. Granular magnesium stearate as a lubricant in tablet formulations. *International journal of pharmaceutics*, 21(3):307–315, 1984.

[122] J. Wang, H. Wen, and D. Desai. Lubrication in tablet formulations. *European Journal of Pharmaceutics and Biopharmaceutics*, 75(1):1–15, 2010.

[123] G. K. Bolhuis, C. F. Lerk, H. T. Zijlstra, and A. H. De Boer. Film formation by magnesium stearate during mixing and its effect on tabletting. *Pharm. Weekbl*, 110:317–325, 1975.

[124] A. H. De Boer, G. K. Bolhuis, and C. F. Lerk. Bonding characteristics by scanning electron microscopy of powders mixed with magnesium stearate. *Powder Technology*, 20(1):75–82, 1978.

[125] M. S. H. Hussain, P. York, P. Timmins, and P. Humphrey. Secondary ion mass spectrometry (sims) evaluation of magnesium stearate distribution and its effects on the physico-technical properties of sodium chloride tablets. *Powder Technology*, 60(1):39–45, 1990.

[126] A. F. Asker, K. M. Saied, and M. M. Abdel-Khalek. Investigation of some materials as dry binders for direct compression in tablet manufacture. part 5: Effects of lubricants and flow conditions. *Die Pharmazie*, 30(6):378–382, 1975.

[127] A. C. Shah and A. R. Mlodozeniec. Mechanism of surface lubrication: Influence of duration of lubricant-excipient mixing on processing characteristics of powders and properties of compressed tablets. *Journal of pharmaceutical sciences*, 66(10): 1377–1382, 1977.

[128] J. Bossert and A. Stains. Effect of mixing on the lubrication of crystalline lactose by magnesium stearate. *Drug Development and Industrial Pharmacy*, 6(6):573–589, 1980.

[129] M. Otsuka, J. I. Gao, and Y. Matsuda. Effects of mixer and mixing time on the pharmaceutical properties of theophylline tablets containing various kinds of lactose as diluents. *Drug development and industrial pharmacy*, 19(3):333–348, 1993.

[130] J. I. Kikuta and N. Kitamori. Effect of mixing time on the lubricating properties of magnesium stearate and the final characteristics of the compressed tablets. *Drug development and industrial pharmacy*, 20(3):343–355, 1994.

[131] M. Otsuka, I. Yamane, and Y. Matsuda. Effects of lubricant mixing on compression properties of various kinds of direct compression excipients and physical properties of the tablets. *Advanced Powder Technology*, 15(4):477–493, 2004.

[132] P. J. Jarosz and E. L. Parrott. Effect of lubricants on tensile strengths of tablets. *Drug Development and Industrial Pharmacy*, 10(2):259–273, 1984.

[133] G. K. Bolhuis and Z. T. Chowhan. Materials for direct compaction. In *Pharmaceutical Powder ComPattion Technology*, pages 419–500. CRC Press, 1995.

[134] A. Mitrevej, N. Sinchaipanid, and D. Faroongsarng. Spray-dried rice starch: comparative evaluation of direct compression fillers. *Drug development and industrial pharmacy*, 22(7):587–594, 1996.

[135] E. Doelker, D. Mordier, H. Iten, and P. Humbert-Droz. Comparative tableting properties of sixteen microcrystalline celluloses. *Drug Development and Industrial Pharmacy*, 13(9-11):1847–1875, 1987.

[136] M. J. Mollan and M. Çelik. The effects of lubrication on the compaction and post-compaction properties of directly compressible maltodextrins. *International journal of pharmaceutics*, 144(1):1–9, 1996.

[137] K. Zuurman, K. Van der Voort Maarschalk, and G. K. Bolhuis. Effect of magnesium stearate on bonding and porosity expansion of tablets produced from materials with different consolidation properties. *International journal of pharmaceutics*, 179(1):107–115, 1999.

[138] M. Llusa, M. Levin, R. D. Snee, and F. J. Muzzio. Measuring the hydrophobicity of lubricated blends of pharmaceutical excipients. *Powder Technology*, 198(1): 101–107, 2010.

[139] A. S. Narang, V. M. Rao, H. Guo, J. Lu, and D. S. Desai. Effect of force feeder on tablet strength during compression. *International journal of pharmaceutics*, 401(1):7–15, 2010.

[140] J. Kushner and F. Moore. Scale-up model describing the impact of lubrication on tablet tensile strength. *International journal of pharmaceutics*, 399(1):19–30, 2010.

[141] S. Nakamura, S. Yamaguchi, Ri. Hiraide, K. Iga, T. Sakamoto, and H. Yuasa. Setting ideal lubricant mixing time for manufacturing tablets by evaluating powder flowability. *AAPS PharmSciTech*, pages 1–9, 2017.

[142] R. J. Roberts and R. C. Rowe. The effect of the relationship between punch velocity and particle size on the compaction behaviour of materials with varying deformation mechanisms. *Journal of pharmacy and pharmacology*, 38(8):567–571, 1986.

[143] A. H. De Boer, H. Vromans, C. F. Leur, G. K. Bolhuis, K. D. Kussendrager, and H. Bosch. Studies on tableting properties of lactose. *Pharmacy World & Science*, 8(2):145–150, 1986.

[144] A. Castellanos. The relationship between attractive interparticle forces and bulk behaviour in dry and uncharged fine powders. *Advances in Physics*, 54(4):263–376, 2005.

[145] A. M. Faqih, B. Chaudhuri, A. W. Alexander, C. Davies, F. J. Muzzio, and M. S. Tomassone. An experimental/computational approach for examining unconfined cohesive powder flow. *International journal of pharmaceutics*, 324(2):116–127, 2006.

[146] E. Shotton and D. Ganderton. The strength of compressed tablets. *Journal of Pharmacy and Pharmacology*, 13(S1):144T–152T, 1961.

[147] J. A. Hersey, G. Bayraktar, and E. Shotton. The effect of particle size on the strength of sodium chloride tablets. *The Journal of pharmacy and pharmacology*, 19:Suppl–24S, 1967.

[148] G. Ragnarsson and J. Sjögren. Force-displacement measurements in tableting. *Journal of pharmacy and pharmacology*, 37(3):145–150, 1985.

[149] F. N. Rhines. Seminar on pressing of metal powders. *AIME Trans.*, 171:518–534, 1947.

[150] H. Vromans, A. H. De Boer, G. K. Bolhuis, C. F. Lerk, K. D. Kussendrager, and H. Bosch. Studies on tableting properties of lactose. *Pharmacy World & Science*, 7(5):186–193, 1985.

[151] G. Alderborn and C. Nyström. Studies on direct compression of tablets. iv. the effect of particle size on the mechanical strength of tablets. *Acta Pharmaceutica Suecica*, 19(5):381, 1982.

[152] P. R. Katikaneni, S. M. Upadrashta, C. E. Rowlings, S. H. Neau, and G. A. Hileman. Consolidation of ethylcellulose: effect of particle size, press speed, and lubricants. *International journal of pharmaceutics*, 117(1):13–21, 1995.

[153] J. G. Van der Watt. The effect of the particle size of microcrystalline cellulose on tablet properties in mixtures with magnesium stearate. *International journal of pharmaceutics*, 36(1):51–54, 1987.

[154] A. Almaya and A. Aburub. Effect of particle size on compaction of materials with different deformation mechanisms with and without lubricants. *AAPS PharmSciTech*, 9(2):414–418, 2008.

[155] Beckman Coulter. Ls 13 320 laser diffraction particle size analyzer: Instructions for use. *URI: https://www. beckmancoulter. com/wsrportal/techdocs*, 2011.

[156] B. Yohannes, M. Gonzalez, A. Abebe, O. Sprockel, F. Nikfar, S. Kang, and A. M. Cuitino. The role of fine particles on compaction and tensile strength of pharmaceutical powders. *Powder Technology*, 274:372–378, 2015.

[157] P. Pawar, H. Joo, G. Callegari, G. Drazer, A. M. Cuitino, and F. J. Muzzio. The effect of mechanical strain on properties of lubricated tablets compacted at different pressures. *Powder Technology*, 301:657–664, 2016.

[158] V. Velasco, A. Muñoz-Ruiz, C. Monedero, and R. Jiménez-Castellanos. Force-displacement parameters of maltodextrins after the addition of lubricants. *International journal of pharmaceutics*, 152(1):111–120, 1997.

[159] D. P. Coffin-Beach and R. G. Hollenbeck. Determination of the energy of tablet formation during compression of selected pharmaceutical powders. *International journal of pharmaceutics*, 17(2-3):313–324, 1983.

[160] NA Armstrong and RF Haines-Nutt. Elastic recovery and surface area changes in compacted powder systems. *The Journal of pharmacy and pharmacology*, 24: Suppl–135P, 1972.

[161] S. M. Razavi, G. Callegari, G. Drazer, and A. M. Cuitiño. Toward predicting tensile strength of pharmaceutical tablets by ultrasound measurement in continuous manufacturing. *International journal of pharmaceutics*, 507(1):83–89, 2016.